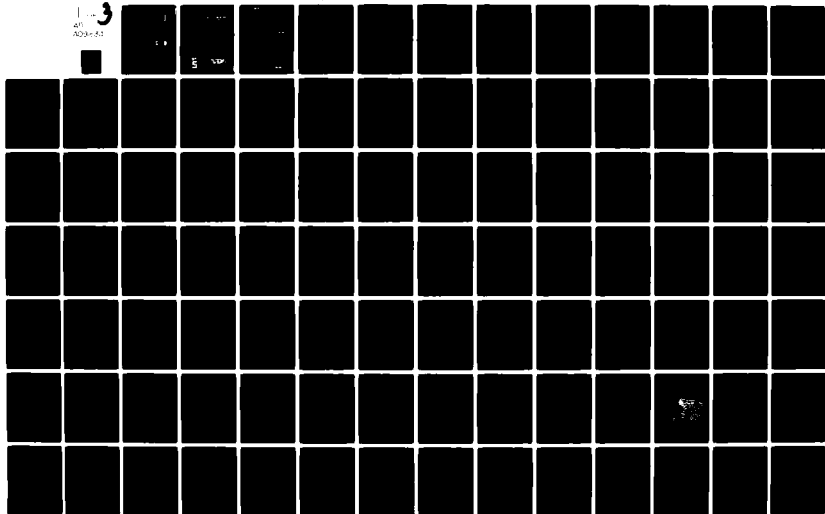


AD-A091 634

EFFECTS TECHNOLOGY INC SANTA BARBARA CA F/G 14/2  
ROCKET SLED IMPROVED VELOCITY MEASURING SYSTEM FEASIBILITY STUD--ETC(U)  
APR 80 W NAUMANN, K ENGBERG, R D HOGG F29601-79-C-0041  
ETI-CR80-770 NL

UNCLASSIFIED

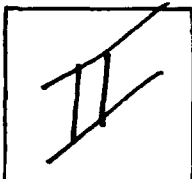
1-3  
AD-A091 634



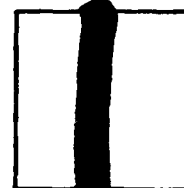
PHOTOGRAPH THIS SHEET

Au A091634

DTIC ACCESSION NUMBER



LEVEL



INVENTORY

Effects Technology, Inc.  
Santa Barbara, CA

"Rocket Sled Improved Velocity Measuring  
System Feasibility Study"

DOCUMENT IDENTIFICATION

Final Rpt., 10 Apr. '80

Contract No. F29601-79-C-0041

Rpt. No. CR80-770

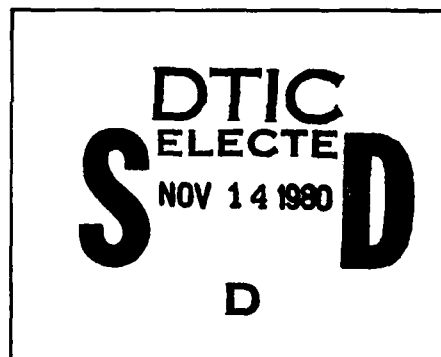
DISTRIBUTION STATEMENT A

Approved for public release;  
Distribution Unlimited

DISTRIBUTION STATEMENT

ACCESSION FOR	
NTIS	GRA&I <input checked="" type="checkbox"/>
DTIC	TAB <input type="checkbox"/>
UNANNOUNCED	<input type="checkbox"/>
JUSTIFICATION	
BY	
DISTRIBUTION /	
AVAILABILITY CODES	
DIST	AVAIL AND/OR SPECIAL
A	

DISTRIBUTION STAMP



DATE ACCESSIONED

80 11 06 028

DATE RECEIVED IN DTIC

PHOTOGRAPH THIS SHEET AND RETURN TO DTIC-DDA-2

AD A091634



**UNCLASSIFIED**

SECURITY CLASSIFICATION OF THIS PAGE (When Data Entered)

REPORT DOCUMENTATION PAGE		READ INSTRUCTIONS BEFORE COMPLETING FORM
1. REPORT NUMBER CR80-770	2. GOVT ACCESSION NO.	3. RECIPIENT'S CATALOG NUMBER
4. TITLE (and Subtitle) ROCKET SLED IMPROVED VELOCITY MEASURING SYSTEM FEASIBILITY STUDY		5. TYPE OF REPORT & PERIOD COVERED Final Report
		6. PERFORMING ORG. REPORT NUMBER
7. AUTHOR(s) Walter Naumann R. Douglas Hogg Kristin Engberg John Hunka		8. CONTRACT OR GRANT NUMBER(s) F29601-79-C-0041
9. PERFORMING ORGANIZATION NAME AND ADDRESS Effects Technology Inc. 5383 Hollister Ave. Santa Barbara CA 93111		10. PROGRAM ELEMENT, PROJECT, TASK AREA & WORK UNIT NUMBERS
11. CONTROLLING OFFICE NAME AND ADDRESS 6585 TESTG/TK Holloman AFB NM 88330		12. REPORT DATE Apr 1980
		13. NUMBER OF PAGES
14. MONITORING AGENCY NAME & ADDRESS (if different from Controlling Office)		15. SECURITY CLASS. (of this report) <b>UNCLASSIFIED</b>
		15a. DECLASSIFICATION/DOWNGRADING SCHEDULE
16. DISTRIBUTION STATEMENT (of this Report)  Approved for public release; distribution unlimited.		
17. DISTRIBUTION STATEMENT (of the abstract entered in Block 20, if different from Report)		
18. SUPPLEMENTARY NOTES		
19. KEY WORDS (Continue on reverse side if necessary and identify by block number) rocket sleds velocity measurement		
20. ABSTRACT (Continue on reverse side if necessary and identify by block number)		

DD FORM 1 JAN 73 1473

**UNCLASSIFIED**

SECURITY CLASSIFICATION OF THIS PAGE (When Data Entered)

ROCKET SLED  
IMPROVED VELOCITY MEASURING SYSTEM  
FEASIBILITY STUDY  
FINAL REPORT

by

Walter Naumann  
Kristin Engberg  
R. Douglas Hogg  
John Hunka  
Glenn Oliver

10 April 1980

EFFECTS TECHNOLOGY, INCORPORATED  
A Subsidiary of Flow General, Inc.  
5383 Hollister Avenue  
Santa Barbara, California 93111  
(805) 964-9831

## ABSTRACT

A study has been performed for the 6585th Test Group at Holloman Air Force Base to determine ways to more accurately measure rocket sled velocity. Extreme accuracies of  $\pm .0003$  meter/sec up to 600 meters/sec (0.001 ft/sec up to 2000 ft/sec) are desired in order to adequately test guidance systems. Measurements are desired every millisecond along the 15 kilometer (10 mile) length of the track. After an extensive search, optical interferometers of 2 types were selected for further study. The first of these looks ahead to a sequence of mirrors mounted next to the track. The second looks vertically down at the rail surface and uses fore and aft scattered light from a laser illuminated spot. An improved version of an existing optical beam break system was also selected as a lower performance, lower cost option.

Areas of investigation have been the high levels of vibration on the sled, alignment fluctuations due to sled flexing and yaw, and signal-to-noise ratio including sources, paths and detectors. Other investigations concerned variations in the speed of light, limits of angle resolution and methods of referencing the velocity to a shock mounted guidance package.

Experiments are recommended to obtain data on the ambient environments, the sled environment, and several environment controlling and instrumentation techniques.

## FORWARD

The work reported here was performed under Air Force Contract Number F29601-79-C-0041 Project 9996. The Project Engineer at Holloman Air Force Base was Captain Larry Shelton who provided invaluable technical data, facility tours, and coordination of technical exchanges with other Holloman AFB personnel.

At Effects Technology, Inc., administrative support came from Frederic Bick and Dr. Richard Parisse. The translational interferometer reported here was conceived by William Isbell who also performed the first experimental verification of its operation. Dr. Hartley King consulted on the aerodynamic aspects and Allen Hunt and Robert Wengler provided concept suggestions and technical exchanges.

## TABLE OF CONTENTS

<u>SECTION</u>	<u>PAGE</u>
1.0 SUMMARY .....	1
2.0 BACKGROUND .....	5
3.0 INTRODUCTION .....	8
3.1 Approach .....	8
3.2 Flag Interferometer .....	12
3.3 Translational Interferometer .....	12
3.4 Conditionally Acceptable Concepts .....	15
3.5 Rejected Concepts .....	15
3.5.1 Millimeter Wave Doppler Radar .....	15
3.5.2 Precision Grids .....	16
3.5.3 Accelerometers .....	16
4.0 GENERAL ANALYSES .....	17
4.1 Sled to Specimen Relative Motion .....	17
4.2 Lasers and Detectors .....	18
4.3 Vibration Effects .....	21
4.4 Flag Interferometer Analyses .....	22
4.4.1 Optical Distortion, Ambient Air .....	24
4.4.2 Shock Wave Effects on Velocity Measurement .....	26
4.4.3 Temperature Measurements .....	28
4.4.4 Active Measurement of the Speed of Light .....	31
4.4.5 Pitch and Yaw .....	33
4.4.6 Beam Steering .....	34
4.4.7 Costs .....	34
4.5 Translational Interferometer Analyses .....	35
4.5.1 Angle Filter Requirements .....	35
4.5.2 Boundary Layer Effects and Slipper Evacuation .....	36
4.5.3 Pitch and Yaw .....	37
4.5.4 Translational Interferometer Experiment .....	38

TABLE OF CONTENTS

(Continued)

<u>SECTION</u>	<u>PAGE</u>
4.5.5 Translational Interferometer Calibration .....	38
4.5.6 Translational Interferometer Costs .....	39
5.0 CONCLUSIONS .....	40
5.1 Flag Interferometer - Conclusions .....	40
5.2 Translational Interferometer - Conclusions .....	43
5.3 Beam Break System - Conclusions .....	44
5.4 Comparison of Systems .....	45
6.0 RECOMMENDATIONS .....	47
REFERENCES .....	49
 <u>APPENDICES</u>	
A.1 VARIATION OF THE SPEED OF LIGHT IN A MOVING MEDIUM .....	A-1
A.2 BEAM COLLIMATION IN A TRANSLATIONAL INTERFEROMETER .....	A-2
A.3 THE EFFECT OF THE BOW SHOCK ON THE FLAG INTERFEROMETER VELOCITY MEASUREMENT .....	A-12
A.4 VARIATIONS IN THE OPTICAL PATH LENGTH DUE TO TEMPERATURE FLUCTUATIONS ON THE FLAG INTERFEROMETER SYSTEM .....	A-42
A.5 TRANSLATIONAL INTERFEROMETER PITCH AND YAW SENSITIVITY .....	A-50
A.6 SPECIMEN TO MEASUREMENT POINT VELOCITY .....	A-53
A.7 VACUUM & AIRFLOW IN ROCKET SLED SLIPPER CAVITIES .....	A-57
A.8 POSSIBLE ERRORS IN THE FLAG INTERFEROMETER VELOCITY MEASUREMENT DUE TO SLED PITCH AND YAW .....	A-79

TABLE OF CONTENTS

(Continued)

<u>SECTION</u>		<u>PAGE</u>
<u>APPENDICES (Continued)</u>		
A.9.	TRANSLATIONAL INTERFEROMETER MODELING EXPERIMENT .....	A-89
A.10	EFFECTS OF MECHANICAL VIBRATION ON THE ACCURACY AND SURVIVABILITY OF PROPOSED DESIGNS FOR THE IMPROVED VELOCITY MEASUREMENT SYSTEM .....	A-91
A.11	REQUIREMENTS ON PINHOLE SIZE AND DIAMETER OF LASER BEAM .....	A-103
A.12	APPLICABILITY OF A TWO-COLOR LASER TO THE PROBLEM OF CORRECTING FOR INDEX OF REFRACTION FLUCTUATIONS ON THE FLAG INTERFEROMETER SYSTEM .....	A-114
A.13	FEASIBILITY OF TEMPERATURE MEASUREMENT .....	A-122
A.14	TRANSONIC BOW WAVE EFFECTS ON THE FLAG INTERFEROMETER VELOCITY MEASUREMENT .....	A-133
A.15	CONSIDERATIONS ON USING EXTENDED (100 METER) MIRROR SPACINGS ON THE FLAG INTERFEROMETER SYSTEM .....	A-148
A.16	OPTICAL DISTORTION IN AMBIENT AIR .....	A-182

## 1.0 SUMMARY

This section briefly describes the results of the study. More detailed descriptions, conclusions and recommendations are contained in the report body while supporting analyses are in the appendices.

The rocket sled at Holloman Air Force Base can be used to evaluate highly accurate guidance systems if an accurate velocity measurement system can be developed. Considerable savings could result from elimination of some flight tests, while at the same time providing data unobtainable in flight.

Performance goals are  $\pm .0003$  m/sec (.001 ft/sec) from 0 to 600 m/sec (2000 ft/sec) with a measurement every millisecond. If completed, this system would provide an unprecedented capability for the track with a velocity accuracy orders of magnitude greater than previously possible.

The above goals imply a position accuracy of  $0.3 \mu\text{m}$  and in screening potential velocity measuring systems it became clear that no mechanical system or electromagnetic wave with wavelength longer than optical could meet this requirement. Therefore, two variations on a visible light laser interferometer were studied in detail. Because of the large amount of development required and the complexity of the interferometers, an option was retained consisting of improvements to the existing optical beam break system. This system would not meet all goals but its required development and unresolved uncertainties are less than for the interferometers.

The first of the interferometers studied was the flat interferometer. This system determined velocity by measuring the difference frequency (of up to 2 GHz) between a reference laser beam and a Doppler shifted beam. The shifted beam is guided by an active tracking system

from the sled mounted laser to and back from one of a series of track mounted mirrors located 100 meters apart. Direct measurement of the velocity of a specimen, which moves within shock mounts on the sled is obtained by passing the reference beam to the specimen and back.

Data corrections are required for ambient temperature, sled pitch and yaw, angle change as the mirrors pass to the side of the measuring device, and varying conditions behind the bow wave in the transonic regime. These corrections require peripheral measurements of temperature, pitch, yaw and mirror position.

Air density fluctuations (scintillation) will reduce velocity measurement accuracy. No data on these fluctuations in the area of the track is available and extrapolation from data at higher elevations is not valid. However if an extrapolation is made, it indicates full accuracy operation at the highest velocities will be possible during meteorologically stable times of each day (usually the hour before sunset). At other times, it is estimated, full accuracy would be available periodically when the sled is close (1 to 10 meters) to a mirror and temperature measurement station. In the transonic velocity range, bow wave stand off distances are large and the ability to correct for the velocity of light behind the bow wave with sufficient accuracy is uncertain.

The other interferometer is called the translational interferometer and in this case the laser is directed perpendicularly against a track rail. Light scattered fore and aft is Doppler shifted by amounts proportional to the sled velocity and when recombined, forms an interference frequency of up to 1.5 GHz. The calibration is sensitive to the observation angle of the scattered light so an angle filter is required. Since this angle cannot be directly measured to the required accuracy, the system will be calibrated on each sled run using a beam interrupt device and the known distance between interrupters along the track.

In order to eliminate velocity of light fluctuations in air, the point of rail illumination is enclosed by a partially evacuated cavity in a special slipper which slides on the rail. Provisions are required for maintaining a close rail to slipper contact and for sweeping debris and water away from the cavity. Isolation from slipper vibration is also required. Corrections for sled yaw are required and a separate interferometer will measure relative specimen motion.

It is uncertain whether the observed angle can be held constant enough. The angle cannot be filtered to the required accuracy because unacceptable attenuation of the light would occur so averaging of angles is required. The other major uncertainty is the ability to evacuate or measure the slipper cavity atmosphere to the degree required.

In the improved beam break system the time between interruptions of a single sled-mounted light beam by two flags and, redundantly, the time between interruption of two sled mounted light beams by one flag will be used to measure velocity. Improvements to existing velocity measuring devices using this concept are high resolution laser light beams and the addition of 2 peripheral interferometers. The first measures relative specimen motion and the second is a track mounted interferometer and sled mounted mirror which provides high data rates just before and after the start of the sled run.

Although accuracy for the beam break system is only on the order of .001 m/sec for individual measurements over a 0.6 m distance and data rate is low at low velocities, it is a marked improvement over the existing system for low cost and with a high certainty of success.

The preferred concept, assuming its uncertainties are favorably resolved, is the translational interferometer because it is operationally simpler than the flag interferometer which should be retained as a back up. It should be emphasized that all of these proposed systems are

complex and that for the flag and translational interferometer systems the uncertainties mentioned earlier remain to be answered before one is selected for fabrication. In order to answer these questions experimental data must be obtained in several areas which are listed in Section 6.0. Finally, this study of sled velocity measurement is encouraging because, of the many potential problems investigated, none appear to be a "fatal flaw". That is, there is no basic reason found to prevent a velocity measuring system of the desired accuracy from being realized.

## 2.0 BACKGROUND

The function of the Test Track at Holloman Air Force Base, NM is to simulate portions of flight trajectories under accurately programmed, closely controlled and rigorously monitored conditions. Payloads and instrumentation are propelled along the track on various rocket sled configurations set upon heavy duty crane rails. The rails span a distance of 15480 meters (50,788 ft.) and are continuously welded and aligned to rigid tolerances. Sled weights can range from 45 kgms (100 lbs.) to over 13000 kgms (15 tons) and speeds in excess of 2400 m/sec (8000 ft/sec) have been obtained. Accelerations and decelerations of 200 g's are possible.

The Test Track is equipped with many support facilities to accomplish a wide range of testing. Sophisticated data acquisition and recording equipment are available to collect data such as velocity, position, acceleration, aerodynamic forces, and various other parameters. Telemetry or on-board recording of data are options to fit the needs of the individual test. Equipment for master timing and communications, versatile enough to adapt to the numerous types of tests performed, is available. Sophisticated optical cameras and instrumentation for documentation of tests and diagnosing of data complement the test facilities at the Test Track.

One of the primary uses for the Test Track Facility is the testing and evaluation of missile guidance systems. Unlike missile flight tests, guidance sled run trajectories are deliberately designed to promote the growth of specified error terms. To accomplish this type of testing, very accurate specimen velocity and position data are required. Moreover, the cumulative errors of the velocity measurement system should be far less than the guidance system being tested.

Presently, the highest precision velocity measurement system (VMS) is the Electro-Optical VMS. This system consists of precisely positioned interrupters on the side of the track. A sled mounted boot contains a light source and detector. The light beam is interrupted by the track mounted posts and this event is telemetered to the instrumentation facility or recorded on board. The limiting error sources for this system are the interrupter spacing accuracy and the light beam cut off time determination. In addition, the sampling rate is low and the output is a distance-time plot rather than a direct velocity output. Also, because of shock isolation of the specimen and the electro-optical VMS's attachment to the sled, the relative sled-specimen velocities are difficult to account for, thus contributing to the combined error.

With the advent of extremely accurate new generation guidance systems, it has become necessary to obtain an orders-of-magnitude improvement in the capabilities of the velocity measurement system. To that end, ETI has investigated the feasibility of developing an Improved Velocity Measurement System (IVMS). An IVMS would prove beneficial in almost all phases of testing that are conducted at the Test Track Facility. For example, more accurate acceleration measurements would be possible in high-G testing. Furthermore, an improved velocity measurement system would permit testing previously prohibited because of velocity accuracy limitations.

The design goals for the IVMS are:

- a) A velocity accuracy of  $\pm 0.0003$  m/sec ( $\pm 0.001$  ft/sec),
- b) A velocity range of 0-600 m/sec (0-2000 fps),
- c) A sampling rate to be 1 KHz,

- d) Operational over entire length of track, and
- e) Able to measure velocity of sleds launched at any point along the track and in both directions.

The above accuracy requirement increases with velocity and reaches  $5 \times 10^{-7}$  per unit velocity, or one part in two million at 600 m/sec.

It should be noted that accuracies are considered to be for an individual velocity measurement obtained in .001 sec. Averaging over longer time intervals and more measurements would reduce some of the error terms.

ETI was charged with investigating the feasibility of achieving the design goals, and in doing so, compiled a list of possible system designs that could possibly meet some or all of the technical requirements.

ETI's objective during this program was to investigate the feasibility of developing a system design or designs that would meet the performance goals, and operate in the harsh sled environment.

### 3.0 INTRODUCTION

#### 3.1 APPROACH

The approach to this complex design problem was to utilize the diversity of skills and disciplines at ETI and to remain open to new approaches throughout the project. The first action was to gather information on the track, its uses, previous velocity measurement systems and past studies. This information was obtained through publications, test and track data, and technical meetings with the Holloman staff. Next, various members of ETI suggested several possible design concepts for the IVMS. A screening process involving simple analysis and comparison of each of the proposed designs was performed resulting in the selection of a few candidates.

The screening process was performed early in the program so that analysis could be initiated on critical technical question areas for each candidate. During later analyses a list of technical questions was maintained and kept current and used to direct new analysis efforts. This list is in Table 3.1. Close interaction with the customer, including a presentation of preliminary results at Holloman, provided much technical information.

ETI's investigation has produced two IVMS designs which received more detailed analyses. Both are laser interferometer systems - the Flag Interferometer and the Translational Interferometer. Other designs have been proposed which were rejected after an initial analysis. These showed performance improvements in some areas but fail to meet all of the design specifications. These are the Improved Beam Break System, the Dual Head Beam Break System, and a system using precision accelerometers. These systems will be described below and detailed analyses for the two primary concepts (the interferometers) will be given in Section 4.0 and in the appendices.

Table 3.1. List of Investigations

1. FLAG INTERFEROMETER CONCEPT

<u>Area of Investigation</u>	<u>Description</u>	<u>Status</u>
1.1 Refraction due to ambient temperature	Changes to optical path length & direction	Appendix A4, 15 & 16. More data needed. May be ok at 4 meter mirror spacing or require restricted use times at 100 meter mirror spacing.
1.2 Refraction due to shock wave	Changes to optical path length & direction, changes in Mach Number vs. time, path, angle	Appendix A3, 14 & 15 Error small.
1.3 Determine track ambient environment	Typical temperature, wind velocity, & humidity gradients must be known	Holloman Data received. Additional data needed.
1.4 Determine shock wave properties	Aerodynamic "fields" around sled must be understood. Include fluctuations.	Appendix A3, 14 & 15. Additional work needed.
1.5 Velocity of light in moving fluid	Determine magnitude of "Fresnel Drag"	Appendix A1 - correction is negligible.
1.6 Active measurements of the speed of light	Want to know speed of light in environment of sled - Two color laser	Appendix A12. Insufficient resolution.
1.7 Optical paths	Determine flag & detector tracking requirements; tracking light source	Appendix A15. Tracking needed.
1.8 Temperature indicators	Use passive liquid crystal temperature indicators mounted at intervals along the track. These would be optically sensed by a detector on the sled	Appendix A13. Twenty conventional thermocouples proposed with restricted use times.
1.9 Lab test model	Lab model to determine sensitivity of measurement to varying parameters. Use ETI internal data.	No problems indicated in brief test.
1.10 Vibration effects - tolerance	Determine vibration effects on measurements	Appendix A10. Best case analysis ok. More analysis indicated.
1.11 Flag and window erosion	Rocket blast and ambient dust concentration erodes flags and optical windows	Data needed.

Table 3.1. (Continued)

2. TRANSLATIONAL INTERFEROMETER CONCEPT (TRANSAR)

<u>Area of Investigation</u>	<u>Description</u>	<u>Status</u>
2.1 Collimation requirements	Determine optical & geometrical limitations	Appendix A2. Resolution limited by optical attenuation. Angle averaging required. Needs work.
2.2 Vibration tolerance	Determine effect of slipper vibration on measurement	Appendix A10. Best case analysis OK. More work indicated.
2.3 Slipper characteristics	Temperature, vibration, wear rate, wear particle flux, distance to rail, pitch & yaw	Needs work.
2.4 Evacuation of slipper cavity	Determine vacuum achievable	Appendix A7. Analysis favorable. Experiments indicated.
2.5 Effects of boundary layer	Will refraction of light in boundary layer of air on the rail significantly distort the measurement angle?	Favorable result.
2.6 Use of window	Does a window near the rail surface allow a better vacuum	Rejected. Window increases angle measurement errors since air at rail surface is critical - no report
2.7 Pitch & Yaw	Effect on accurate measurement of angle.	Appendix A5. Gyro corrections required.
2.8 Rail roughness specifications necessary	Determination of how the rail surface affects the velocity measurement	Experiments needed.
2.9 Lab Test	Set up a translational interferometer in the lab to test sensitivity of system to varying parameters.	Appendix A9. Operation achieved. Sensitivities to be determined.
2.10 Sensitivity calculation	Calculation of fringe rate vs. velocity.	Appendix A9.
2.11 Calibration method	Determine whether angle can be measured or system calibrated to sufficient accuracy	Use improved beam interrupt device and known distance between interrupters on each sled run.

Table 3.1. (Continued)

3. <u>GENERAL TOPICS</u>	<u>Area of Interest</u>	<u>Description</u>	<u>Status</u>
3.1	Sled-specimen differential motion	Evaluate different accelerometer techniques, and the possibility of running a light signal through optical fibers to eliminate shock wave refraction effects.	Appendix A6. Accelerometers not accurate enough. Fiber optic or air path interferometer is favorable
3.2	Lasers & Detectors	Locate suitable devices for the task	Section 4.2
3.3	Optical power calculations	Determine losses, and a power budget for each suggested VMS. Consider tracking device, shockwave light and solar light.	Section 4.2
3.4	Hardware	Determine Optical and mechanical hardware required.	Appendix A10. More work needed.
3.5	Data analysis methods	Investigate circuits for interpolating fringe count	Not started

### 3.2 FLAG INTERFEROMETER

The Flag Interferometer was the system described in the original proposal and the current configuration is shown in Figure 3.1. A coherent laser beam is split into a reference leg and a leg that is directed to strike a mirrored surface ahead of the sled next to the track (in similar positions as existing interrupters). The reflected beam is thus doppler shifted and returns to the sled where it interferes with the reference beam to produce a fringe rate that is proportional to velocity. The mirrors are positioned to pass between windows for the laser and detector. The Flag Interferometer has the capability to resolve the velocity to plus or minus .0003 m/sec. (.001 ft/sec) in one millisecond. An added advantage of the Flag Interferometer is that an optical leg can be directed to the specimen thus enabling true specimen velocity to be measured directly. Environmental effects such as transonic and supersonic bow shocks, temperature gradients, air turbulence, and flag reflectivity have the potential to adversely affect the accuracy of the system.

The few millisecond signal drop out in transitioning from one mirror to the next is tolerable. (Refer to Section 4.4.6.) A control system to direct the beam at the appropriate flags is probably necessary. Results of analyses of the Flag Interferometer are discussed in Section 4.4.

### 3.3 TRANSLATIONAL INTERFEROMETER

The Translational Interferometer (TRANSAR) as shown in Figure 3.2 is self contained in a non-load bearing slipper or in a monorail sled and uses the diffuse reflections from the rail surface to obtain a doppler fringe rate. This system has advantages over the Flag Interferometer in that it is independent of the ambient environment and with adequate evacuation of the slipper cavity, the environmental effects

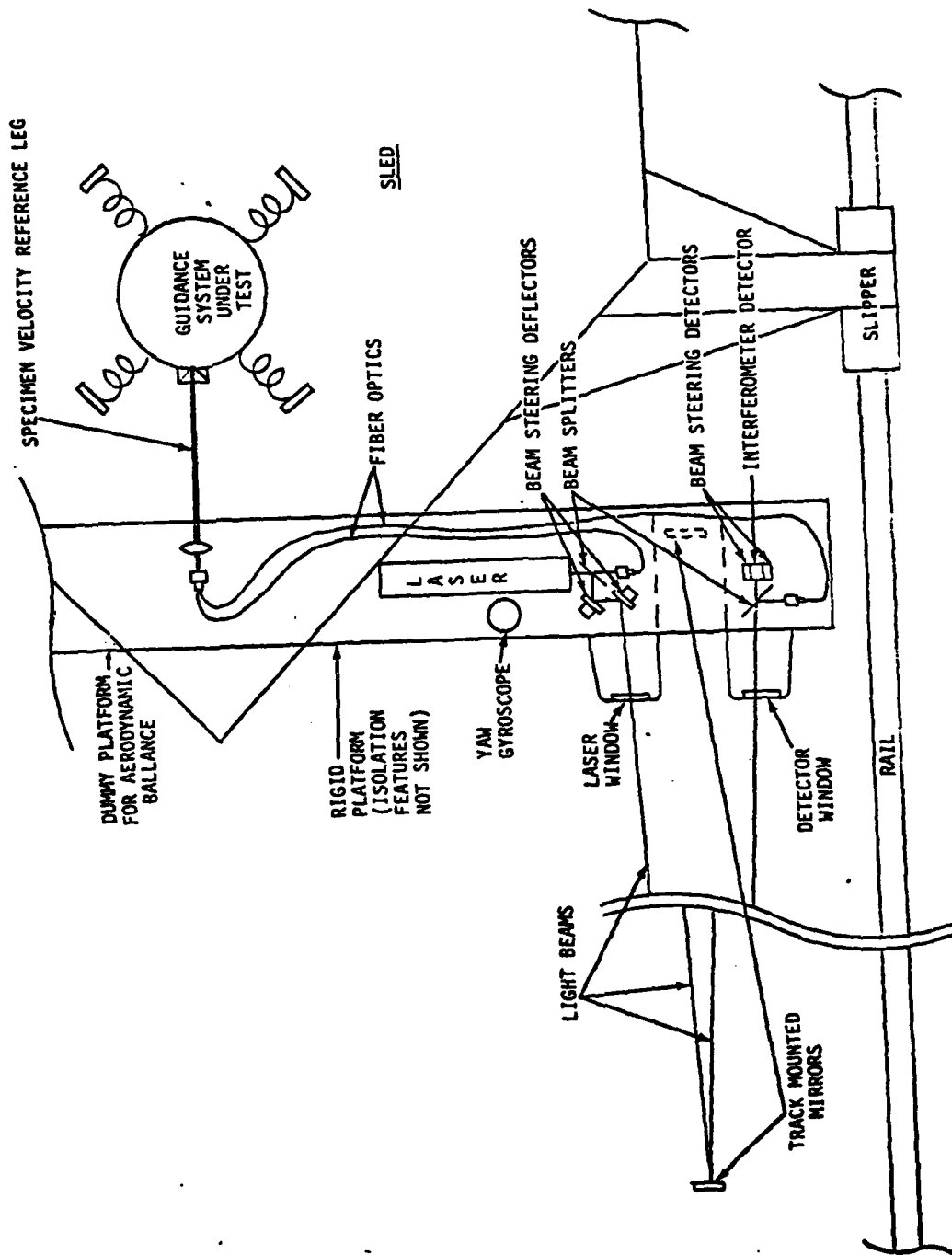


Figure 3.1. Schematic Diagram of Flag Interferometer, Top View (not to scale).

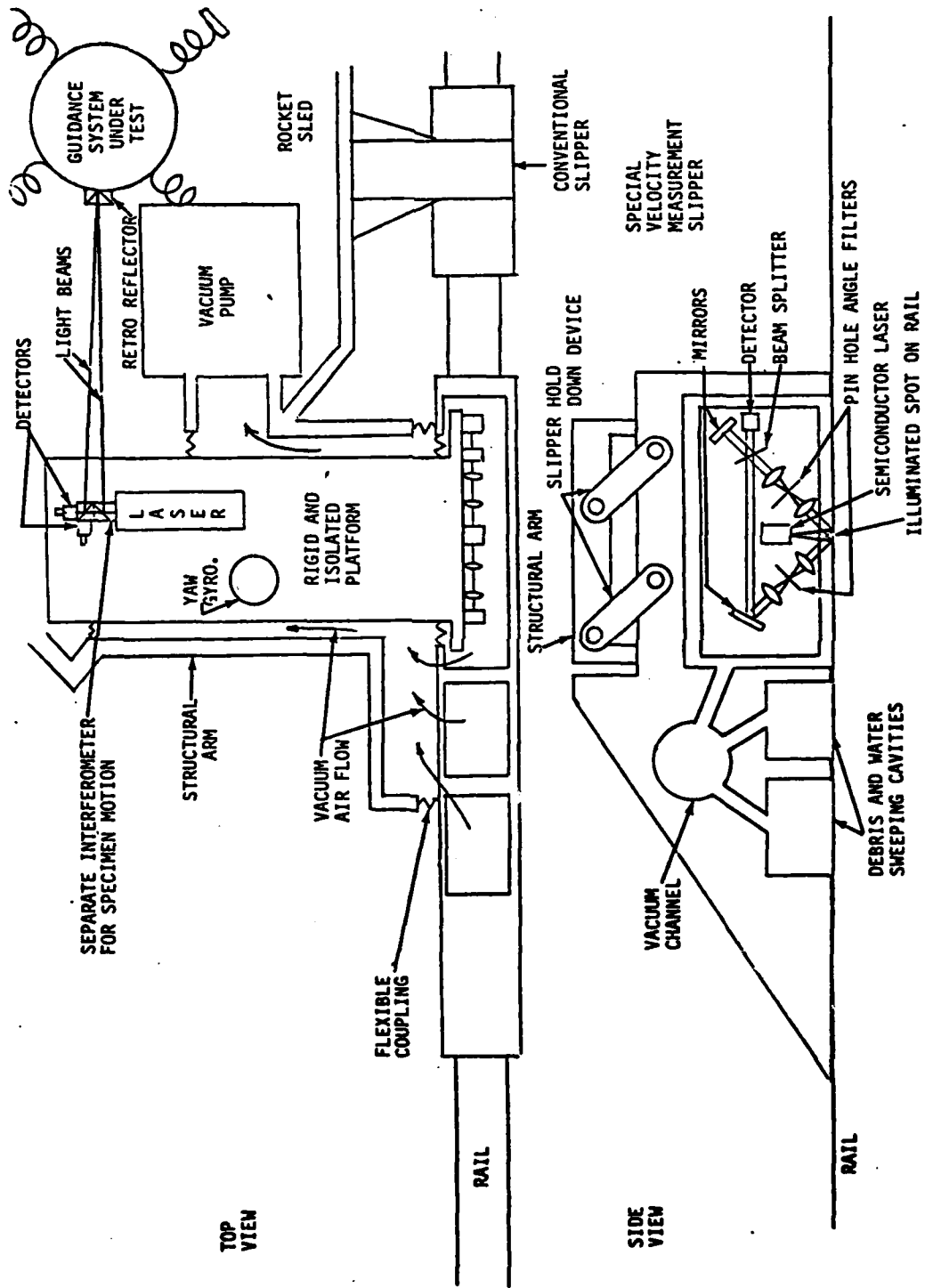


Figure 3.2. Schematic Diagram of Translational Interferometer (not to scale).

are greatly reduced or eliminated. In this system a separate interferometer is required to measure the relative motion of the sample with respect to the sled. One leg cannot be sent to the specimen as in the Flag Interferometer because the diffuse reflection results in a short coherence length and a necessity for equal path lengths. Performance of the TRANSAR system is presented and analyzed in Section 4.3.

#### 3.4 CONDITIONALLY ACCEPTABLE CONCEPTS

An Improved Beam Break system would update many of the components of the existing beam break system (VMS). The incandescant light source would be replaced by a semiconductor laser thereby greatly increasing the power of the light incident on the detector and the superior collimation would lend to more accurate beam break determination. The electronics system would be replaced with reliable high speed integrated circuitry. Improved interferometer techniques are to be used to re-survey the interrupters to greater accuracy.

A Dual Head Beam Break system uses the improved light source and electronics of the improved beam break system but has two or more precisely aligned sensing heads. The velocity is computed by the time difference between beam breaks and thus the flag spacings are not required to be accurately determined. As with the Improved Beam Break system, sampling rates at low velocities are poor. The advantage of these systems is that they are simple and rugged and therefore reliable under demanding conditions.

#### 3.5 REJECTED CONCEPTS

##### 3.5.1 Millimeter Wave Doppler Radar

The primary reason for rejecting this concept was its inability to meet the resolution requirement of 1 part in 2 million. A 600 m/sec

(2000 ft/sec) velocity and a wavelength of one millimeter results in a doppler shift of 0.6 MHz. Since a measurement per millisecond is required 600 fringes are obtained which limits resolution to less than 1 part in 600. Several technological considerations such as poor signal-to-noise and beam width added to the evidence for rejection. These considerations can also be applied to any RF system whose frequency is lower than optical frequencies.

### 3.5.2 Precision Grids

If a tape attached to or near the track, or the track itself, is inscribed with precision grid markings on its surface, a photodetector could detect the moving grid spacings much like the fringes of an interferometer. This would be a simple and rugged system. However, to obtain the desired accuracy, the grid spacings would have to be  $.3 \mu\text{m}$  resulting in fabrication and detection problems.

### 3.5.3 Accelerometers

Designing a velocity measurement system using precision accelerometers is possible but at reduced accuracy. The major drawbacks are that this is the same type of system used in the guidance packages being tested and therefore is not any more accurate, and the same sort of errors occur in both systems making testing by comparison difficult.

#### 4.0 GENERAL ANALYSES

The following analyses apply to both primary candidate interferometer systems. Analyses unique to one or the other system are contained in Sections 4.4 and 4.5. The common analyses are 1) Sled to Specimen Relative Motion, 2) Lasers and Detectors, and 3) Vibration Effects.

Throughout these analyses, error sources are compared to the maximum error budget of 1 part in two million ( $5 \times 10^{-7}$ ). This is the largest error for the stated accuracy (.001 fps) at 2000 fps. Obviously at lower velocities, the fractional error allowed is larger so the discussions consider the worst case situation.

The error analyses presented here are for the individual contributions considered. We have not attempted to provide an overall accuracy figure for either interferometer system because of the unresolved experimental areas which may contain the largest errors. Until the experimental investigations are completed and the results used in the error analysis, no overall accuracy can be given. However, it is possible to state the maximum potential accuracy for each system and to characterize possible problems. This has been done. The flag interferometer has a possible accuracy of  $\pm .001$  fps at 2000 fps with a .001 second sample time, and the translational interferometer  $\pm .0014$  fps at 2000 fps with a .001 second sample rate. These figures are the raw accuracy and no special averaging or processing of the data has been included. Whether or not these limits can be reached can not be determined in a study program without experimental input.

The unresolved experimental areas are discussed in the text and summarized in Section 6.0 under recommendations for further investigation.

#### 4.1 SLED TO SPECIMEN RELATIVE MOTION

Because of the tremendous vibrational shock environment of the rocket sled, and shock mounting of the specimen, significant differences in relative velocity occur between the sled and the specimen. The guidance systems being tested are so sensitive as to make this relative velocity large compared to the error goal. The goal of the IVMS is to measure specimen rather than sled velocity. The Flag Interferometer is designed to do just that but the Translational Interferometer measures slipper velocity and requires a separate slipper to specimen interferometer.

Linear Accelerometers cannot be used to provide relative motion as explained in Appendix A.6 because the accuracy requirement is the same as for using accelerometers to make the velocity measurement independently.

A separate interferometer can measure the specimen to sled velocity. A rigid mechanical beam joins the two interferometers as shown in Figure 3.2. This assembly is vibration isolated from the sled and corrections are made for its yaw relative to the track using a gyroscope. See Appendix A.10.

For the flag interferometer, a separate interferometer is not required, but the rigid beam and gyroscope are. Fiber optics may be used to run the reference light beam to the specimen as shown in Figure 3.1.

#### 4.2 LASERS AND DETECTORS

The sled-borne Flag and Translational Interferometer systems place enormous operational and environmental demands upon the individual optical components. A study was conducted to assess the feasibility of

obtaining commercially available optical components capable of meeting the operational specification and withstanding the harsh environment. The two areas of emphasis were laser systems and detectors.

The laser systems considered had to be CW, simple, reliable, and rugged. Particular emphasis was placed on obtaining vibration and shock survivability data. A specification of withstanding 40 g vibration and 150 g steady acceleration would have been ideal. Table 4.1 lists those CW laser systems which had some type of vibration or shock testing data and which appeared to be rugged enough to be considered. High power is desirable, however, as can be seen from Table 5.1, there is considerable tradeoff of power for ruggedness. All ion laser systems were eliminated because of the fragility of the optics<sup>(1)</sup>. Dye lasers and solid state (e.g., Ruby) lasers were rejected for their complexity and fragility. Semiconductor lasers are a possibility for the Transar Interferometer because of the short distance involved but are effectively ruled out for the Flag Interferometer due to their short coherence lengths.

In considering detectors, two major categories were studied: photomultipliers and semiconductor photodetectors. A bandwidth specification of 2 to 4 GHz and high responsivity were essential for the interferometer system since the return power to the detector for both systems would be diminished by orders of magnitude. Photomultipliers are ideally suited for low power level applications, however, only a very few were found to have the bandwidth capacity. Of these, none were tested for any vibrational or shock tolerance and all were of questionable ruggedness. Some systems houses have tested photomultipliers, but not by a systematic method whereby one could be compared to others. The cost of photomultipliers which are specially designed and manufactured units would be high.

Table 4.1. CW Laser Systems

CW LASER SYSTEMS

LASER MFR MODEL TYPE	$\lambda_0$ $\mu\text{m}$	TEM <sub>00</sub> POWER mW	BEAM DIAM. mm	BEAM DIV. mrad	TESTED FOR VI- BRATION/ SHOCK	STABIL- IZED	POLAR- IZATION	PRICE \$	COMMENTS
METROLOGIC ME-845 He-Ne	0.6328	3.5	15 mm ø 300 m		NOTE 1	No	RANDOM	0.79K	BUILT-IN COLLIMATOR
METROLOGIC ME-840 He-Ne	0.6328	3.5	0.68	1.2	NOTE 1	No	RANDOM	0.70K	CYLINDRICAL HEAD
HUGHES 3025-H He-Ne	0.6328	5	0.81	1	NOTE 2	No	RANDOM	0.71K	RUGGED SHORT/COMPACT
HUGHES 3025-H-P He-Ne	0.6328	5	0.81	1	NOTE 2	No	LINEAR 500:1	0.78K	RUGGED AVAILABLE IN 4,2,1 mm
HUGHES 3035-H He-Ne	0.6328	10	1.37	0.6	NOTE 2	No	RANDOM	1.36K	QUESTIONABLE RUGGEDNESS DUE TO LONGER LENGTH
HUGHES 3035-H-P He-Ne	0.6328	10	1.37	0.6	NOTE 2	No	LINEAR 500:1	1.59K	QUESTIONABLE RUGGEDNESS DUE TO LONGER LENGTH
LICOMIX 4110 Series He-Cd	0.442	13	0.9	0.7	NOTE 3	NOTE 4	LINEAR 100:1	4.2K	QUESTIONABLE RUGGEDNESS
LICOMIX 4050 Series He-Cd	0.442	50	0.91	0.62	NOTE 3	NOTE 4	LINEAR 100:1	7.6K	QUESTIONABLE RUGGEDNESS
MITSUBISHI ML2200-2300 Series GaAlAs	0.83	3	----	----	-----	-----	-----	0.82K	SEMICONDUCTOR
RCA C3000 & C8000 Series GaAlAs	0.82	10	----	----	-----	-----	-----	0.35K	SEMICONDUCTOR

NOTES: 1. 26/200 Hz/2 MIN 2. 15g for 11 ms 50g for 1 ms  
3. >20g SHOCK 4. Model V Stabilized Reduce Power Increased Price

Of all the semiconductor photodetectors categories considered, the avalanche photodiodes offered the best characteristics. The main advantage of an avalanche photodiode is the increased sensitivity over standard photodiodes. Finding avalanche photodiodes with the required bandwidth is not as simple. One particular photodiode stood apart from all others when specifications were compared. That was the Mitsubishi PD-1000 series. A synopsis of its specifications is as follows:

Spectral Response 0.5 - 1  $\mu\text{m}$  .78  $\mu\text{m}$  peak

Responsivity - 0.45 a/w no multiplication

~ 300 a/w max with multiplication

~ 100 a/w at 0.6328  $\mu\text{m}$

Bandwidth - 2 GHz (150 ps rise time)

Noise Equivalent Power -  $10^{-14}$  w/ $\sqrt{\text{Hz}}$

Price - \$300.

It is estimated in Appendix A.11 that the drop in power from source to detector in the flag interferometer could be as much as  $10^{-4}$  (40 dB). If we assume we have a 5 mw He-Ne laser, this implies there will be about 0.5  $\mu\text{w}$  at the detector. The minimum amount of power required to voltage signal to noise ratio of 10 for the detector is given by

$$\begin{aligned} P &= 10^2 (\text{NEP}) (\text{BW})^{1/2} \\ &= 10^2 (10^{-14}) (2 \times 10^9)^{1/2} \\ &= 0.05 \mu\text{w} \end{aligned}$$

This is an order of magnitude below the actual power and thus obtaining a good signal to noise ratio should be possible.

The amount of signal generated by  $0.5 \mu\text{w}$  can be found from the responsivity  $R_o$

$$\begin{aligned} I_{\text{sig}} &= R_o P \\ &= (100 \text{ a/w}) (5 \times 10^{-7} \text{ w}) \\ &= 50 \mu\text{amps} . \end{aligned}$$

This is a small current but is detectable by many amplifier systems. It does point to the need to have as high power as possible from the laser.

This investigation demonstrates that there exist commercially available components that are capable of meeting the operational and environmental specifications of the interferometer systems at reasonable cost. The actual implementation of these components and its cost is not addressed here. However, there are available commercially, optical receiver systems which have these components in optimum configurations and which meet or exceed the bandwidth specifications<sup>(2)</sup>.

#### 4.3 VIBRATION EFFECTS

The sled can be subjected to over 200 g accelerations and the slippers can experience vibrations and shocks as high as 500 g's. At these levels of vibration and shock, the deformation of components and the question of their survivability become important. An analysis effort was conducted to determine what effect these vibrations would have on the accuracy and survivability of the two proposed interferometer systems.

Because of the properties of interferometer systems, small movements in the mirror positions on the order of fractions of a wavelength of light can exceed error goals in the velocity measurement accuracy. The analysis assumed the system had to maintain the  $\pm .0003$  m/sec (.001 ft/sec) accuracy goal at 600 m/sec (2000 ft/sec) and assumed a He-Ne laser system radiating at  $0.6328 \mu\text{m}$  and a maximum acceleration of 200 g's. Vibrational analysis on the support plate and a typical optical component were conducted for both interferometer systems (see Appendices A.6 and A.10). The conclusions drawn from the analysis were:

1. A simplified best case analysis indicates the mounts can be made sufficiently rugged. Additional analyses or tests are indicated.
2. The two meter support I-Beam for the Flag Interferometer, used to convey the optical beams from the flag to the specimen axis, would have to be shock isolated to 1/2 g in the lateral direction. Shock isolation and/or servo control are proposed to achieve this isolation but more work is needed.

#### 4.4 FLAG INTERFEROMETER ANALYSES

The Flag Interferometer, described in Section 3.2, was investigated in those areas which could cause excessive error or failure. Detailed analyses are contained in several of the appendices and the results are summarized below.

The requirement of making a measurement once every .001 second of the sled velocity to an accuracy of .0003 m/sec (.001 ft/sec) requires measurement of the sled displacement to an accuracy on the order of a wavelength of light. Because of this requirement even small distorting effects on the signal beam, or changes in the interferometer's optical

path lengths due to effects other than sled displacement can induce significant errors into the velocity measurement.

The Flag Interferometer optical signal is subject to degradation due to atmospheric turbulence, scattered debris, aerosols, and shock waves. In addition, misalignment between the sled and reflecting surfaces arising from sled pitch, yaw, and vibration is apt to introduce errors into the velocity measurement.

In order to calculate the magnitude of the error introduced by these various effects the relevant system parameters must be known. The original Flag Interferometer used divergent beams to track the reflecting surfaces placed every 4 meters (13 ft.) along the track. Refer to Figure 3.1. This system has two problems. The first is the installation and maintenance requirements inherent in using a 4 meter spacing between the mirrors. This would require about 4000 mirrored surfaces along the track which would have to be installed, aligned and kept polished. Second, the use of divergent beams necessitates very small detector apertures in the receiver plane to meet the angular filtering requirements of the signal. This causes such a large optical attenuation that the signal to noise requirements of the interferometer system could not be met. Refer to Appendix A.11.

A study of possible design modifications was undertaken to remedy this situation. The improved system design uses larger spacings between the mirrors and a small diameter collimated laser beam for the signal. Refer to Appendix A.15.

If spacings of 100 meters were used the number of mirrors required would be about 150 to cover the entire track. Use of a collimated beam for the signal requires a different method of angular filtering than that originally proposed. Neglecting angle of arrival fluctuations (which can be smoothed out with aperture averaging) the angular

sensitivity of the velocity measurement across the face of a collimated beam will be constant, and a detector diameter the same size as that of the beam could be used. This would ensure minimum signal loss.

Use of a collimated beam requires some form of tracking system to keep the beam aligned on the detector as the sled pitches and yaws and as the beam wanders and deflects due to atmospheric effects. See figures in Appendix 8. The performance requirements of such a tracking system would be quite stringent. A fast response is required due to the high frequency sled vibrations, and the system must be capable of retracking the beam very rapidly after signal dropout occurs. Such a tracking system is feasible.

The following discussion of the error sources of the Flag Interferometer velocity measurement pertains to the improved system design which incorporates 100 meter inter-mirror spacings, and a collimated laser beam with a diameter on the order of 1 mm for the signal.

#### 4.4.1 Optical Distortion, Ambient Air

Atmospherically induced variations in the optical path length to the flag mirror and back are of concern because changes on the order of one wavelength of light equal the total error allowance at 2000 ft/sec. Optical distortion in undisturbed air in front of the sled is analyzed in Appendix A.16 and summarized below.

The  $5 \times 10^{-7}$  per unit velocity error allowance can be produced by variations in the speed of light (or index of refraction,  $n$ ) of this same magnitude which in turn can be produced by about a  $0.5^{\circ}\text{C}$  change in temperature of the air. Section 4.4.3 discusses temperature variations and measurement.

Local turbulence can deflect portions of the beam preventing

interferometer operation. Data are available at 8 meters above the ground at White Sands Missile Range (refer to Appendicies A.4 and A.16) and under worst conditions the smallest characteristic distance for this turbulence is about 5 mm. Using a 20X beam shaping telescope (Metrologic 45-200), the beam of a Helium Neon laser can be adjusted to be on this order for the 200 m paths so these effects can be minimized. More sophisticated methods (spatial filtering, for example) can further reduce the beam diameter. Turbulence near the rail will be greater and scaling laws break down near the source of heating so measurements are needed.

The 5 mm distance mentioned above is also marginal for introducing errors from motion of the beam laterally during the one milli-second measurement interval such as would occur with pitch and yaw of the sled.

A brief test of an existing stationary interferometer was conducted in Santa Barbara on a parking lot on a sunny August midday. Operation was successful at a 3 meter mirror distance, but not at 10 meters. The frequencies of beam position fluctuations appeared low enough that active beam tracking may have helped. Unknown are the effects of the black asphalt surface and the relative degree of turbulence or scintillation present.

At Holloman, a sharp decrease in the level of atmosphere turbulence at selected morning and evening times indicate at least a factor of ten improvement in the value of the turbulence parameter,  $C_n$  (refer to Appendicies A.4 and A.16).

Optical distortions from ambient air inhomogeneities therefore are uncertain, but under best meteorologic conditions should allow 100 meter mirror distances. These conditions occur usually during the hour before sunset. At other times operation may only be possible when the sled is near a mirror. Although this places a constraint on the test schedule, it is not severe. Only one maximum accuracy run could be made per day and it possible that a thunder storm or other weather disturbance could cause cancellation.

Turbulence behind the bow wave or shock has not been addressed because of the lack of data.

#### 4.4.2 Shock Wave Effects on Velocity Measurement

The original design for the Flag Interferometer system proposed positioning the optical sensing head far enough in front of the sled to allow the signal beam to be ahead of the supersonic shock wave from the sled body. An investigation of shock effects determined that this would be unfeasible in the transonic regime, below about Mach 1.3 where the sled shock will extend over 3 m ahead of the sled. In the transonic regime just around Mach 1 the shock will still be supersonic in form but may extend 10 m ahead of the sled. In this speed regime the entire optical path to the reflecting surface and back can lie within the sled shock region. At subsonic velocities no shock will exist, but a disturbed region of air will extend quite far ahead of the sled, the temperature and density gradients decreasing smoothly to their free stream values.

The amount of optical degradation that will occur as a result of the laser beam propagating through the higher density turbulent shock regions, or areas of disturbed air, is difficult to predict. An experimental investigation of shock induced signal degradation and optical distortion caused by ambient conditions is necessary to determine the feasibility of the system. Other error sources may be correctable, but distortion must be kept small to allow continuous velocity data.

Once turbulence induced optical degradation has been considered, the remaining errors must be taken into account in order to determine the possible system accuracy. The three major causes of error predicted by an analysis of the system are: 1) Angular errors introduced due to beam refraction at the shock front, 2) Optical path length changes (transit-time changes) as the shock density and stand-off distance vary over the .001 sec sampling time, and 3) An inability to determine an accurate enough value for the index of refraction when the entire path of the beam lies in a shock region.

The magnitude of the angular error is dependent on the system

geometry used. The errors calculated in Appendices A.3 and A.14 assumed off-axis mirrors with a baseline of 2.5 cm (source to detector distance) and a distance of closest approach to the reflecting surface of 1.5 m. These results are applicable to sled design in Figure 4.1. Angular errors would also be introduced into the measurement due to refractive effects if a large detector were to intercept the return signal, because the actual angle of the refracted ray would be undetermined and the measurement is a function of the cosine of this angle. If a beam tracking system were used, and a coaxial detector and laser, the error would be eliminated because the angle would be zero. However, the mirror would get in the way of the detector and laser and would have to be removed before impact. This complexity is not warranted since small detectors and a tracking system alone will allow correction for the angle.

As the shock parameters (density profile and stand-off distance of the shock) increase or decrease over the .001 sec sampling time due to sled acceleration, the induced change in the signal beam's optical path will appear as an error on the sled displacement measurement. The magnitude of the change in the shock parameters depends on the sled acceleration and on the stand-off distance of the shock. The error increases at lower velocities where the shock extends further, and at higher sled accelerations. Assuming a maximum acceleration of 200 g's for the sled, the change in Mach number over .001 sec will be,  $\Delta M \approx .006$ .

The worst error arises in the transonic regime where the shock extends far ahead of the sled, and the sensing head is behind the shock. The apparent displacement of the sled caused by the changes in the shock parameters is on the order of  $10^{-4}$  ft, two orders of magnitude larger than the minimum design goal. If the entire path of the beam to the reflector and back lies within a shock region, some correction to the value of the index of refraction must be made to

interpret the fringe count accurately. The uncertainty in the index of refraction value affects the measurement accuracy directly. The following section discusses possible corrections for the value of the index of refraction in a shock region.

The Flag Interferometer can achieve the required accuracy at low velocities where the percent accuracy requirement is low and at supersonic velocities ( $M > 1.3$ ) where shock standoffs are small. Serious problems exist in the intermediate range and will be discussed in the conclusions.

#### 4.4.3 Temperature Measurements

In Flag Interferometer system the speed of light along the displaced optical path must be known to the same accuracy as that required of the velocity measurement. A part per 2 million accuracy is required at the highest velocity.

Different techniques for measuring the speed of light were investigated. The two methods most applicable to the Flag Interferometer system are stationary measurements of temperature at different positions along the track, prior to sled arrival (see Appendix A.13) and a measure of atmospheric dispersion through use of a sled mounted two-color laser (see Appendix A.12). The preference of one of these methods over the other depends on the extent of the bow shock of the sled, i.e., on the sled velocity range, since a stationary measurement will not accurately measure temperature behind the bow shock.

Temperature measurements will be discussed in this section and the two-color laser in Section 4.4.4.

The slow variance of the index of the refraction with temperature changes in the atmosphere enables the required accurate measurement of

the speed of light in a region.

Neglecting the effects of humidity, which are negligible at optical wavelengths, the relationship between temperature, T, pressure, P, and the index of refraction, n, in the atmosphere is given by<sup>(3)</sup>, (See Appendix A.13)

$$n = (77.6 \times 10^{-6}) \frac{P}{T} + 1 .$$

Therefore, the variance in the index of refraction arising from changes in the temperature and pressure is given by,

$$\Delta n = n_2 - n_1 = (77.6 \times 10^{-6}) \left( \frac{P_2}{T_2} - \frac{P_1}{T_1} \right) .$$

As shown in Appendix A.16, the spatial variation for pressure is much less than for temperature, so only temperature variations are considered. At normal atmospheric conditions, P is approximately 900 mbars, and  $T \approx 300^\circ\text{K}$ . Putting these values into the above equation yields.

$$\Delta n \approx 10^{-6} \Delta T .$$

If n is to be known to  $\pm 5 \times 10^{-7}$ , the sensitivity required of a temperature measurement is on the order of  $\pm .5^\circ\text{K}$ .

The temporal and spatial variations of temperature along the track depend on the strength of the atmospheric turbulence in the track environment. Assuming the worst case, a structure function  $C_n^2$  (defined in Appendix A.13) of  $10^{-12} \text{m}^{-2/3}$ , the r.m.s. temperature variance between two points separated by a distance of 1 meter is roughly  $1.5^\circ\text{K}$ . When the value of  $C_n^2$  decreases to  $10^{-14} \text{m}^{-2/3}$  this variance is on the order of  $.15^\circ\text{K}$  over 1 meter (see Appendix A.13). At all times of the year daily minimums in  $C_n^2$  of about  $2 \times 10^{-16}$  are observed. Therefore, operation at worst case conditions is not feasible, but at best conditions is feasible from several considerations.

Over points separated by a distance much greater than 1 meter the turbulence structure functions are not applicable for predicting temperature fluctuations. The variance of T over long distances is dependent on changes in the environment. The ambient conditions can also vary due to cooling effects from trackside pools of water, or the water brake system troughs. Therefore, in front of the sled bow shock, turbulence decreases with distance to the side or above the track.

A previous investigation of the applicability of laser systems to the problem of determining the rocket sled velocity (Ref. 4) reported data taken at the track of the long-term temperature variations along the track. The sensors were positioned at intervals of 3000 ft, at the benchmarks. At a height of 6 ft above the ground the temperature difference between benchmarks never exceeded  $4.5^{\circ}\text{C}$  during any season and in some cases were  $0.5^{\circ}\text{C}$ . Before a very precise estimate of the magnitude of the error could be made, more data on temperature variance along the track at the exact position of the beam, would be required. From 10 to 1000 measurement points might be adequate for determining a value of n to the required accuracy depending on the atmospheric turbulence.

Several methods of making temperature measurements have been investigated: 1) A 50,000 ft (track length) thermocouple wire with magnetic reed relays activated by a magnet on the passing sled. Depending on the desired accuracy, the spatial frequency of the relays could be increased or decreased. 2) Liquid crystal temperature indicators mounted track side and read by a sensing head on the passing sled. 3) Thermistors mounted similarly to the thermocouple set-ups. Any of these three techniques requires only one electronics package and data recording channel and would automatically read the temperature at the sled location.

Another consideration in choosing a method of temperature measurement is the installation and maintenance required versus the obtained accuracy. Sensitive temperature measurements in the atmosphere require shades because of radiative heating effects. The accuracy of uncalibrated thermocouples is  $\pm 4^{\circ}\text{K}$  so calibration is necessary.

Since the measurement device is simple the cost per added temperature measuring channel would be small ( $\sim \$25$ ), Installation costs would be similar to that for other trackside mounted equipment but has not been determined.

Individual trackside devices could also be used to measure the Air temperature just prior to sled arrival. This would be more practical if only 10 measurement locations are required.

As discussed in Section 4.4.2 in the transonic speed range the sled shock will extend far ahead of the sled. As the speed decreases through the subsonic range, no distinct shock exists, but the region of disturbed air in front of the sled extends for a large distance before standard conditions are obtained<sup>(5,6,7)</sup>. Depending on the distance of closest approach between the sled and reflecting surface the entire length of the signal beam may fall within a shock region, or within a region of greatly disturbed air. If this is the case then the speed of light measurement would have to be made within this disturbed region. At the lowest velocities, the percent error goal is larger and atmospheric corrections are not necessary.

#### 4.4.4 Active Measurement of the Speed of Light

A two-color laser has the advantage of providing just this type of

measurement. When two signal beams of different optical wavelengths are used in the interferometer a comparison of the difference in the number of fringes generated at the two wavelengths, with that expected at standard conditions yields a correction to the index of refraction. The system accuracy is limited, though, due to the fact that the minimum measurable  $\Delta(N_1-N_2)$ , where  $N_1$  and  $N_2$  are the number of fringes generated at the two wavelengths, is  $\pm 2$  fringes. This determines the sensitivity of the measurement of the change in the index of refraction from its value at standard conditions. The change in the optical path lengths for the two beams over the .001 sec measuring interval depends directly on the sled velocity. The greater this change is the larger the value of  $\Delta(N_1-N_2)$  and so the sensitivity of the instrument increases at higher velocities. An investigation of the theoretical limiting accuracy of the instrument shows it to be almost two orders of magnitude below the design goal of  $5 \times 10^{-7}$  in the sled velocity range of 600 m/sec. Around Mach 1 if no correction were made for the value of  $T$  from its value in free stream the maximum error in  $n$  would be about  $5 \times 10^{-5}$ . This is assuming the temperature behind the shock is the stagnation temperature  $T_o$ . This is not actually the case.  $T$  will decrease ahead of the sled approximately exponentially to its free stream value. Therefore, the error would be less than the value given above, depending on how close to the sled the reflecting surface was. The error that arises from using the ambient value of  $n$  rather than the shock value could be decreased by estimating a correction to the ambient value from knowledge of the approximate sled velocity and position. Below the transonic speed regime the temperature change in the disturbed air will introduce a smaller error. These results indicate that the accuracy obtainable using a two-color laser will not be as good as that of a conventional temperature measurement.

The most accurate correction over a large velocity range for the speed of light is made by measurements of the ambient atmospheric temperature. Stationary trackside temperature thermocouples or other

devices are suitable with the number required being a function of the meteorologic conditions. Although additional data is required, almost all days contain a time near sunrise and sunset when the required accuracy could be attained with 10 measurements. In the transonic range, uncorrected errors as high as  $5 \times 10^{-5}$  can occur which is 100 times the goal. The amount of correction attainable by using sled velocity to predict bow wave conditions has not been determined.

#### 4.4.5 Pitch and Yaw

The magnitude of the error introduced into the velocity measurement by sled pitch and yaw is determined in Appendix A.8. A simplified system diagram to show this effect is in Figure A.8.2.

Changes in sensitivity due to angle change alone are negligible since a tracking system returns the beams to alignment. However, as the sled pitches and yaws the signal beam's optical path length is changed. Depending on the location of the axis of rotation of the sled, and the relative positioning of the laser and the specimen, the change in the signal beam optical path length will be different.

The maximum error occurs if the sled pitches and yaws through its maximum available angle in the .001 sec sampling time. With typical sled dimensions, path length changes would occur on the order of a millimeter. This is 3 to 4 orders of magnitude outside of the design goal. The sled cannot yaw the maximum amount in .001 sec so the error will be smaller, but corrections using gyros or angular accelerometers will still be required.

Errors from pitch are smaller due to the specimen being more nearly in line with the laser but gyros or angular accelerometers may be required.

#### 4.4.6 Beam Steering

The sled-based beam steering system in two axis must be able to withstand the severe vibrational environment of the sled, and must have a very fast response time. Rapid re-tracking after signal drop-outs is also required, to insure a minimum amount of signal loss. Detectors to the side of the primary interferometer detector will measure any deflection of the beam and provide the feedback to recenter the beam.

Various types of systems have been investigated. The two most promising are 1) an acousto-optic modulator system which steers the beam by inducing a "grating" in a piezo-electric crystal, using a high frequency oscillator, 2) a mirrored piezoelectric crystal which deflects the beam through crystal surface deformation.

The response time of both systems is on the order of microseconds which is small enough since the vibrations to be tracked are below 1000 Hz and the sled moves 0.6 m or less in a millisecond. An investigation of their performance in a high vibration environment, and of their re-tracking capabilities is needed. If acousto-optic modulators are used, the frequency shift which they produce will require an additional correction.

During acquisition of the next mirror, which might take one or two milliseconds, velocity will not be measured. At worst (highest velocity), this would eliminate about 1% of the measurements but not affect the accuracy of the remaining measurements. A separate sled mounted system overlapping the first would avoid the missed data but the added expense would not be warranted.

A further investigation of beam tracking systems to determine their performance capabilities on the sled environment is required. A preliminary investigation shows that they will be complex systems, but could probably meet the tracking requirements on the Flag Interferometer velocity measuring system.

#### 4.4.7 Costs

This early in a feasibility study, life cycle costs are only as certain as the technical solutions to remaining problems many of which are unresolved. An estimate of development costs is best determined when proposals for this work are made. An estimate of replacement cost for the sled borne interferometer and electronics will probably be on the order of \$50,000. Track mounted mirrors and temperature measurement devices will cost a similar amount. The risk to these components will depend on operation policies of the track. In addition

to replacement due to accidents, maintenance will include cleaning, aligning of mirrors, recalibration of thermometers, set-up and alignment of the interferometer and miscellaneous repair.

#### 4.5 TRANSLATIONAL INTERFEROMETER ANALYSES

The TRANSAR system error modeling to be described in the following is not as complex as it is for the Flag Interferometer because the system performance is not affected by the ambient environment and the bow wave. The major area of concern is the boundary layer of air at the base of the slipper which can produce refractive effects and change the angular sensitivity of the signal. Sled pitch and yaw will also affect the angular sensitivity. Another area of concern is the performance of the optical system in the high vibration sled environment. Finally of concern is the vacuum level in the measurement cavity and its freedom from debris.

##### 4.5.1 Angle Filter Requirements

The accuracy obtainable with the TRANSAR system is directly dependent on the angular resolution obtainable, and on the variations of this sampling angle during the sled run. The angular sensitivity is greater for the Translational Interferometer than for the Flag Interferometer, because a larger angle between the sampled ray and sled velocity vector is required to allow for adequate light from the rail. Therefore, the angle accuracy is more critical since  $\cos \theta$  varies more

rapidly at large  $\theta$ . Assuming randomly oriented diffuse reflections (no preferred direction) angular filtering on the order of the required  $5 \times 10^{-7}$  radians resolution would cause power attenuation on the order of the square of this value. The resulting power would be unusable so some trade-off between angular resolution and signal to noise requirements is necessary. To reduce the attenuation to the  $10^{-4}$  value discussed in section 4.2 would require angular filtering of about  $10^{-2}$  radians which is over  $10^4$  times that required for direct compliance with the velocity accuracy. Power absorbed at the rail surface has been neglected so although poor, this is a best case. Averaging over a relatively large angle is possible, as a means of improving the directivity of the returned signal. This would require a consistent intensity with angle, a property which has not been observed in preliminary qualitative tests. Additional tests are required before conclusions can be drawn.

#### 4.5.2 Boundary Layer Effects and Slipper Evacuation

The fringe count generated by the sled displacement is given by  $\frac{v}{\lambda} (\cos\theta_1 + \cos\theta_2)$ , where  $v$  is the sled velocity,  $\lambda$  is the wavelength of the light used for a signal and  $\theta_1$  and  $\theta_2$  refer to the angles of the forward and backward scattered light with respect to the sled velocity vector. From this it can be seen that the accuracy of the system is determined directly by the error in the measurement of the speed of light in the slipper cavity, and the uncertainty in the value of the sampled angles.

To eliminate refractive effects and keep the uncertainty in the speed of light to a minimum, a pressure of 1 torr or less must be maintained in the cavity. Since at the higher Mach numbers the pressure differential from the front to the back of the slipper is a couple of thousand torr a high performance pumping system would be required to maintain the required cavity pressure.

Some of the possible approaches to the problem include using a pre-vacuum cavity, or a series of such cavities, which would successively reduce the pressure in front of the slipper (Refer to Appendix A.7). Since the pressure is reduced as a power of the pressure drop for each pumping cavity, a great reduction in the pressure could be achieved. This would result in a complex slipper and pumping system. The simplified analysis in Appendix A.7 indicates the required evacuation may be possible, but significant assumptions were made and additional analysis and testing is indicated.

A separate velocity measuring slipper with aerodynamic design to keep the slipper close to the rail may be required. A simplified calculation (Appendix A.7) shows the required slipper gap to be on the order of 0.3 mm to maintain a cavity pressure of 1 torr. A more exact analysis and testing would be required to determine the feasibility of maintaining this gap distance, but it should be possible using a combination of aerodynamic vacuum and mechanical downloading.

Another method of controlling the environment inside the slipper cavity is to pressurize it with a clean gas (e.g., Air or Helium). This would act to sweep debris from under the front of the slipper and prevent it from entering the cavity.

#### 4.5.3 Pitch and Yaw

Refer to Appendix A.5 for a detailed analysis. Assuming a rigid sled with slippers and an all around slipper-rail clearance of 1.5 mm and 2.5 m slipper-spacing the maximum pitch and yaw angles for the sled are approximately  $1.2 \times 10^{-3}$  radians peak to peak. The allowable angular changes are just below this value.

A separate slipper is also under consideration which is supported so that it can remain against the top of the rail. If either of the

above configurations cannot achieve the required angular stability angular accelerometers or gyroscopes will be required.

Effects of vertical motion combined with pitch have not been analyzed.

#### 4.5.4 Translational Interferometer Experiment

The laboratory experiments are described in Appendix A.9. A simplified model of the Translational Interferometer was assembled in the lab at ETI. Figure A9.1 shows the modified design used for the experiment. The edge of a rotating aluminum wheel was used to simulate the surface of the rail.

Proof of principle was demonstrated. Operation was achieved with a greater than 0.1 radian angle filter. This was a larger angle than was thought useable from analysis and suggested aperture averaging would be effective. Calibration tests were limited in accuracy to 2% by the oscilloscope used.

#### 4.5.5 Translational Interferometer Calibration

The Translational Interferometer is subject to the same calibration uncertainties in principle as the Flag Interferometer. These are frequency of the laser, velocity of light, and the angle of observation. Sensitivity to the frequency of the laser is of course the same but the velocity of light is controlled in the Translational Interferometer by controlling the measurement cavity environment.

The changes in angle due to pitch and yaw of the slipper can be minimized mechanically using linkages and measured using gyroscopes. Finally, the cosine of angle of observation of the rail must be known and this must be measured indirectly.

In the flag interferometer the angle of observation to the track is near zero. In order to obtain sufficient reflected light in the transar the angle between the rail surface and the line of observation of the rail must be much greater than zero. This results in a large sensitivity to small changes in the angle in the transar. In fact the total error budget of  $5 \times 10^{-7}$  requires an angle accuracy of  $5 \times 10^{-7} / \sin \theta$ . While it is too early to establish an error budget the accuracy required is at least twice this.

Angles cannot be directly measured to this accuracy. However, if the velocity can be measured independently, the angle can be calculated. Again in the laboratory there is no known method for achieving and measuring the velocity to the required accuracy, but at the rocket sled track the average velocity over long distances can be measured to the required accuracy using a beam break device and improvements in surveying track bench marks. Then the Translational Interferometer can be calibrated on each use by constraining the average velocity obtained from its numerous velocity measurements to agree with the few measurements obtained with the beam break velocity measuring system. In other words, the integrated velocity must agree with the track length.

#### 4.5.6 Translational Interferometer Costs

As with the Flag Interferometer it is too early to compile comprehensive costs, but an estimate will be of value. Again development cost estimates will require a significant effort which is best done as part of a proposal for this work.

Replacement cost for the sled borne interferometer system will also probably be on the order of \$50,000. Need for a separate rail has not been determined and is not included. The risk to these components will depend on operational policies of the track. Maintenance will include an undetermined amount of rail surface preparation.

## 5.0 CONCLUSIONS

After analysis of numerous concepts it was concluded that only an interferometer of some type operating at optical wavelengths could meet the performance goals. Any system using longer wavelengths, such as microwave or millimeter wavelengths, inherently lacks the required resolution. Two optical interferometers have analytically been shown to be possible, but experimental data are required since several difficulties have been identified either on the interferometers or in the track or sled environment. The improved beam break system is also included because it represents a cost effective compromise between the large amount of development required for the interferometers and the performance limitations of the existing velocity measuring system (VMS).

Conclusions and comparisons follow for the two Interferometer systems and an improved beam break system. Features, advantages, disadvantages and difficulties are listed in Table 5.1.

### 5.1 FLAG INTERFEROMETER — CONCLUSIONS

After evaluating a number of flag interferometer variations, the following system was selected. 150 mirrors would be mounted along the track at 100 meter intervals. Active beam steering would be used to track the mirror as it passes to the side and to account for pitch, yaw and vibration. Although dual overlapping systems would be required to prevent signal drop out when the next mirror is acquired, it is more practical to tolerate a few millisecond drop out every 100 meters. On the order of 20 temperature measuring stations along the track (about every 750 meters) will correct for speed of light changes. In order to determine specimen velocity, a fiber optic or airpath beam is carried to and from the specimen using a rigid and shock isolated mechanical beam. Gyroscopes will correct for path length changes produced by yaw of the sled. Frequency doubling of the fringe rate raises the maximum frequency to 4 GHz and allows resolution of  $\pm .00015$  m/sec

Table 5.1. Comparison of Candidate Concepts

	<u>ADVANTAGES</u>	<u>DISADVANTAGES</u>	<u>DIFFICULTIES OR UNCERTAINTIES</u>
<b>Flag Interferometer</b>	<ul style="list-style-type: none"> <li>- Performance goals achieved under selected conditions</li> <li>- Inherent calibration</li> <li>- Operation from before sled start.</li> <li>- Direct measurement of specimen velocity.</li> </ul>	<ul style="list-style-type: none"> <li>- Full performance restricted to minimum scintillation times of day.</li> <li>- Installation and maintenance of mirrors and thermocouples</li> <li>- Data drop outs of a few milliseconds each 100 meters for mirror switching.</li> <li>- Complexity</li> </ul>	<ul style="list-style-type: none"> <li>- Uncertain accuracy near Mach 1 due to need for calculating conditions behind large bow wave.</li> </ul>
<b>Translational Interferometer</b>	<ul style="list-style-type: none"> <li>- Essentially all performance goals achieved under all conditions</li> <li>- Operation from before sled start</li> <li>- Independence from ambient conditions</li> </ul>	<ul style="list-style-type: none"> <li>- Slight (50%) increase in measurement interval over goal</li> <li>- Rail surface maintenance or separate rail</li> <li>- Necessary external calibration from a beam break system on each sled run.</li> <li>- Separate specimen velocity interferometer.</li> <li>- Complexity</li> </ul>	<ul style="list-style-type: none"> <li>- Uncertain accuracy due to undetermined calibration stability</li> <li>- Uncertain accuracy due to undetermined slipper cavity environment</li> </ul>
<b>Improved Beam Break</b>	<ul style="list-style-type: none"> <li>- Low cost and low uncertainty</li> <li>- Improved performance over current capability.</li> <li>- Simplicity</li> </ul>	<ul style="list-style-type: none"> <li>- Performance compromised to <math>\pm .001</math> m/sec accuracy with long measurement intervals determined by flag spacing.</li> </ul>	<ul style="list-style-type: none"> <li>- No major uncertainties</li> </ul>

and an accuracy of  $\pm .0003$  m/sec. These performance tolerances estimates are subject to verification.

Advantage of this system follow. Except in the vicinity of Mach 1, simultaneous achievement of all design goals is predicted at selected meteorologic conditions. Accuracy is determined only by the frequency of the laser and the speed of light with corrections due to sled yaw and measuring angle. Measurements can begin before the rocket firing and continue after the stop. Measurement of a point on a shock mounted specimen is made.

Disadvantages of the Flag Interferometer are, first that it can only operate continuously when atmospheric turbulence is at a minimum (usually the hour before sunset). At other times it would work only near each mirror which are at 100 meter intervals and full accuracy would be achieved only near temperature measurement points at 750 meter intervals. Near other mirrors, accuracy would be reduced by up to an order of magnitude. The system could be upgraded with more mirrors and temperature measurements temporarily for special runs. Drop outs of one or two milliseconds for mirror switching will occur every 100 meters unless dual overlapping sled systems are used. Finally, cleaning and alignment checks on the 150 mirrors must be accomplished at undetermined intervals.

A number of difficulties or uncertainties exist which, after additional investigation, may or may not be disadvantages. Uncertainties exist in the environment at the track. Also uncertain is the accuracy achievable at velocities near Mach 1 due to variations in the speed of light behind the bow wave and the large bow wave stand off distances in this velocity range. A prediction can be made of the velocity of light behind a bow wave in the transonic region using a knowledge of ambient conditions and the approximate sled velocity. A 1% or less error in this correction is required to achieve the full accuracy goal.

## 5.2 TRANSLATIONAL INTERFEROMETER - CONCLUSIONS

The Translational Interferometer is configured as follows. The measuring head would be vibration isolated from and mounted in a separate, non-load bearing slipper which would remain in contact with the top surface of a rail. In order to eliminate atmospheric effects and to remove debris, the slipper measurement cavity would be evacuated, or pressurized and accurately characterized. Absolute calibration independent of the track is not possible with this system, so beam break data over large distances will be used to calibrate the system on each run. Velocity of the specimen is determined with a separate interferometer from the measurement slipper to the specimen and gyroscopes will be used to correct for relative velocity between the specimen and the measurement head due to sled yaw and pitch.

The advantage of the Translational Interferometer is that it can potentially achieve a velocity accuracy of  $\pm .001$  ft/sec (.0003 m/sec) over the full range of 0 to 2000 ft/sec (0 to 600 m/sec). Measurements can begin before the start and after the stop of a run. Measurement of a point on the shock mounted specimen is made. Measurements are independent of meteorologic conditions and can be done day or night.

The Translational Interferometer has a few disadvantages. Special rail surface preparation and maintenance or a separate measurement rail may be required. Also, the accuracy goal is achievable only with measurement intervals of .0015 sec which is slightly greater than the .001 sec goal. Finally, the system is not inherently accurate but must be calibrated on each run using beam break data.

A number of uncertainties or difficulties exist which, after further investigation, may or may not result in disadvantages. Scale factor (fringe frequency per velocity) is a strong function of the angle of observation and in order to achieve adequate light power a large

angle range must be observed. This angle range must be larger than the range which would directly satisfy the accuracy goal and serious questions exist whether averaging over these angles can be sufficiently constant to achieve the accuracy goal. Variations in the surface of the rail may cause undesired fluctuations in this averaging but the required laboratory experiments have not been done.

Another uncertainty is the feasibility of achieving a system which will ride close enough to the rail, and which will achieve debris sweeping and evacuation requirements.

### 5.3 BEAM BREAK SYSTEM — CONCLUSIONS

Improvements to the existing beam break can improve its performance. It cannot meet all the performance goals but its cost would be much lower than the previous two concepts. The incandescent light source would be replaced by a semiconductor laser thereby greatly increasing the power of the light incident on the detector, and the superior collimation would lend to more accurate beam break determination. The electronics would be replaced with reliable high speed integrated circuitry.

The dual head beam break system which has been used on the track operates by measuring the time between passage of a single flag by two heads mounted on the sled.

To supplement data rate at the start of the run, a stationary interferometer and a sled mounted mirror could provide velocity data from before the start until the sled is from 3 to 100 meters along the track, depending on meteorologic conditions.

Velocity of a shock mounted specimen can be obtained by using the same fiber optic interferometer previously proposed for use with

the Translational Interferometer. Refer to Section 5.2 and Appendix A.6. This relative velocity of the specimen measurement is much simpler than either the Flag or Translational Interferometers.

This system has the advantage of not requiring accurately surveyed flags. However, accurately surveyed flags at the track bench marks would provide an accuracy cross check. In addition, the beam break system is proven and improvements are relatively low cost and low risk. An accuracy of .001 m/sec (.03 ft/sec) can probably be achieved at reduced sampling rates which are at fixed distances rather than the design goal frequency of 1 kHz. At the maximum design goal velocity of 600 m/sec (2000 ft/sec) the sampling interval can be .001 sec if 0.6 meter flag spacings are used.

Disadvantages of the beam break systems are reduced accuracy and reduced frequency of measurement.

#### 5.4 COMPARISON OF SYSTEMS

The listing of advantages and disadvantages in Table 5.1 reveals some comparisons.

The only system potentially capable of achieving the design goal accuracy is the Flag Interferometer. Uncertainties are less than with the Translational Interferometer. If its uncertain accuracy near Mach 1 does not rule it out, this concept would be favored.

The potential accuracy of the Translational Interferometer comes close to the design goals and it eliminates the sensitivity to ambient conditions. However experimental data are needed to resolve uncertainties in scale factor and slipper evacuation.

This concept would be favored if these uncertainties are answered favorably.

The most cost effective concept is improvements to the beam break system. This is then the concept of choice if its reduced sampling rate and accuracy can be tolerated.

While these qualified conclusions can be made, it cannot be easily concluded that any one system is superior at this time.

Similarly, detailed design specifications cannot be developed at this time. However, the requirements and specifications for the various portions of the systems are discussed in the analyses and summarized in Tables 5.2 and 5.3. When further experimental data are available, detailed specifications for the system can be finished.

The design specifications that can be determined now and the expected performance from the two interferometers are given in Tables 5.2 and 5.3.

Table 5.2

Flag Interferometer

System Requirements:

Laser:	Ruggedized He-Ne. Single frequency. Power level of several mw.
Detector:	APD with bandwidth of at least 2GHz.
Beam Steering:	Capable of tracking beam angle change between flags and correct for pitch and yaw. Signal processing to control electronics are required.
Electronics:	Preamp for APD must have a bandwidth greater than 2 GHz. Frequency counter range to 2 GHz without prescaling.
Telemetry:	Digital link with approximately 250 Kbps for timing, data and angle correction data.
Secondary Measurements:	Off sled pressure and temperature measurements necessary.

System Specifications:

Maximum Accuracy:	.001 fps at 2000 fps in .001 sec without averaging.
Major Corrections:	Index of refraction of air.
Accuracy With No Corrections:	About .1 fps at 2000 fps without averaging.

Table 5.3

Translational Interferometer

System Requirements:

Laser:	Ruggedized He-Ne. Single frequency. Power level of several mw.
Detector:	APD with bandwidth of at least 1.4 GHz.
Mounting Slipper:	Maintain rail contact within .3 mm during run.
Vacuum:	For .3 mm clearance need 50 $\mu$ /sec pump. May be turbine driven by the sled since the lowest pressure is required only at the highest velocity.
Electronics:	Preamp for the APD must have bandwidth greater than 1.4 GHz. Frequency counter required with a range to 1.4 GHz without prescaling.
Telemetry:	Digital link with approximately 100 Kbps rate for data and timing.
Secondary Measurements:	Low accuracy system required for sled to sample motion correction. Pitch and yaw may need to be measured. Rail surface preparation may be necessary.

System Specifications:

Maximum Accuracy:	.0014 fps at 2000 fps in .001 second without averaging.
Major Corrections:	Angle collimation Sample to slipper motion.
Accuracy with No Correction Or Slipper Evacuation:	About .1 fps at 2000 fps without averaging.

## 6.0 RECOMMENDATIONS

To provide the best chance for achieving the design goals, it is recommended that a single concept not be chosen at this point. Either of the two interferometers appear feasible, so that a two step process is necessary to achieve success. A two phase program would first obtain the experimental data required to address the difficulties of operation for both interferometers, as well as to ensure that in areas where the analysis indicated no problems exist, that the analysis was sufficient. These data should be obtained in both a laboratory and at the Test Track during sled runs. Upon successful completion of this phase, it will be justified to go ahead with a second phase of selecting one system and making it operational at the Test Track Facility. Some of the areas to be investigated are:

### AREAS OF INVESTIGATION

#### Flag Interferometer

1. Ambient atmospheric fluctuations near the track
2. Atmospheric fluctuations behind bow waves
3. Prediction of the speed of light behind transonic bow waves
4. Temperature profiles around the track
5. Interferometer operation in the vibration environment
6. Erosion of mirrors and sled windows and beam interruption due to debris
7. Optical and electronic circuit feasibility
8. Fiber optic interferometer feasibility on the sled.

### Translational Interferometer

1. Calibration stability
2. Rail surface finish effects
3. Feasibility of slipper evacuation and debris sweeping
4. Interferometer operation in the vibration environment
5. Optical and electronic circuit feasibility
6. Fiber optic interferometer feasibility on the sled.

### Improved Beam Break

1. Overall proof test.

The analysis and limited experimentation performed in this program show possible hardware systems can be designed to obtain substantial increases in accuracy. The realization of a working system requires acknowledging that any further analysis must be in conjunction with experiments to determine if the substantial difficulties identified in the analysis impose actual limitations on performance. It is important to emphasize that the operation of either interferometric technique in this environment is not trivial. Each of the enumerated difficulties must be addressed experimentally. It is also important that the analysis that led to these two interferometric techniques did not as yet find the design goal to be impossible.

## REFERENCES

1. Personal communication with Spectra Physics, 1250 West Middlefield Road, Mountain View, California 94042 and Quantronix, 225 Engineers Road, Smithtown, New York 11787
2. B & H Electronics Company, Box 490, Chester, New York 10918, Data Sheet AC2500-DC3000-AC3000.
3. Liepmann and Roshko, Gas Dynamics, (London and New York: Wiley, 1957).
4. TRW System Group, October 1971, "Concepts for Improved Range Tracking During Sled Test Evaluation of Inertial Guidance Systems".
5. Heberle, Wood, Gooderum, Data on Shape and Location of Detached Shock Waves on Cones and Spheres, NACA TN 2000, (1950).
6. Ames Research Staff, Equations, Tables, and Charts for Compressible Flow, NACA, Report 1135.
7. Hayes and Probstein, Hypersonic Flow Theory, Vol. I. (New York: Academic Press, 1966), p. 462.

## APPENDIX A.1

### VARIATION OF THE SPEED OF LIGHT IN A MOVING MEDIUM

In the Flag Interferometer concept, the light initiated on the sled encounters air which is moving with respect to the sled. First, since the velocity of light is independent of the coordinate system

$$V \approx V_o = \frac{c}{n}$$

where  $V_o$  is the velocity of light in the coordinate system of the moving medium,  $V$  is the velocity of light to the observer,  $c$  is the speed of light in a vacuum and  $n$  is the index of refraction of the air. A more accurate description is obtained from the Lorentz transformation between coordinate systems which gives

$$V = V_o + v \left(1 - \frac{1}{n^2}\right)$$

or

$$\frac{V}{V_o} = 1 + \frac{v}{V_o} \left(1 - \frac{1}{n^2}\right)$$

where  $v$  is the velocity of the medium to the observer. The second term is proportional to this velocity so in a moving medium a small correction is required. For the sled  $v = 600$  m/sec, and  $n = 1.000291$ , so

$$\frac{V}{V_o} = 1 + 1.2 \times 10^{-9} .$$

This correction to the speed of light is negligible.

## APPENDIX A.2

### BEAM COLLIMATION IN A TRANSLATIONAL INTERFEROMETER

In the Translational Interferometer the scale factor of fringes per unit velocity is a function of the angle of observation of the rail. In order to maintain an accuracy of  $5 \times 10^{-7}$  this effective angle  $\theta$  must be constant enough that  $\cos\theta$  changes less than  $5 \times 10^{-7}$ . In practice the effective angle will be some weighted average of the range of angles observed. This will vary with the rail surface. Additional averaging occurs over the rail length traversed in the 1 msec measurement interval. Of interest is the increased accuracy obtained at high velocities due to a longer length of rail to average which corresponds to the higher % accuracy required at high velocities.

The paper will address the angle filtering accuracy achievable and effects of a boundary layer attached to the rail on the angle of observation.

#### Angle Filtering

Figure A.2.1 shows use of a lens and a pinhole system placed at the lens focal length to filter out all but a band of angles. The lens collects rays from any illuminated point, but only rays of a narrow band of angles pass through the pinhole.

The beam collimation possible is determined by the resolution of the lens system and the size of the pinhole. (The pinhole is not diffraction limited because one only wants to know what angular component of the diffuse reflection passes through the pinhole onto the detector.) The requirement is that the pinhole be large enough to allow a "useable" intensity signal to pass, but small enough to keep the required 1 part per 2 million accuracy.

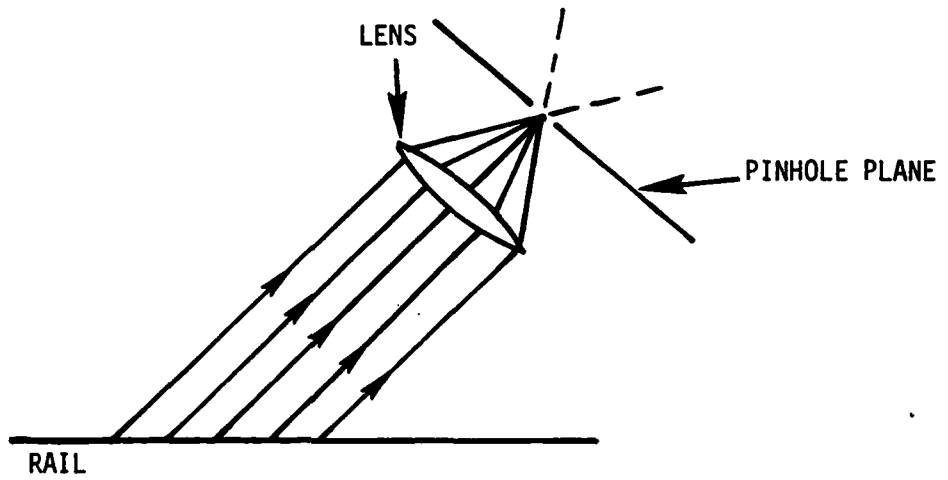


Figure A.2.1

An achromatic lens provides the best resolution of any single lens.\* The resolution decreases by about 5% as the angle between the lens axis and a line from the focal point to the point where the ray intercepts the lens, increases from 0° to about 5°. (A larger focal length helps reduce this effect.) A value for the exact "spot size" was not calculated but to practical limiting resolution is 0.5 μm.\*

An estimate of the resolution was made using a Plano-Convex Lens, which would be the next best lens to use after the achromat. The formula\* is as follows

$$\theta = \frac{K(n)}{2f^3} D^3 + \frac{1.22 \lambda}{D}$$

where  $\theta$  is the angular radius of the image spot.

$K(N)$  = a function of the refractive index of the lens  
 $f$  = the focal length  
 $\lambda$  = HeNe 0.6328 μm (6.328 x 10<sup>4</sup> mm)  
 $D$  = lens diameter.

The first term is due to aberration and the second to diffraction.

It is apparent from this formula that one should maximize the focal length of the lens to increase the resolution. With the slipper dimensions as they are the focal length of the lens couldn't be any larger than about 100 mm.

The first term is proportional to  $D^3$  and the second to  $1/D$ . The optimum  $D$  value and  $f/D$  ratio, to minimize  $\theta$ , are \*

---

\*Melles Griot Optics Guide, (1975 edition), pp. 20 and 174.

$$D_{\text{opt}} = \left[ \frac{(2)(1.22)}{3} \cdot \frac{\lambda}{K(n)} \right]^{1/4} f^{3/4}$$

$$\left( \frac{f}{D} \right)_{\text{opt}} = \left[ \frac{3}{2(1.22)} \cdot \frac{f K(n)}{\lambda} \right]^{1/4}$$

where  $K(n)$  for a Plano-Convex lens is given by

$$K(n) = \frac{1}{32(n-1)^2} \left( n^2 - 2n + \frac{2}{n} \right)$$

Using  $n = 1.5$  this works out to

$$K(n) = .07$$

$$\text{Therefore } D_{\text{opt}} = .29f^{3/4}$$

using  $f = 100 \text{ mm}$ ,  $D_{\text{opt}} = 9.16 \text{ mm}$ .

Therefore, using a 100 mm focal length lens you have an optimum aperture of 9.16 mm using a Plano-Convex lens.

The resolution is:

$$\theta = \frac{.07}{2(100 \text{ mm})^3} (9.16 \text{ mm})^3 + \frac{1.22(6.328 \times 10^{-4} \text{ mm})}{9.16 \text{ mm}}$$

$$\theta = 1.1 \times 10^{-4} \text{ (radians) .}$$

Actually the resolution is determined by the cosine of the angle.  
Assuming this angle is  $45^\circ$ ,

$$\text{resolution} = \frac{\Delta \cos \theta}{\cos \theta} = \frac{\cos \pi/4 - \cos(\pi/4 + 1.112(-4))}{\cos \pi/4}$$

$$\text{resolution} = 1.1 \times 10^{-4} .$$

Therefore, the required angular resolution of  $5 \times 10^{-7}$  couldn't be achieved with this lens without averaging over the angle.

#### Pinhole Size

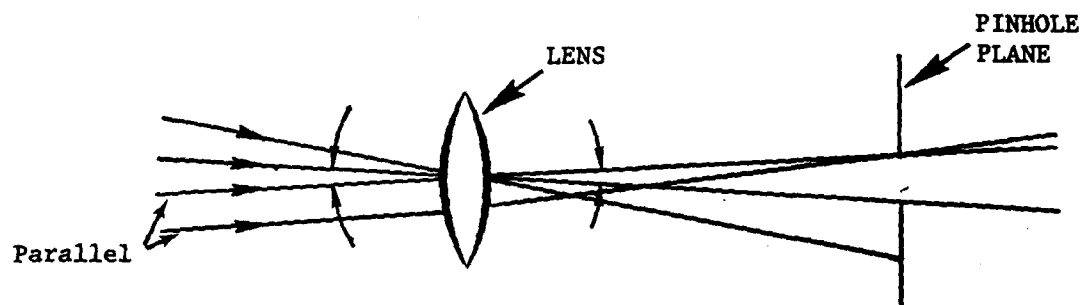
Now let us calculate the size of the pinhole necessary to maintain angular resolution. Let  $\theta$  = angle of resolution = angle defined by the pinhole diameter,  $d$ , and the distance from the lens to the pinhole,  $f$ , (the focal length)

$$\theta = \frac{d}{f} .$$

The wavelength of the He-Ne laser is  $\sim .6 \mu$ . To keep the angular resolution obtained above ( $1.1 \times 10^{-4}$ ) with the 100 mm pinhole to lens spacing assumed above the pinhole would be

$$d = \theta f = (1.1 \times 10^{-4})(100 \text{ mm}) = 11 \mu \text{m} .$$

In Figure A.2.2, assume the cavity has been evacuated except for a boundary layer adhering to the rail. Since the scale factor of the transar is a function of the angle  $\theta$ , refraction of light at the boundary layer will cause an error.



Note incoming parallel rays are accepted by the pinhole and rays outside  $\theta$  are rejected by the pinhole, thus providing angle filtering.

Figure A.2.2  
Pinhole Size

Assume beam is at angle  $45^\circ$  and look at variations in  $\sin\theta$  where  $\theta$  is redefined by Figure A.2.3. From Snell's law:

$$1) \quad n_1 \sin\theta_1 = n_b \sin\theta_2 \quad .$$

Pressure difference from boundary layer to cavity = 5% variation\* .

$$2) \quad n_1 = 1 + \beta \rho_1 / \rho_s \quad \rho_s = \rho \text{ at STP}$$

$$n_b = 1 + \beta \rho_b / \rho_s \quad \beta = .000291$$

$\rho_1$  = The air density inside the cavity

$\rho_b$  = Air density in the boundary layer

$n_1$  = Index of refraction in the cavity

$n_b$  = Index of refraction in the boundary layer.

Using equations 1 and 2 we have that

$$n_1 / n_b \sin\theta_1 = \sin\theta_2$$

and

$$n_1 / n_b = (1 + \beta \rho_1 / \rho_s) / (1 + \beta \rho_b / \rho_s) \quad .$$

Now, assuming a 5% variation between  $\rho_1$  and  $\rho_b$

$$\rho_1 = \rho_b (1 - .05) = .95 \rho_b \quad .$$

Therefore,

$$n_1 / n_b = \frac{1 + \beta \frac{.95 \rho_b}{\rho_s}}{(1 + \beta \rho_b / \rho_s)} \quad .$$

\* Personal communication with Dr. H. King, ETI.

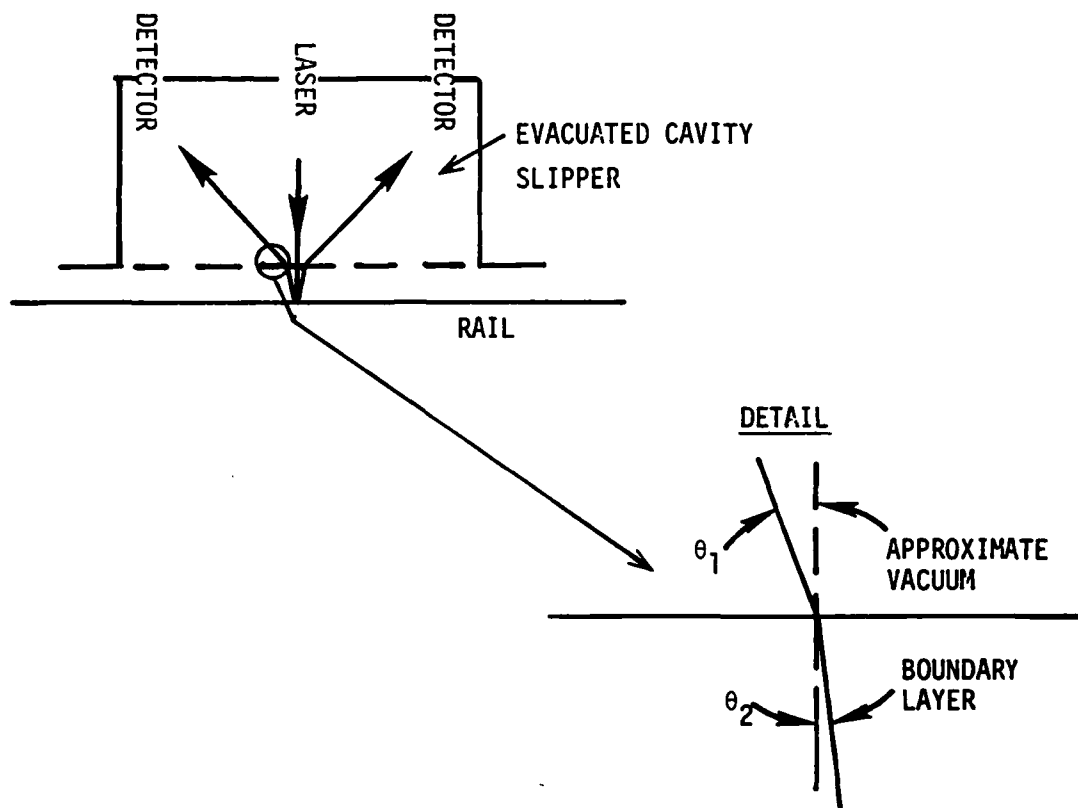


Figure A.2.3  
Translational Interferometer Boundary Layer

Let  $\rho_b = 1/100 \rho_s$  (assuming the pumping capability is sufficient to yield this value)

$$\text{Then } n_1/n_b = \frac{1 + \beta (.95) (1/100)}{1 + \beta \left(\frac{1}{100}\right)} = .9999985 .$$

$$\text{So } \sin\theta_2 = .9999985 \sin\theta_1$$

$$\begin{aligned} \text{and } \Delta\sin\theta &= \sin\theta_1 (1 - .9999985) \\ &= 1.46 \times 10^{-7} \sin\theta_1 . \end{aligned}$$

$$\text{Since } \theta = 45^\circ, \sin\theta_1 = .707 .$$

$$\text{At } \theta = 45^\circ, \sin\theta = \cos\theta$$

$$\text{and } \Delta\sin\theta \approx \Delta\cos\theta$$

$$\text{so } \frac{\Delta\sin\theta}{\sin\theta} \approx \frac{\Delta\cos\theta}{\cos\theta} .$$

$$\text{Now } \frac{\Delta\sin\theta}{\sin\theta} = \frac{1.46 \times 10^{-7} \sin\theta}{\sin\theta} = 1.46 \times 10^{-7}$$

$$\text{therefore, } \Delta\cos\theta/\cos\theta \approx 1.46 \times 10^{-7} .$$

This error is smaller than but a significant part of the  $5 \times 10^{-7}$  requirement so boundary layer refraction is tolerable.

If it can be assumed that there is always a 5% difference between the air density inside the slipper and that in the boundary layer then the better evacuated the slipper is, the less the effect due to refraction at the boundary layer will be since the ratio

$$\frac{n_1}{n_b} = \frac{1 + \beta \rho_{\text{cavity}}/\rho_s}{1 + 1.05 \beta \rho_{\text{cavity}}/\rho_s} \rightarrow 1 \text{ as } \rho_{\text{cavity}} \rightarrow 0 .$$

The resolution on a microscope objective is diffraction limited, so the resolution is determined by the  $.61\lambda/D$  term. If  $s$  is the resolution in units of length,  $\theta = s/\text{focal length} = \text{angular resolution in radians}$ . Therefore,  $\theta$  is defined as  $\frac{.61\lambda}{\text{N.A.}/\text{focal length}}$

$$\lambda = 632.8 \text{ nm}$$

N.A. = the numerical aperture.

The greatest value of N.A. x focal length available from Melles Griot is on a 10 x magnification lens (Products #04 OAS 015), with a numerical aperture of .30 and a focal length of 16.0 mm, yields a resolution of

$$\theta = 8.04 \times 10^{-5} \text{ radians}$$

or two orders of magnitude greater than required by the two part per million specification.

### APPENDIX A.3

#### THE EFFECT OF THE BOW SHOCK ON THE FLAG INTERFEROMETER VELOCITY MEASUREMENT

PURPOSE: To determine the effect of the Supersonic bow shock ahead of the flag interferometer sensing head on the velocity measurement accuracy obtainable using this system.

ASSUMPTIONS: That the sensing head is mounted so as to stand ahead of the supersonic bow shock of the sled itself. In this case the sensing head bow shock forms in undisturbed air. This is a reasonable assumption in the supersonic regime. Refer also to Appendix A.14 "Transonic Bow Wave Effects on the Flag Interferometer Velocity Measurement," and Appendix A.15 addresses larger spacings. A flag spacing of 13 ft. is also assumed.

#### INTRODUCTION TO PROBLEM

The accuracy of the sled velocity measurement is affected in two ways by the sensing head bow shock.

The first is an "absolute" effect and depends on the value of the shock parameters at the time of the measurement. This effect is that as the laser beam traverses the distance from the source to the flag mirror, it is refracted at the shock wave front ahead of the sensing head. (See Figure A.3.1.)

Since the indicated velocity depends directly on the value of  $\cos\theta$ , any error in the calculated value of this quantity will cause a corresponding error in the velocity calculated.  $\cos\theta$  is calculated from the knowledge of the values of  $a$  and  $b$ , see Figure A.3.2. It is assumed in this calculation that no refraction occurs as the ray traverses the

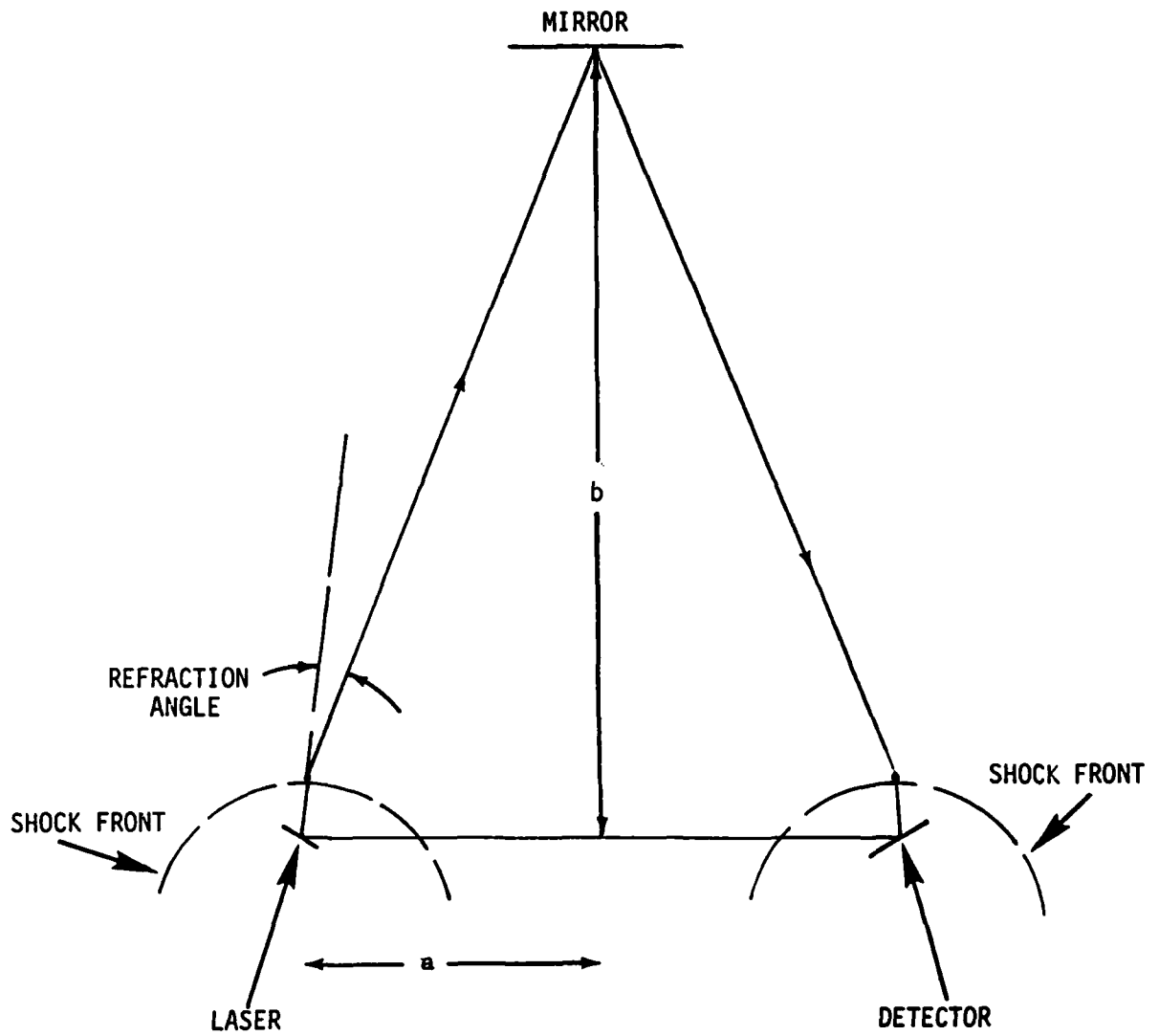


Figure A.3.1. Refraction of Laser Beam at Shock Front

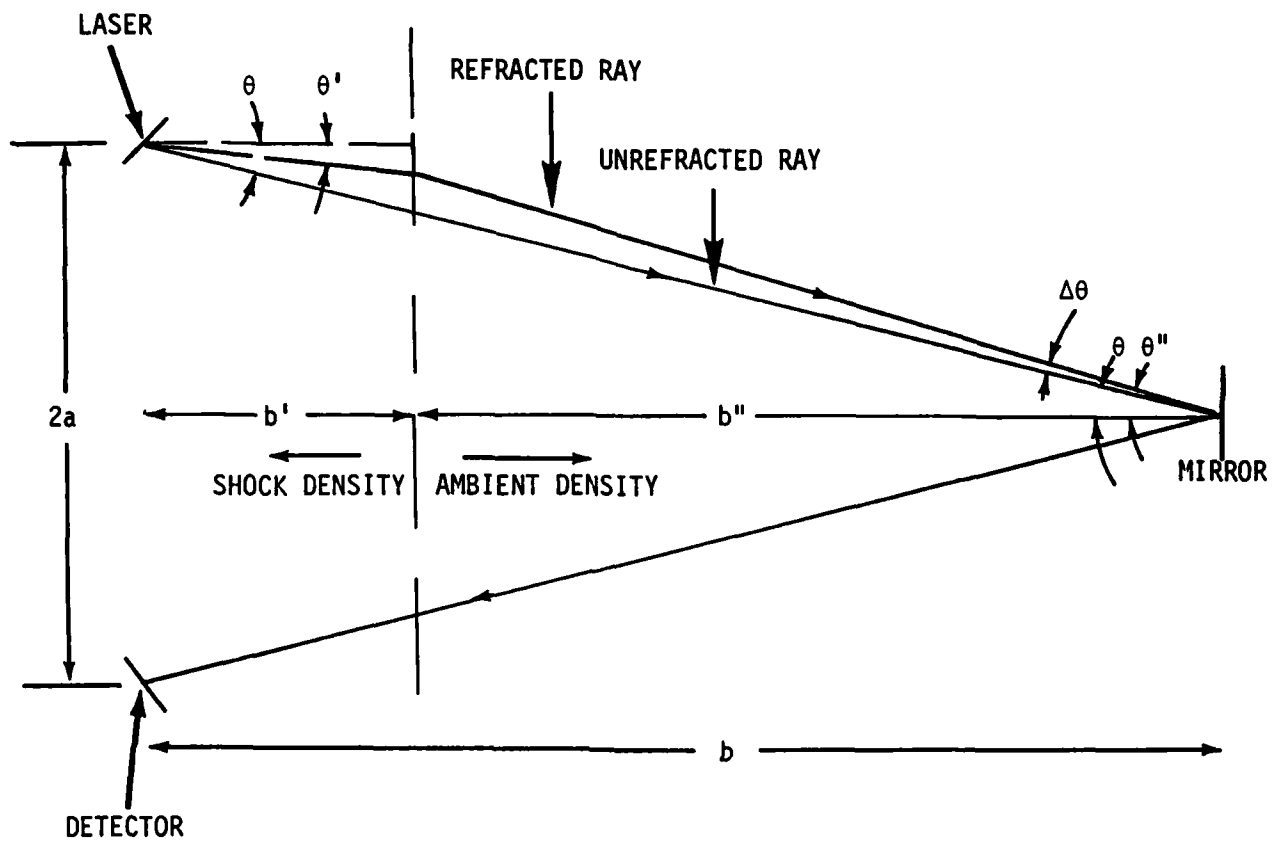


Figure A.3.2. Simplified Refraction Diagram

source-mirror distance. Actually the ray is refracted at the shock front introducing an error into the velocity measurement. The magnitude of this error depends on the shock parameters and the angle between the ray and the shock front, and will be discussed later.

The second effect of the bow shock on the velocity measurement accuracy depends on the "rate of change" of the shock parameters, that is, how they vary from one measurement time to the next. This depends on the sled acceleration and a worst case analysis (200 g acceleration) is given later in this report. As the shock parameters vary over one measurement interval they change the beam's optical paths in such a way as to induce an "apparent displacement" of the sled. (This is the displacement that would be measured even if the sled were to be static relative to the flag, but the shock parameters were varied over the time interval.) The requirement on these changes is that the "apparent displacement" due to changing shock parameters be less than 1 part per 2 million of the actual sled displacement during the 1 millisecond measurement interval.

#### EFFECT OF REFRACTION AT THE SHOCK WAVE FRONT ON THE ACCURATE MEASUREMENT OF $\cos\theta$

To find the value of the possible error in  $\cos\theta$  it is necessary to know how the ray is refracted at the shock front. To first order, the net angle of refraction of the ray as it propagates through the shock depends on the difference in the density of the air from the stagnation point, on the face of the sensing head, to the region outside the shock, rather than on the density profile. Therefore the density change, approximated to occur at a point (the shock front), will be the difference between the stagnation density and the free stream density.

The angle the ray is refracted through is also dependent on its angle with respect to the shockfront. This angle depends in turn on

the sensing head geometry, since the shock shape is dependent in a complex way on this geometry. A good approximation to the refraction effects can be made assuming the sled shock front is parallel to the reflecting mirror. This is a reasonable assumption since the shock normal at the front of the shock is parallel to the sled velocity vector, and this is the region where the optical paths traverse the shock (see Figure A.3.3).

#### LIST OF THE SYMBOLS USED FOR THE ANALYSIS

$\theta$  = arc tan  $a/b$  = angle of undeflected ray with respect to sled velocity vector and shock normal

$a$  = 1/2 (laser to detector distance)

$b$  = laser or detector to mirror distance

$b'$  = shock stand off distance

$b''$  = distance from shock front to mirror

$\theta'$  = angle of ray behind shock with respect to sled velocity vector and shock normal

$\theta''$  = angle of ray in front of shock with respect to sled velocity vector and shock normal

$\Delta b$  = the sled displacement over the measuring interval

$\Delta d$  = the measured change in optical paths (fringe count)

$\Delta\theta = \theta'' - \theta$  = the difference between the deflected and undeflected rays' angles.

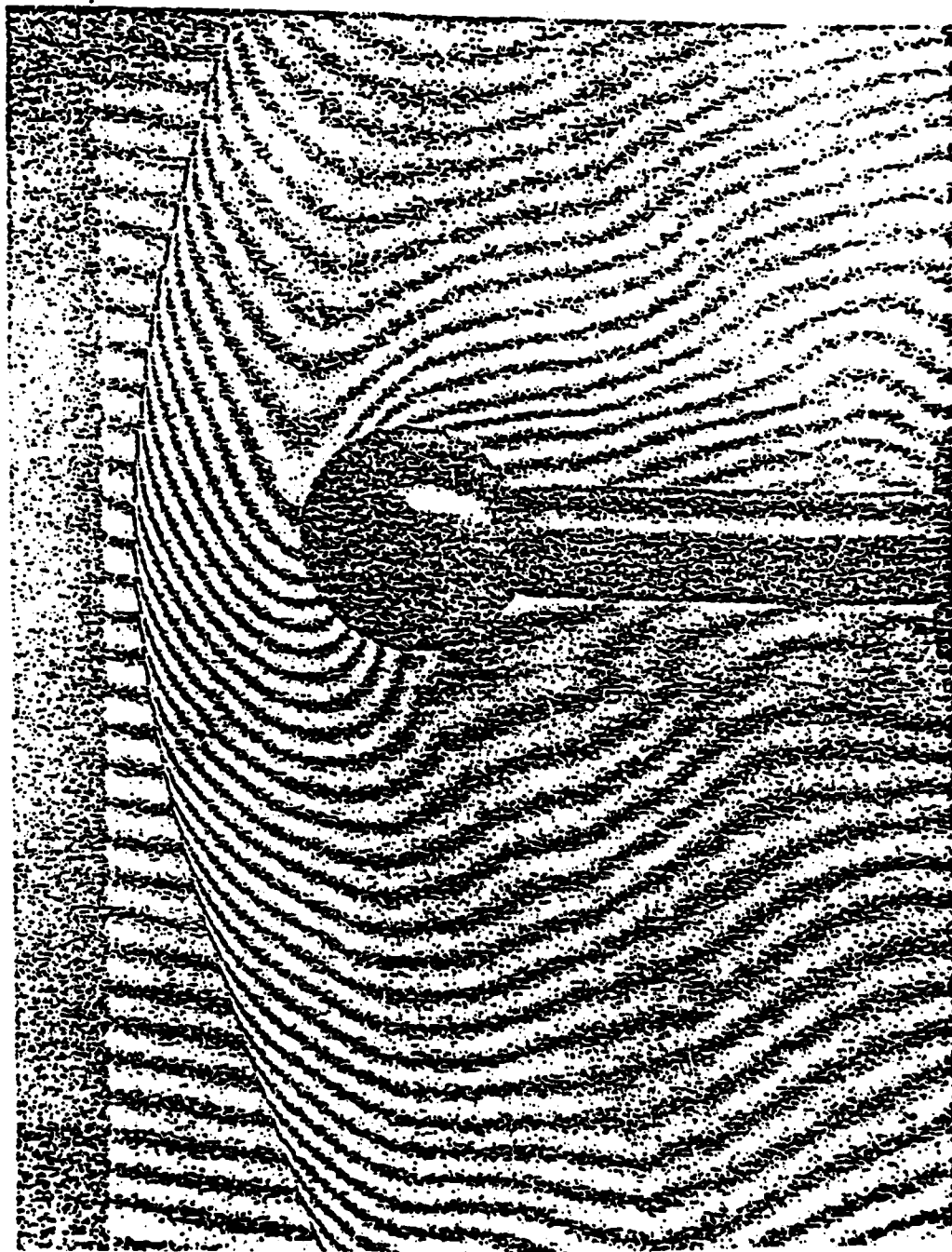


Figure A.3.3. Interferogram of flow around sphere at  
Mach number 1.17;  $d = 1/4$  inches.

At Mach 2, the change in density across the shock wave front corresponds to a value of  $\rho_{\text{shock}}/\rho_s$  of about 4.3 ( $\rho_{\text{shock}}$  = the air density behind the shock at the stagnation point, and  $\rho_s$  = that in front of the shock). Since the index of refraction in air of fixed composition depends only on the air density, the change in index of refraction across the shock front can be calculated from a knowledge of the change in density. Although the ambient conditions outside the shock area are not known exactly, it is reasonable to assume that the density of air outside the shock is just that at standard conditions,  $\rho_s$ . Then the index of refraction outside the shock is just  $1 + \beta$ , and the index of refraction behind the shock is  $1 + \beta (\rho_{\text{shock}}/\rho_s)$ .

Therefore

$$\frac{n_{\text{shock}}}{n} = \frac{1 + \beta (\rho_{\text{shock}}/\rho_s)}{1 + \beta}$$

where

- $n_{\text{shock}}$  = the index of refraction behind the shock
- $n$  = the index of refraction in front of the shock
- $\rho_{\text{shock}}$  = the air density behind the shock = the stagnation density
- $\rho_s$  = the air density in front of the shock
- $\beta$  = .000291 for He-Ne laser wave length

and from tables  $\rho_{\text{shock}}/\rho_s$  at Mach 2 = 4.3

so

$$\frac{n_{\text{shock}}}{n} = 1.00096$$

Next consider  $\Delta b$ , the sled displacement over the sampling time. If an undeflected ray is assumed, this quantity will be calculated as the change in the optical path multiplied by the cosine of the angle

$\theta = \text{arc tan } a/b$ . This is in error, because the actual angle of the ray with respect to the sled velocity is  $\theta''$ . The magnitude of the error introduced into the velocity measurement will then depend on the difference between the values of  $\cos\theta$  and  $\cos\theta''$ . Using the previously mentioned assumptions, this difference can be calculated as follows.

From geometrical considerations

$$b' \tan \theta' + b'' \tan \theta'' = a$$

and, applying the laws of refraction,

$$\sin\theta' = \frac{n}{n_{\text{shock}}} \sin\theta''$$

Combining these two results,

$$b' \frac{n}{n_{\text{shock}}} \sin\theta'' / \cos\theta' + b'' \frac{\sin\theta''}{\cos\theta''} = a$$

$$\text{so } \sin\theta'' = \frac{a}{b' \left( \frac{n}{n_{\text{shock}}} \frac{1}{\cos\theta'} - \frac{1}{\cos\theta''} \right) + \frac{b}{\cos\theta''}}$$

Since  $b' \ll b$ , and  $\cos\theta' \approx \cos\theta''$

this can be estimated as

$$\sin\theta'' = \frac{a}{\frac{b'}{\cos\theta''} \left( \frac{n}{n_{\text{shock}}} - 1 \right) + \frac{b}{\cos\theta''}}$$

or

$$\tan\theta'' = \frac{a}{b' \left( \frac{n}{n_{\text{shock}}} - 1 \right) + b}$$

so,

$$\Delta\theta = \text{arc tan} \left( \frac{a}{b' \frac{n}{n_{\text{shock}}} - 1 + b} \right) - \text{arc tan } a/b .$$

Remembering that the exact form of this equation, and the relevant parameters depend on the exact positioning of the laser and detector, and on the sled shape and Mach number, a rough approximation to the magnitude of the error can be obtained with reference to the shock parameter tables and an assumed geometry for the interferometer.

Now the smallest tolerance which must be placed on  $\theta$  during a sled run will be calculated. Since the value of  $\cos\theta$  is approximately equal to 1, the part per 2 million accuracy goal requires a determination of  $\cos\theta$  to 1 part per 2 million of 1 which is  $5 \times 10^{-7}$ . The corresponding error allowed in  $\theta$  can be found from the relationship between  $\Delta\theta$  and  $\Delta\cos\theta$  at the angle of interest,

$$(\Delta\theta)_{\text{max}} = (\Delta\cos\theta)_{\text{max}} \left( \frac{d\theta}{d\cos\theta} \right) .$$

The smallest error budget allowance for  $\theta$  will occur when

$$\frac{d\theta}{d\cos\theta}$$

assumes its smallest value. This will be when

$$\theta = \arctan \frac{a}{b}$$

is a maximum, or equivalently, when  $b$  is a minimum (see Figure A.3.1). The minimum value obtained by  $b$  is 60 inches therefore the angle of

$$\theta = \arctan \frac{.5 \text{ inches}}{60 \text{ inches}} = .008 \text{ radians.}$$

$$\left( \frac{d\theta}{d\cos\theta} \right) \text{ at } .008 \text{ radians} = 125 .$$

Therefore,

$$(\Delta\theta)_{\max} = (5 \times 10^{-7}) \times 125$$

$$(\Delta\theta)_{\max} = 6 \times 10^{-5} .$$

An inspection of the equation for  $\Delta\theta$  shows that  $\Delta\theta$  decreases as  $b$  increases. Therefore the worst case would be the distance of closest approach between the sensing head and the mirror,  $b = 5 \text{ ft.}$  Also assume  $a = .04 \text{ ft.}$

Using these values,

$$\Delta\theta = \arctan \frac{.04 \text{ ft.}}{b' \left( \frac{n}{n_{\text{shock}}} - 1 \right) + 5 \text{ ft.}} = .008 \text{ radians} .$$

At Mach 2,  $\frac{n_{\text{shock}}}{n} = 1.00096$ . The value of  $b'$  can be found from the ratio of shock standoff distance to projectile diameter, which at Mach 2  $\approx .38$ . Assuming a 20 mm sensing head diameter (the exact geometry has not been designed but this is a reasonable approximation),

the value of  $b'$  would be 3.8 mm. Substituting these values into the above equation gives:

$$\Delta\theta = 2.0 \times 10^{-8} \text{ radians} .$$

This is over 3 orders of magnitude below the tolerable error, and is a negligible effect.

A problem could arise if the alignment of the ray relative to the shock was such that the angle between the two increased above the previously assumed value. An estimate of the effect of increasing this angle can be obtained as follows. Refer to Figure A.3.4.

The only new quantity here is the angle  $\alpha$ , which the shock makes with the normal to the sled velocity vector.  $b'$  and  $b''$  are now measured from the sensing head and mirror respectively to the point where the ray intercepts the shock front.

From geometrical considerations,

$$b' \Delta\theta' \approx b'' \Delta\theta$$

$$\text{or} \quad \Delta\theta' \approx b''/b' \Delta\theta \quad (1)$$

and, from the laws of refraction

$$\sin(\theta' + \alpha) = n/n_{\text{shock}} \sin(\theta'' + \alpha)$$

$$\begin{aligned} \text{so} \quad \Delta\theta' &= \theta - \theta' \\ &= \theta - \arcsin \left[ n/n_{\text{shock}} \sin(\theta'' + \alpha) \right] + \alpha \end{aligned} \quad (2)$$

but,

$$\sin(\theta'' + \alpha) = \sin(\theta + \Delta\theta + \alpha) .$$

The expansion for this into the equation for  $\Delta\theta'$ , and combining Equations 1 and 2

$$\frac{b''}{b'} \Delta\theta = \theta - \arcsin \left[ \frac{n}{n_{\text{shock}}} \left( (\sin\theta \cos\Delta\theta + \cos\theta \sin\Delta\theta) \cos\alpha + (\cos\theta \cos\Delta\theta - \sin\theta \sin\Delta\theta) \sin\alpha \right) \right] + \alpha .$$

Assuming a closest approach between the sled and mirror (largest refraction effect), and the proposed system dimensions of

$$b'' \approx b = 5 \text{ ft.}, \quad a = .04 \text{ ft.}, \quad \theta = \arcsin \frac{.04 \text{ ft.}}{5 \text{ ft.}} ,$$

$$\Delta\theta \text{ (maximum)} = 6 \times 10^{-5} \text{ rads}$$

$$n/n_{\text{shock}} \text{ at Mach 2} = 1/1.00096$$

$$b' \text{ at Mach 2, with a 10 mm radius sensing head} \\ = .5 \text{ cm} - .02 \text{ ft.}$$

Substituting these values

$$|\theta'| = .007 = |-\arcsin (.008 \cos\alpha + .999 \sin\alpha) + \alpha| .$$

By trial and error the maximum allowable value for the angle  $\alpha$  is about .8 rads = 45°, much larger angle than would occur with the proposed system geometry.

### Conclusions

Refractive effects due to the sensing head shock in the supersonic regime should be negligible.

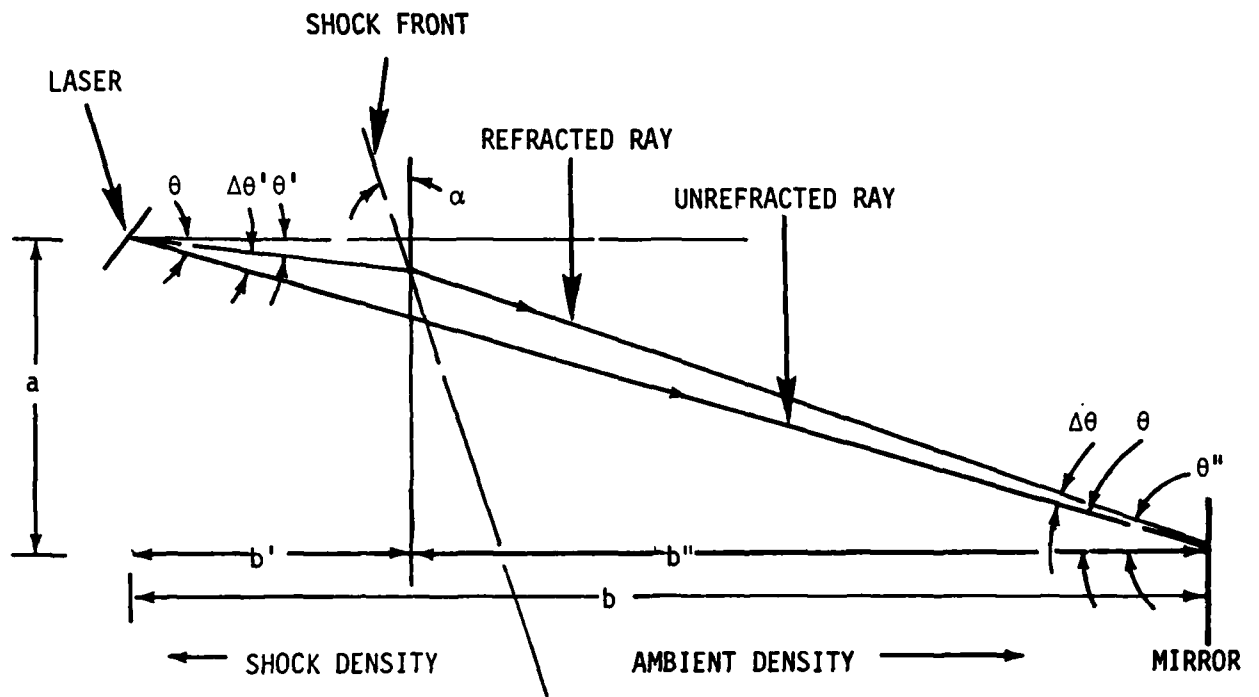


Figure A.3.4 Angled Shock Front

EFFECTS OF BOW SHOCK IN INTRODUCING AN APPARENT DISPLACEMENT  
OF THE SLED OVER THE .001 SEC SAMPLING TIME

Since the shock parameters change with the sled velocity, their maximum change per unit time will be at the maximum value of sled acceleration. So for a worst case, assume an acceleration of 200 g =  $6.4 \text{ ft}/\frac{1}{1000} \text{ sec}^2$ .

The tables in Reference 1 show that the changes in shock density with change in Mach number is approximately linear between Mach 1 and 2. Also, the greatest change in stand-off distance (of the shock from the sensing head) with Mach number occurs closer to Mach 1 rather than Mach 2, see Figure A.3.5. Let  $\Delta p$  = virtual change in path length due to the changing shock parameters. This is the distance it would "look like" the sled had traveled in 1/1000 sec if you were to hold the sled at a constant distance, and only vary the shock density and stand-off distance of the wave front.

The velocity must be known to an accuracy of  $\pm .001$  fps.

$$.001 \text{ ft/sec} \times .001 \text{ sec} = 10^{-6} \text{ ft.}$$

This is the value of  $\Delta p$  which corresponds to the entire error budget.

$$\Delta p \text{ (maximum)} = 10^{-6} \text{ ft.}$$

As the shock parameters change  $\Delta p$  is caused by two effects which will be calculated separately.

The first is that as the density behind the shock front changes over  $\frac{1}{1000}$  of a second, the refraction angle changes and so the optical path changes, as can be seen from Figure A.3.6.

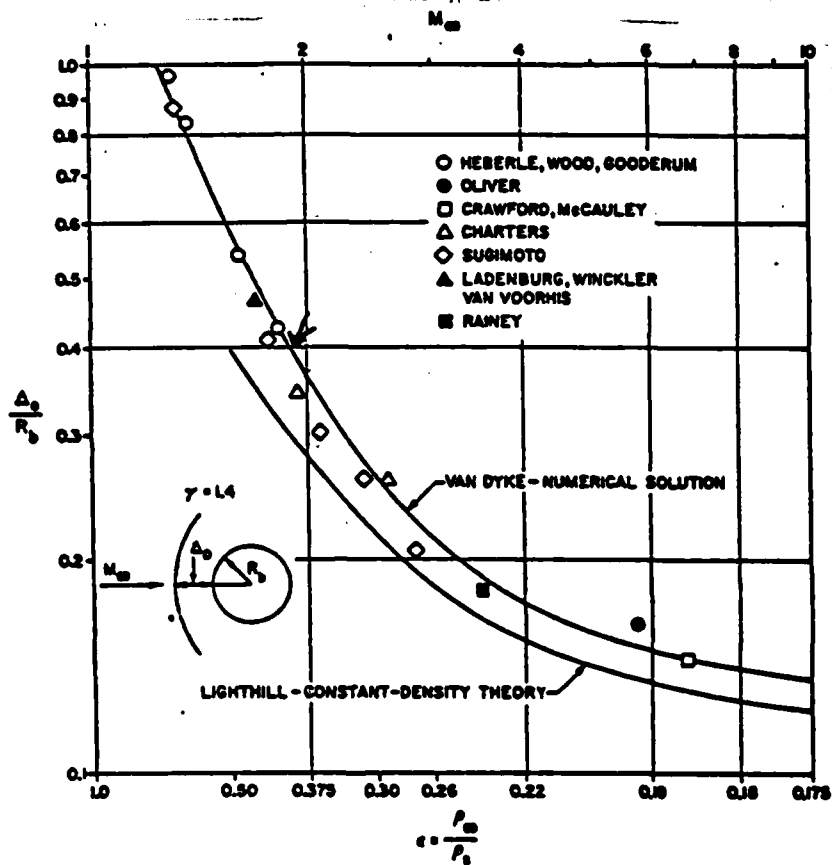


Figure A.3.5. Stagnation point detachment distance for a sphere

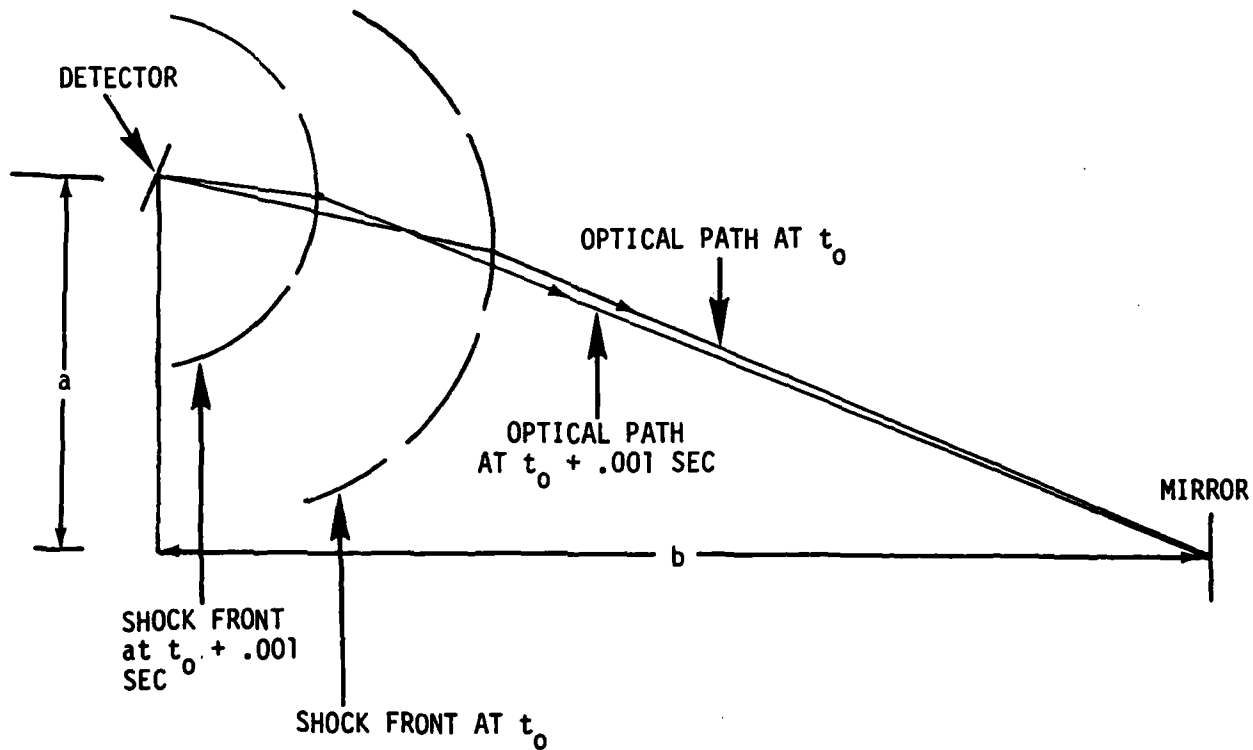


Figure A.3.6 Changes with Time

The second effect arises as the index of refraction behind the shock increases (or decreases) over  $\frac{1}{1000}$  sec, and the shock stand-off distance increases (or decreases) thus changing the optical path length through the shock region.

OPTICAL PATH LENGTH CHANGES OVER .001 SEC DUE  
TO REFRACTION AT THE SHOCK WAVE FRONT

In order to consider refraction alone, approximate the geometry as shown in Figure A.3.7.

$$\text{Path A} = 2(P_1 + P_2)$$

$$\text{Path B} = 2(P_3 + P_4)$$

Path A = the path of the ray at  $t_0$

Path B = the path of the ray at  $t_0 + 1/1000$  sec

Where  $t_0$  = the time at the start of the measuring interval, and  
 $(t_0 + \frac{1}{1000}$  sec) = that at the end.

As the index of refraction of the compressed air behind the shock wave changes, the path changes from A to B.

Figure A.3.7 shows the front "flat". This approximation is valid since you are concerned with changes in the refraction angle. To determine the exact magnitude of refraction changes you would have to know the shape of the shock exactly, because as the sled interrupter distance changes, the way the angle of the ray through the shock changes depends on the shape of the shock around the sensing head.

In assuming a flat shock front you can determine the maximum angle allowable between a ray incident from behind the shock front and the

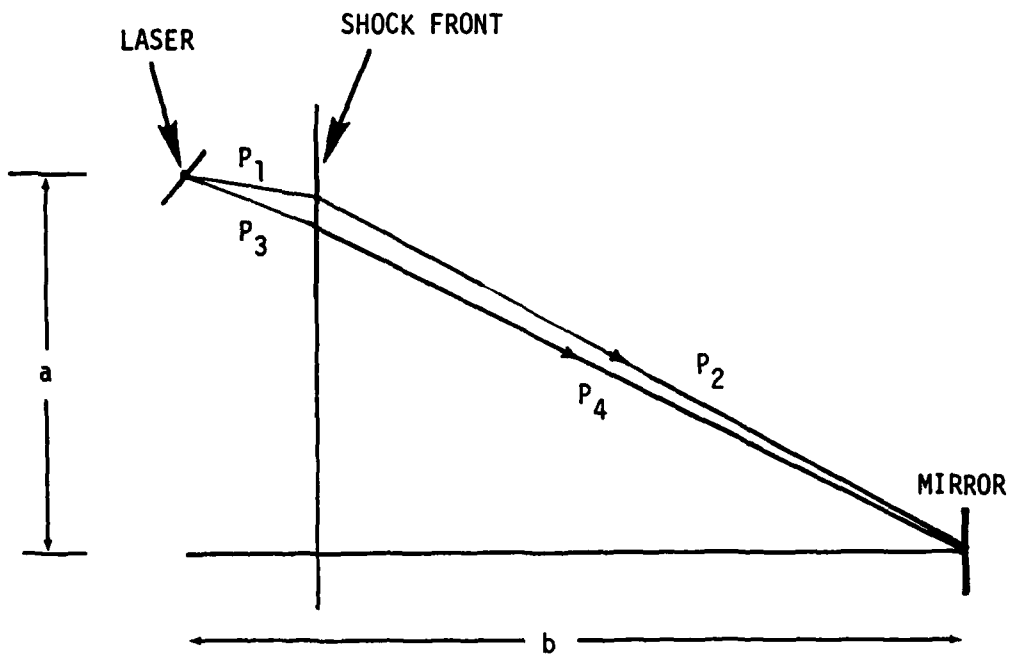


Figure A.3.7 Refraction Approximation

be  $t_0 + 1/1000$  sec. What you need to calculate refraction effects is the ratio  $\frac{n_{\text{shock}}}{n}$  at  $(t_0)$  and at  $(t_0 + 1/1000 \text{ sec})$ .

Since M at

$$t_0 = 1$$

$$n_{\text{shock}} \text{ at } t_0 = n \text{ at } t_0$$

so 
$$\frac{n_{\text{shock}}}{n} \text{ at } t_0 = 1 .$$

$$\begin{aligned} M \text{ at } (t_0 + 1/1000 \text{ sec}) &= M \text{ at } (t_0) + 6 \times 10^{-3} \\ &= 1.006 \end{aligned}$$

and  $n_{\text{shock}}$  can be calculated from fact that  $n_{\text{shock}} = 1 + \beta \frac{\rho_{\text{shock}}}{\rho_s}$

$$= 1 + \beta \left( \frac{\rho_{\text{shock}}}{\rho_s} \text{ (at } t_0) + \Delta \left( \frac{\rho_{\text{shock}}}{\rho_s} \right) \right)$$

$$= 1 + \beta (1 + 0.010)$$

$$= 1 + .000291 (1.010)$$

$$= 1.000294 .$$

So 
$$\frac{n_{\text{shock}}}{n} \text{ (at } t_0 + 1/1000 \text{ sec)} = \frac{1.000294}{1.000291}$$

$$= 1.00000297 .$$

So you have

$$\frac{n_{\text{shock}}}{n} = 1 \text{ at } (t_0)$$

$$= 1.00000297 \text{ at } (t_0 + 1/1000 \text{ sec}) .$$

front normal. This then sets the specifications on the sensing head geometry required to keep this angle always below its maximum value.

The larger part of the change in path length can be found by calculating the difference in the lengths of  $P_2$  and  $P_4$

$$\Delta p = P_2 - P_4 < 10^{-6} \text{ ft.}$$

Now,

$$\begin{aligned} \text{Maximum acceleration of sled} &= 200 \text{ g} = 6400 \text{ ft/sec}^2 \\ &= 6.4 \text{ ft}/\frac{1}{1000} \text{ sec}^2 . \end{aligned}$$

Maximum velocity change over 1/1000 sec = 6.4 ft/sec.

$$\text{Mach \#} = \frac{\text{vel}}{1090 \text{ fps}} \quad \Delta \text{Mach \#} = \frac{\Delta v}{1090 \text{ fps}} = \frac{6.4}{1090} = 6 \times 10^{-3}$$

Using data from Liepmann & Roshko<sup>(1)</sup>,  $\rho_{\text{shock}}/\rho_s$  varies approximately linearly with changing Mach #. Linear interpolation yields the following values.

$$(M(\text{Mach \#}) \text{ at } t_0) = 1.000; M \text{ at } t_0 + 1/1000 \text{ sec} = 1.006 .$$

$$\text{From the tables, at } M = 1; \frac{\rho_{\text{shock}}}{\rho_s} = 1.000$$

$$M = 1.01; \frac{\rho_{\text{shock}}}{\rho_s} = 1.017$$

So by interpolation at  $M = 1.006$ ,  $\rho_{\text{shock}}/\rho_s = 1.010$ ,

and 0.010 = change in value of  $\rho_{\text{shock}}/\rho_s$  in 1/1000 sec.

Let the beginning time of the measuring interval be  $t_0$  and the end time be  $t_0 + .001$  sec.

If  $\frac{n_{\text{shock}}}{n}$  at Mach 1 = 1 the ray is not refracted at  $t_0$ , but continues straight to the interrupter. Then  $P_2 - P_4$  can be calculated from Figure A.3.8.

$$P_2 - P_4 = \sqrt{a^2 + b^2} - \sqrt{(a - \Delta a)^2 + b^2}$$

where  $\Delta a \approx \Delta \alpha b$ .

Therefore, the maximum value of  $\Delta a$  occurs when  $b$  is a maximum = 18 ft. (each flag is used when it is between 5 and 18 ft. away) and  $\Delta a \approx \Delta \alpha \times 18$  ft.

Now  $\Delta \alpha$  is just the change in refraction angle at the shock wave front over 1/1000 sec

Letting  $\alpha_1$  = angle of refraction of ray incident from behind shock front at  $t_0$ .

$\alpha_2$  = angle of refraction of ray incident from behind shock at  $(t_0 + 1/1000 \text{ sec})$ .

Then to first approximation (assuming both rays are incident from behind the shock front at the same angle  $\alpha$ )

$$\begin{aligned} \Delta \alpha &= \alpha_1 - \alpha_2 = \text{arc sin} \left( \frac{n_{\text{shock}}}{n} \left( \text{at } t_0 + \frac{1}{1000} \text{ sec} \right) \text{ sin } \alpha \right) \\ &\quad - \text{arc sin} \left( \frac{n_{\text{shock}}}{n} \left( \text{at } t_0 \right) \text{ sin } \alpha \right) \\ &= \text{arc sin} (1.00000297 \text{ sin } \alpha) - \text{arc sin} (\text{sin } \alpha) \\ &= \text{arc sin} (1.00000297 \text{ sin } \alpha) - \alpha \end{aligned}$$

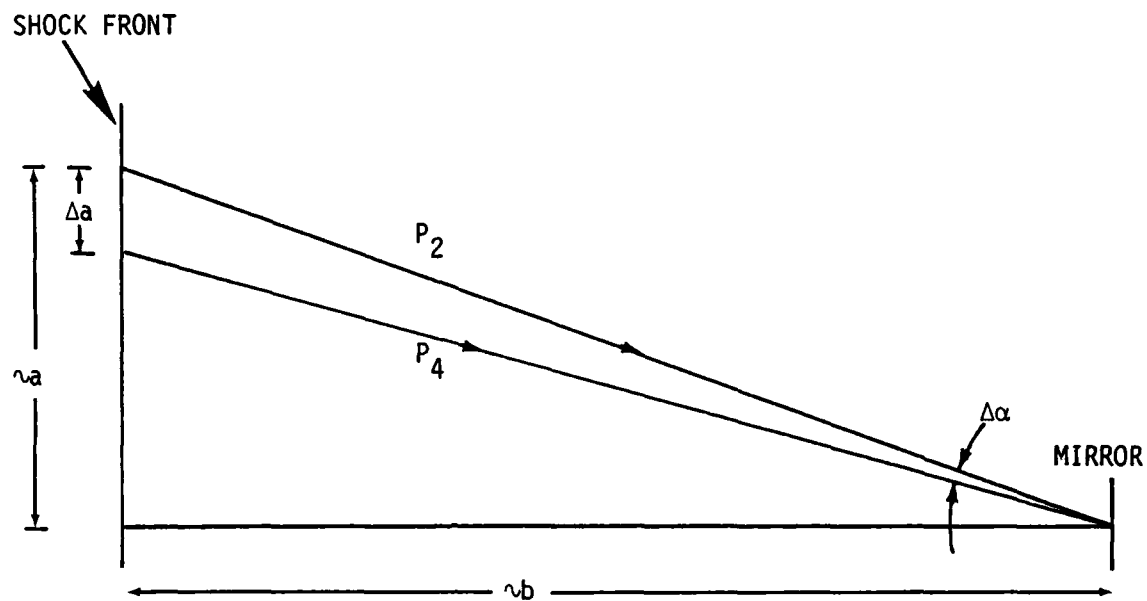


Figure A.3.8 No-Refraction Approximation



$$\text{Now } P_2 - P_4 = \sqrt{a^2 + b^2} - \sqrt{[a - (\Delta\alpha b)]^2 + b^2} .$$

Using  $b = 18 \text{ ft.}$

$$a = .5''$$

$$\text{and } P_2 - P_4 < 10^{-6} \text{ ft.}$$

By trial and error  $\Delta\alpha$  maximum  $\approx 2 \times 10^{-6}$  radians (assuming the  $\Delta\alpha$  change in refraction angle depends only on the change in the shock wave density over 1/1000 sec).

$$\begin{aligned} \text{So } \Delta\alpha (\text{max}) &= 2 \times 10^{-6} \text{ radians} \\ &= \text{arc sin } (1.00000297 \text{ sin } \alpha) - \alpha . \end{aligned}$$

Use this to solve for  $\alpha$  (max) = the maximum allowable angle between the ray incident from behind the shock front and the normal to the front.

$$\begin{aligned} \text{Solving gives } \alpha \text{ max} &= .6 \text{ radians} \\ &= 35^\circ . \end{aligned}$$

Comparing this to the maximum value set on this angle due to the absolute value of refraction above, it can be seen that this condition is the limiting one although neither is critical.

#### SHOCK TRANSIT TIME EFFECTS

As the stand-off distance of the shock from the sensing head, and the speed of light in the shock area change, the optical path length varies, because the ray to the flag spends more, or less time traversing the shock area.

We want to calculate the change in optical path length  $\Delta P$  due to these effects. We can find this from the fact that  $\Delta P =$  the change in

traversal time of the ray due to changing shock parameters, multiplied by the value of C (speed of light) used to calculate the sled velocity from the observed doppler shift. (Call this value  $C_{\text{air}}$ ). (See Figure A.3.9).

$$\text{Then } \Delta P = \Delta t \times C_{\text{air}} .$$

Where  $t$  = the change in light traversal time over .001 sec due to the changing shock parameters. This equals the change in traversal time as the stand-off distance of the shock front  $\Delta_o$  changes in 1/1000 sec plus the change in traversal time due to the increased (or decreased) air density behind the shock wave, or

$$t = \left[ \frac{-\Delta(\Delta_o)}{C_{\text{air}}} + \frac{\Delta(\Delta_o)}{C'_{\text{shock}}} \right] + \left[ \frac{\Delta_o}{C'_{\text{shock}}} - \frac{\Delta_o}{C_{\text{shock}}} \right] .$$

$\Delta_o$  = stand-off distance at  $t_o$

$\Delta(\Delta_o)$  = change in stand-off distance from  $t_o$  to  $t_o + 1/1000$  sec

$C_{\text{air}}$  = the velocity of light in air

$C'_{\text{shock}}$  = the velocity of light behind the shock wave at  $t_o + 1/1000$  sec

$C_{\text{shock}}$  = the velocity of light behind the shock at  $t_o$ .

The velocity of light in the region of interest is found from

$$n = \frac{C_{\text{vacuum}}}{C_{\text{region}}} = 1 + \beta \frac{\rho_{\text{region}}}{\rho_s}$$

$$\beta = .000291 \text{ at } 6328 \text{ \AA}$$

$\rho_s$  = density of air at standard conditions

$\rho_{\text{region}}$  = density of air in the region of interest.

Since the velocity of light used to determine the sled velocity ( $C_{\text{air}}$ ) depends on measurements to be made at the track prior to a sled run, a good approximation to make for  $C_{\text{air}}$  would be that  $C_{\text{air}}$  = the speed of light in air at standard conditions.

( $\Delta P$  depends on the difference between  $C_{\text{air}}$  and  $C_{\text{shock}}$ ) .

Therefore,

$$\Delta t = \frac{\Delta(\Delta_o)}{C_{\text{vacuum}}} \left( \left( 1 + \beta \frac{\rho'_{\text{shock}}}{\rho_s} \right) - \left( 1 + \beta \frac{\rho_s}{\rho_s} \right) \right) + \frac{\Delta_o}{C_{\text{vacuum}}} \left( \left( 1 + \beta \frac{\rho'_{\text{shock}}}{\rho_s} \right) - \left( 1 + \beta \frac{\rho_{\text{shock}}}{\rho_s} \right) \right)$$

where as before the primed values refer to values at  $t_o + 1/1000$  sec, and the unprimed at  $t_o$ .

Cancelling terms

$$\Delta t = \frac{\Delta(\Delta_o)}{C_{\text{vacuum}}} \beta \left( \frac{\rho'_{\text{shock}}}{\rho_s} - 1 \right) + \frac{\Delta_o}{C_{\text{vacuum}}} \beta \left( \frac{\rho'_{\text{shock}}}{\rho_s} - \frac{\rho_{\text{shock}}}{\rho_s} \right)$$

Substituting values for  $\rho_{\text{shock}}/\rho_s$  and  $\rho'_{\text{shock}}/\rho_s$  from above:

$$\rho_{\text{shock}}/\rho_s = 1.0000 \qquad \rho'_{\text{shock}}/\rho_s = 1.0102$$

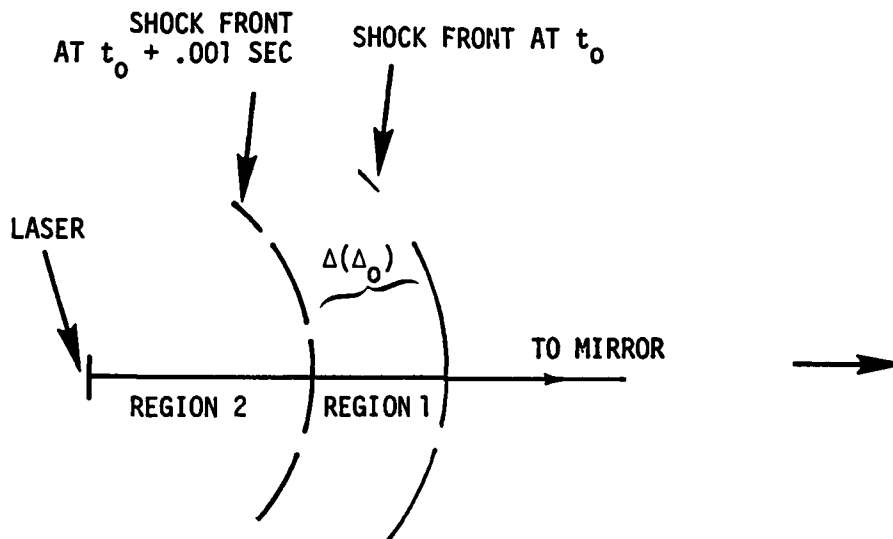


Figure A.3.9 Shock Transit Time Effects

$$\Delta t = \frac{2.968 \times 10^{-6}}{C_{\text{vacuum}}} \times [\Delta(\Delta_o) + \Delta_o]$$

and  $\Delta p = \Delta t \times C_{\text{air}}$

$$= 2.968 \times 10^{-6} \times \frac{1}{n_{\text{air}}} \times [\Delta(\Delta_o) + \Delta_o]$$

$$= 2.968 \times 10^{-6} \times \frac{1}{1.000291} \times [\Delta(\Delta_o) + \Delta_o]$$

$$= 2.969 \times 10^{-6} \times [\Delta(\Delta_o) + \Delta_o].$$

Now the values of  $\Delta(\Delta_o)$  and  $\Delta_o$  both depend on the geometry of the sensing head that the shock forms around. Since the requirement on  $\Delta p$  is that it be less than  $10^{-6}$  ft., the above equation sets a requirement on the value of  $[\Delta(\Delta_o) + \Delta_o]$ . This requirement is:

$$\frac{10^{-6} \text{ ft.}}{2.969 \times 10^{-6}} > [\Delta(\Delta_o) + \Delta_o]$$

or

$$.34 \text{ ft.} > \Delta(\Delta_o) + \Delta_o.$$

Since  $\Delta(\Delta_o)$  is  $\ll \Delta_o$

this requirement is basically that

$$\Delta_o < .34 \text{ ft. at Mach 1.}$$

Around Mach 1 the stand-off distance of the shock is approximately equal to one body diameter of a blunt shaped projectile. Therefore, an approximate requirement on the sensing head shape would be that its diameter be less than .34 ft. or 10 cm.

One way of achieving a smaller stand-off distance is to make the shape of the sensing head more pointed than round. (See Figure A.2.10).

The problem with doing this is that as the laser beam tracks the flag the stand-off distance the beam sees varies more than it would with a "flatter" shock, so  $\Delta(\Delta_0)$  becomes a larger fraction of  $\Delta_0$ . Also, as the sled pitches and yaws the ray sees a smaller or larger stand-off distance. (See Figure A.3.11). But, given the maximum yaw angle is about  $10^{-3}$  radians, and the angular change of the ray as the flag moves from 18 ft. to 5 ft. ahead of the sled is around  $6 \times 10^{-3}$  radians, the value of  $\Delta(\Delta_0)$  over 1/1000 sec would still be a small part of  $\Delta_0$ .

To keep the body diameter of the sensing head small (that is, the diameter determining the shock shape) dual sensing heads could be used. Then one head would be the source of the laser beam, and the second would contain the detector pinhole. (See Figure A.3.12).

### Conclusions

Refraction effects on the velocity measurement should be negligible in the supersonic regime.

To keep changes on the optical path length due to changing shock parameters to less than 1 part per 2 million over the 1/1000 sec sampling time, the sensing head must have a diameter (seen by the shock) of less than about 10 cm.

The above conclusions are for supersonic flow and more work on what happens to the optical path lengths when the sled traverses the transonic regime is given in Appendix A.14.

SUPERSONIC SHOCK FRONT

SENSING HEAD

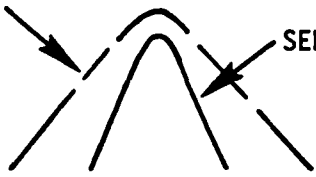


Figure A.3.10 Pointed Sensing Head

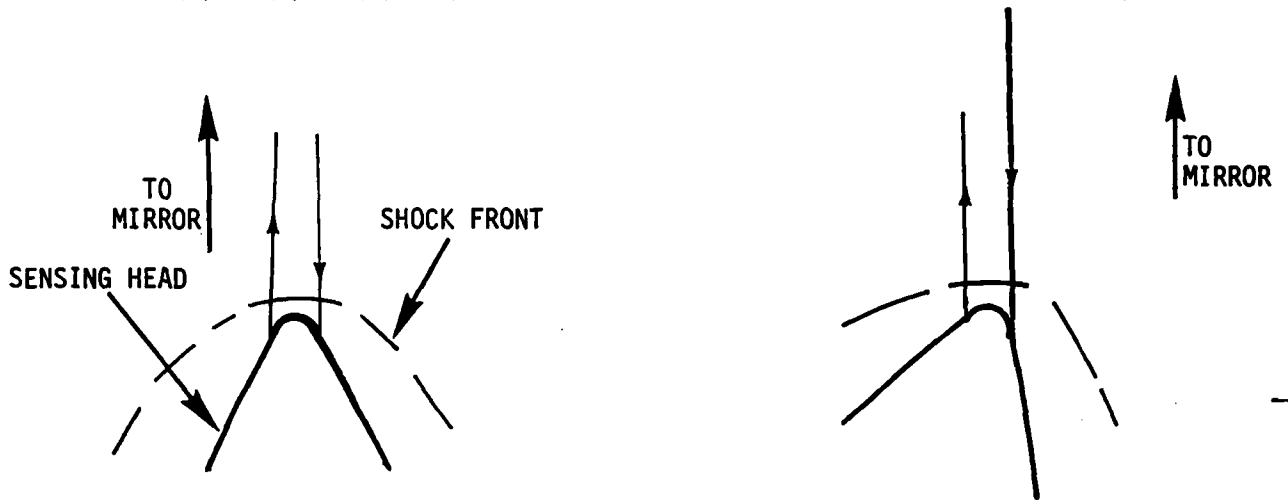


Figure A.3.11 Yaw Effects

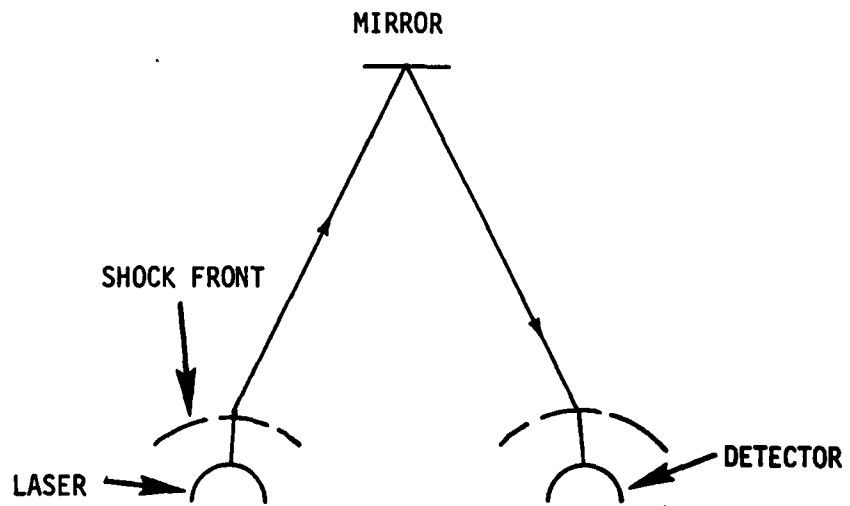


Figure A.3.12



#### APPENDIX A.4

##### VARIATIONS IN THE OPTICAL PATH LENGTH DUE TO TEMPERATURE FLUCTUATIONS ON THE FLAG INTERFEROMETER SYSTEM

Temperature fluctuations in the atmosphere induce corresponding fluctuations in the optical path lengths of the laser beam used in the flag interferometer system. The problem is to determine how, and to what degree these temperature fluctuations may affect the velocity measurement made using this system.

One error introduced by atmospheric variations arises if the temporal or spatial structure of the temperature fluctuations is such as to induce an apparent displacement  $\Delta p$  from one measuring time to the next. This is the displacement that would be measured even if the sled was stationary and only the atmospheric parameters were changing. This apparent displacement appears as "noise" on the actual measurement. An estimate of the apparent displacement can be calculated as follows:

Assume the sled is travelling at 2000 fps. Then in the 1/1000 sec interval used for the measurement the sled travels 2 ft.

As can be seen from Figure A.1 the spatial structure of the temperature fluctuations will affect the velocity measurement because  $\overline{DB}$  and  $\overline{FB}$  do not overlap, so the beam is not travelling through the same atmospheric paths. If  $\overline{FB}$  differs from  $\overline{DB}$  by more than geometrical considerations dictate there is an error introduced. To estimate this error the theoretical value for optical path length variations from V.I. Tatarski's book Wave Propagation in a Turbulent Medium<sup>(1)</sup> has been used. Tatarski defines a structure function  $D_\phi$  which predicts the mean square phase variations of rays leaving the same source, and propagating through the atmosphere at a lateral distance  $\rho$  from each other. (See Figure A.4.2.)

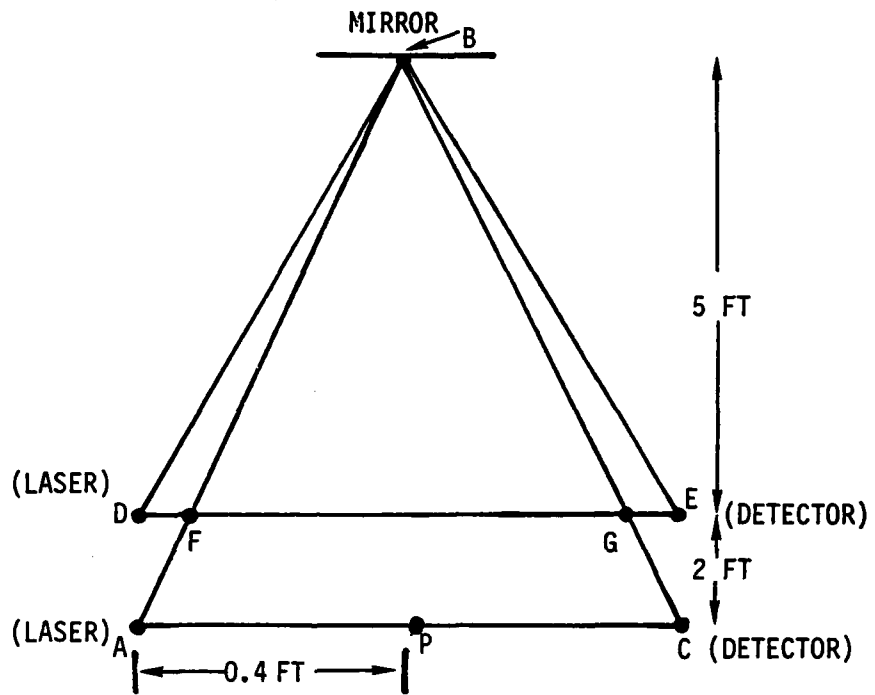


Figure A.4.1  
Flag Interferometer Paths

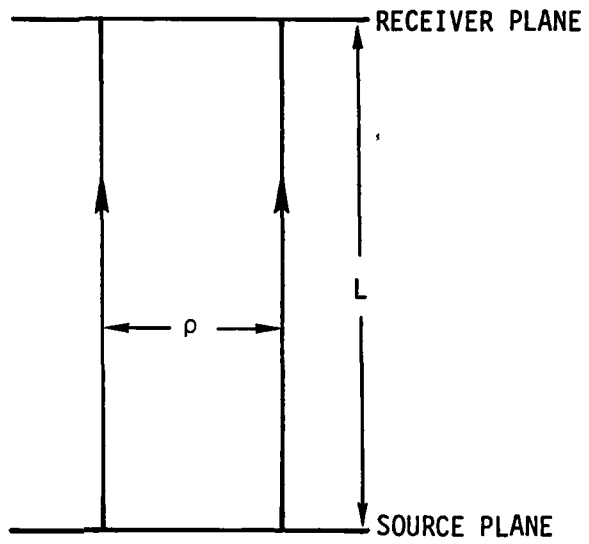


Figure A.4.2

$$D_{\phi}(\rho) = \langle [\phi(\bar{r} + \bar{\rho}) - \phi(\bar{r})]^2 \rangle \quad (\phi = \text{phase}) .$$

Where  $D_{\phi}(\rho)$ , the structure function, is the mean square phase difference in the detector plane between the two rays. The value given in the above reference for  $D_{\phi}$  is:

$$D_{\phi}(\rho) = 2.91 k^2 C_n^2 L \rho^{5/3}$$

where  $k^2 = (2\pi/\lambda)^2$  ( $\lambda$  = the wavelength of light used)

$\rho$  = the lateral separation (see Figure A.4.2) (zero to 1 cm in the 1 VMS)

$L$  = the length of the path (see Figure A.4.2) (1 to 100 m in the 1 VMS)

$C_n^2$  = the index of refraction structure function. This is derived from the temperature structure function  $C_T^2$  which is defined as the mean square temperature difference between 2 points (averaged over a time span of about 1 minute), divided by the distance between the two points raised to the 2/3 power.  $C_n^2 = \langle [T_1 - T_2]^2 \rangle / d^{2/3}$ . Over a horizontal distance equal roughly to the height of the horizontal plane above the ground, this quantity is independent of distance between the two points used for the measurement.

$C_T^2$  is related to  $C_n^2$  by the formula

$$C_n^2 = [(79P/T^2) \times 10^{-6}]^2 C_T^2$$

(also from Tatarski's Wave Propagation in a Turbulent Medium).

Table A.4.1 contains values for  $C_n^2$  taken at Holloman, by Dr. K. Kunkel<sup>(2)</sup>. Referring again to Figure A.1, let ABC = the optical path at  $t_0$  and DBE = the optical path at  $t' = t_0 + 1/1000$  sec. The above formula for  $D_{\phi}(\rho)$  can be used to estimate the magnitude of the optical path length difference, due to index of refraction fluctuations, between  $\overline{DB}$  and  $\overline{FB}$ . In this case the distance  $\rho$  will be the average lateral

TABLE A.4.1

Fluctuation Indices  $C_n^2$  measured at 8 meters above the ground

	<u>NIGHT</u>	<u>1/2 HOUR AFTER SUNRISE</u>	<u>DAY</u>	<u>1/2 HOUR AFTER SUNSET</u>
SPRING	$3 \times 10^{-14}$	$2 \times 10^{-15}$	$10^{-13}$	$2 \times 10^{-16}$
SUMMER	$1 \times 10^{-14}$		$6 \times 10^{-14}$	$2 \times 10^{-16}$
FALL	$3 \times 10^{-14}$		$4 \times 10^{-14}$	$2 \times 10^{-16}$
WINTER	$4 \times 10^{-14}$		$4 \times 10^{-14}$	$2 \times 10^{-16}$

where  $C_n^2 = (\text{time average of difference in index of refraction over distance } d)^2 \times d^{-2/3}$

d = measurement distance

displacement of  $\overline{FB}$  from  $\overline{DB}$ , which is approximately equal to 1/2 the distance  $\overline{DF}$ . (See Figure A.1.) Therefore, in order to calculate  $\rho$  it is necessary to know the magnitude of  $\overline{DF}$ . From geometry  $\overline{DF}/\overline{DA} = \overline{AP}/\overline{BP}$  or

$$\overline{DF} = (\overline{AP}/\overline{BP}) \times \overline{DA}$$

where

$$\overline{DA} = 2 \text{ ft. (when the sled velocity} = 2000 \text{ fps)}$$

$$\overline{AP} = .04 \text{ ft. (taken from the original proposal)}$$

$$\overline{BP} = 7 \text{ ft.}$$

therefore,  $\overline{DF} = .01 \text{ ft.} = .0035 \text{ meters}$   
 $1/2 (.0035 \text{ meters}) = 1.6 \times 10^{-3} \text{ meters} \rightarrow$  this is approximately the average value of  $\rho$  between the rays.

To get a value for  $C_n^2$  we used the results taken from Holloman, and the fact that  $C_n^2$  varies as  $h^{-4/3}$  where  $h$  = the height above the ground. Assuming the measuring plane we are interested in is around .25 meters off the ground  $\rightarrow C_n^2$  at .25 meters  $\approx C_n^2$  at 8 meters  $\times (8 \text{ meters})^{4/3}$  using the maximum value of  $C_n^2$  at 8 meters, from the Holloman tabulation =  $10^{-13}$

$$C_n^2 \text{ (at .25 meters)} = 10^{-13} \times (8\text{m})^{4/3} / (.25 \text{ m})^{4/3}$$

$$= 1.01 \times 10^{-11} \text{ m}^{-2/3}$$

$L$  here = 5 ft.  $\times 2 = 3$  meters because the light must travel to the flag and back. Therefore:  $D_\phi = 2.91 \times 3.0\text{m} \times 1.01 \times 10^{-11} \times (1.6 \times 10^{-3} \text{ m})^{5/3} \times k^2$   
 $= 1.8 \times 10^{-15} k^2$

$$\sqrt{D_\phi} = \text{root mean square phase variation}$$

$$= 4.2 \times 10^{-8} \times k \text{ radians.}$$

So the corresponding apparent displacement = the phase shift divided by  $2\pi/\lambda$  or

$$\begin{aligned}\Delta p &= \sqrt{D_\phi}/k = 4.2 \times 10^{-8} \text{ meters} \\ &= 1.4 \times 10^{-7} \text{ ft.}\end{aligned}$$

This is the rms path length change due to spatial temperature fluctuations.

$$1.4 \times 10^{-7} \text{ ft}/2 \text{ ft} = 7 \times 10^{-8} = .07 \text{ parts per million.}$$

Therefore, assuming a  $C_n^2$  value of around  $10^{-12}$ , the rms value of  $\Delta p$  is about an order of magnitude better than tolerance, and so the effect of spatial temperature variations on the velocity measurement is not a problem.

Another source of error with regard to atmospheric effects, would arise if the frequency of the temperature fluctuations was such as to allow the possibility of the atmospheric parameters changing significantly over the 1/1000 sec measuring interval. Clifford, et al., in an article in the Journal of the Optical Society of America entitled "Phase Variations in Atmospheric Optical Propagation"<sup>(3)</sup>, have determined experimentally the frequency spectrum of the phase differences induced by the atmosphere. Their results show the frequency power spectrum falling to zero well below 1000 hertz, so the frequency of these variations would appear to be slow enough to make their effect over 1 measurement interval negligible. (The atmospheric parameters don't change significantly from  $t_0$  to  $t_0 + 1/1000$  sec.)

### Conclusions

Assuming that  $C_n^2$  at the height aboveground of the optical paths used in the flag interferometer can be calculated from Kunkel's data

using a  $h^{4/3}$  variance, the temperature fluctuations along the track will not have a significant effect on the velocity measurement.

Even if a greater amount of turbulence than predicted by the  $h^{4/3}$  variance exists along the track, the effect of the turbulence can be neglected up to values of  $C_n^2$   $5 \times 10^{-10}$  (very strong turbulence).

More temperature data taken from the immediate rail environment is necessary to determine the actual magnitude of the turbulence effect.

NOTE: These conclusions assume 4 meter flag spacing.  
Greater flag spacings are considered in  
Appendix A.15.

#### REFERENCES

1. Tatarski, V. I., Wave Propagation in a Turbulent Medium, McGraw Hill, 1961.
2. Dr. Kenneth Kunkel, Personal Communication with Walter Naumann, Effects Technology, Incorporated, Santa Barbara, California.
3. Clifford, Bouricius, Ochs, Ackley, Phase Variations in Atmospheric Optical Propagation, Journal of the Optical Society of America; 61, pp. 1279-1284, (1971).

## APPENDIX A.5

### TRANSLATIONAL INTERFEROMETER PITCH AND YAW SENSITIVITY

Direct vertical motion of the measuring head with respect to the rail changes both paths of reflection equally so no fringe output from the interferometer results. Angle changes are examined below.

#### Translational Interferometer Pitch Sensitivity

The transar recombines the two scattered beams A and B as shown in Figure A.5.1.

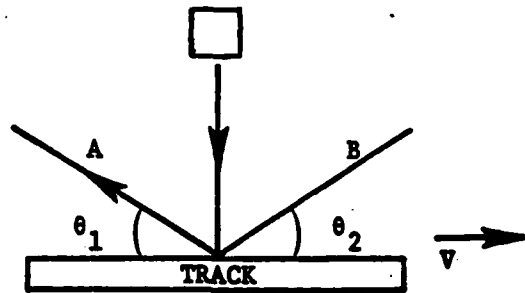


Figure A.5.1

The fringe rate (F) for the translational velocity V is given by

$$F = \frac{V}{\lambda} (\cos\theta_1 + \cos\theta_2)$$

where  $\lambda$  is the light wavelength.

To see the effects of the angular rotation in the plane of the paper we take the angular derivative:

$$dF = \frac{-V}{\lambda} \left( \sin\theta_1 \frac{d\theta_1}{d\theta} + \sin\theta_2 \frac{d\theta_2}{d\theta} \right) d\theta = \frac{-V}{\lambda} (\sin\theta_1 - \sin\theta_2) d\theta .$$

The signs of  $\sin\theta_1$  and  $\sin\theta_2$  are opposite because the changes in  $\theta_1$  and  $\theta_2$  under pitch are in the opposite directions.

We want the fractional change in F versus  $\theta$ . This is given by:

$$\frac{\Delta F}{F} = \frac{\frac{-V}{\lambda} (\sin\theta_1 + \sin\theta_2)}{\frac{V}{\lambda} (\cos\theta_1 + \cos\theta_2)} \Delta\theta .$$

After rotation,  $\theta_1' = \theta_1 - \Delta\theta = \theta_2 + \Delta\theta$ . Using this and the initial condition,  $\theta_1 = \theta_2$  gives for the fractional change in the fringe rate:

$$\frac{\Delta F}{F} \approx \frac{(\sin\theta_1 - \sin(\theta_1 + 2\Delta\theta))}{2 \cos\theta_1} \Delta\theta = \frac{(2 \sin\Delta\theta \cos\theta_1)}{2 \cos\theta_1} \Delta\theta = \Delta\theta^2$$

$$\Delta\theta = (5 \times 10^{-7})^{1/2} = 7 \times 10^{-4} .$$

This means that  $\Delta\theta = 7 \times 10^{-4}$  radians corresponds to the entire error budget.

Assuming a 1.5 mm (.06") clearance around each side of the slipper and a 2.5 m (8 ft.) sled length, the maximum pitch angle is  $\sim 10^{-3}$  radians, which is slightly above the error budget at maximum velocity. Therefore, an angular accelerometer or gyroscope must be used for the short term corrections. Note that if the vibrations average to zero, equivalent to the constraint that the sled remains on the track, this will not be a long term scale change.

### Transar Yaw Sensitivity

The pitch angle changes the calibration of the Transar while yaw does not. However, yaw causes the measurement plane to be at an angle to the track. The fringe rate, F, including yaw is given by:

$$F = \frac{V}{\lambda} (\cos\theta_1 + \cos\theta_2) \cos\alpha$$

where

V is the velocity along the track

$\lambda$  is the light wavelength

$\theta_1$  and  $\theta_2$  are the angles of the scattered light with respect to the track in the pitch axis

$\alpha$  is the yaw angle with respect to a track parallel.

At small  $\alpha$ , this reduces to

$$F = F_0 (1 - 1/2 \alpha^2)$$

and

$$\alpha = \left(2 \frac{\Delta F}{F_0}\right)^{1/2} = 10^{-3}$$

Therefore to keep the change in fringe rate below  $5 \times 10^{-7}$ , the stated maximum accuracy,  $\alpha$  must be less than  $10^{-3}$  radians. The maximum yaw angle is also about  $10^{-3}$  radians (.06" slipper clearance on each side and an 8 ft. slipper spacing).

The acceleration required to pitch or yaw the sled the maximum in the 1 msec measurement interval can be calculated as follows assuming constant acceleration

$$a = \frac{2s}{t^2} = 2(3 \times 10^{-3} \text{ m}) / (10^{-3} \text{ sec})^2 = 6000 \text{ m/sec}^2 \approx 600 \text{ g.}$$

This acceleration level has not been observed. Since maximum pitch or yaw cannot occur in the 1 msec measurement interval, the error will be small.

## APPENDIX A.6

### SPECIMEN TO MEASUREMENT POINT VELOCITY

#### Statement of Problem

The object of this report is to analyze methods of measuring specimen velocity rather than the sled velocity. The systems to be discussed are: (1) the use of accelerometers to either determine the absolute velocity of the test specimen or as a secondary system to correct for the relative velocity of the specimen and the primary IVMS, and (2) the flag interferometer concept utilizing a mechanically stabilized light path between the velocity measuring system and the specimen.

In some instances it will be appropriate to assume that vibrational effects are limited if the parts of the system can be shock isolated. In addition, the analyses have made numerous simplifying assumptions which will be given. Some analyses are applicable to more than one measurement concept. Limited applicability will be noted.

One requirement of the IVMS is to measure the velocity of the specimen instead of the sled. One way to accomplish this is to directly measure the accelerations in 3 axis and integrate to get a velocity reading.

The other possible use of accelerometers is to measure the relative acceleration between the specimen and a primary IVMS, then integrate to obtain the relative velocity and use this as a correction term to the velocity output of the primary IVMS.

#### Accelerometers as the Primary IVMS

Consider the use of an accelerometer for the IVMS. We want an accuracy of .001 ft/sec with a measurement every .001/sec. To calculate

the accelerometer accuracy required, assume the total time of the seld run is 25 sec.

$$\Delta a = \frac{\Delta v}{\Delta t} = \frac{.001 \text{ ft/sec}}{25 \text{ sec}} = 4 \times 10^{-5} \text{ ft/sec}^2 = 1.25 \times 10^{-6} \text{ g's}$$

Assuming a maximum sled acceleration of 125 g's, this amounts to 1 part in  $10^8$ .

A brief survey of current industrial literature shows no existing capabilities to measure acceleration to such accuracy.

If sufficient accuracy is possible, a "strap down" guidance system could be used as the IVMS. Its frame mounted design eliminates the need for a platform gimbal system. In this system, three single axis gyros (one-degree of freedom) are mounted on a base fixed to the specimen, input axes set orthogonal. The gyros are provided with high precision input axis angle measuring devices (e.g., an induction type device). The accelerometers (three of them, also orthogonal) are also mounted on the base. The computer, or recorder, receives the incremental angular motion signals from the angle measuring devices and with the timing signal reconstructs a space fixed coordinate system equivalent to a framework provided by a gimbal or other stabilized element. Then it interprets the accelerometer outputs in terms of accelerations in this frame.

Shocks and vibrations are important in that they determine the instantaneous accelerations, velocities and position of the specimen. And theoretically, these shocks should be calculated into the absolute velocity. But the problem lies in not only resolving these minute changes in acceleration but in maintaining the necessary 1 part in  $10^8$  accuracy at the 100 g level of the shocks. There is also the problem of retaining accuracy in determining the orientation of the specimen (i.e., precision angular measurements) but this is a much less severe

problem. Also important is the necessary response time of the computer or processor receiving and analyzing the signals.

A major disadvantage of accelerometers as the primary IVMS is that they are the same devices used in the guidance systems under test. A different concept is desirable so that its errors will be different functions of the sled run parameters and could be more easily identified.

#### Accelerometers to Correct for IVMS to Specimen Velocity

Now consider the use of accelerometers to determine the difference in velocity between the specimen and an IVMS mounted remotely from the specimen (such as the "translational interferometer").

The principle here is to use accelerometers mounted on the specimen and on the velocity measuring device (for example an interferometer). The difference between these two accelerations can be used to measure differences in velocity between the specimen and the interferometer. To maintain the required velocity measurement accuracy, the accelerometers would have to have the same accuracy as calculated above for use of accelerometers as the primary velocity measuring device.

To reduce the accuracy requirement for the accelerometers, let us investigate the possibility of requiring accelerometer accuracy only over short intervals and rezeroing the accelerometers with each other at longer time intervals by making use of the fact that no large relative displacements can occur (assuming nothing breaks on the sled).

This concept unfortunately will not work because relative displacements and therefore, accelerations are too large. To see this, assume parameters which are optimistic. Assume a maximum relative displacement of  $\pm 1$  mm due to sled frame flexing and specimen shock mounts. Also, let the accelerometer be rezeroed using 10 sec averages.

Then, frequencies higher than 0.1 Hz (= 1/10 sec) will be measured by the accelerometers. The error in rezeroing will be the maximum accelerations (a) which can occur with a displacement ( $s_0$ ) of  $\pm 1$  mm at a frequency (b) of 0.1 Hz.

$$s = s_0 \sin 2\pi ft$$

$$v = \frac{ds}{dt} = 2\pi b s_0 \cos 2\pi ft$$

$$a = \frac{d^2s}{dt^2} = 4\pi^2 b^2 s_0 \sin 2\pi ft$$

$$a_{\max} = 4\pi^2 b^2 s_0 = 0.39 \text{ mm/sec}^2 = 4 \times 10^{-5} g$$

This is the maximum error in rezeroing the accelerometer. The accelerometer accuracy required is that necessary to keep the velocity accurate to .001 ft/sec (.03 cm/sec) in the 10 second interval above. This is

$$a = \frac{\Delta v}{\Delta t} = \frac{.03 \text{ cm/sec}}{10 \text{ sec}} = .003 \text{ cm/sec} = 3.2 \times 10^{-5} g$$

The error achievable ( $3.2 \times 10^{-5} g$ ) is marginally greater than the maximum error allowed ( $4 \times 10^{-5} g$ ) which is to say, rezeroing will not help even under optimistic assumptions. It can be seen that shorter rezeroing intervals or, larger relative displacements will make matters worse and longer rezeroing intervals and smaller relative displacements are not practical or possible. The conclusion is that reasonable relative motion between the specimen and a remote velocity measuring device cannot be corrected to the required accuracy using accelerometers on each unless the accelerometers are accurate enough to be used to measure the specimen velocity directly without the aid of a separate velocity measuring device.

## APPENDIX A.7

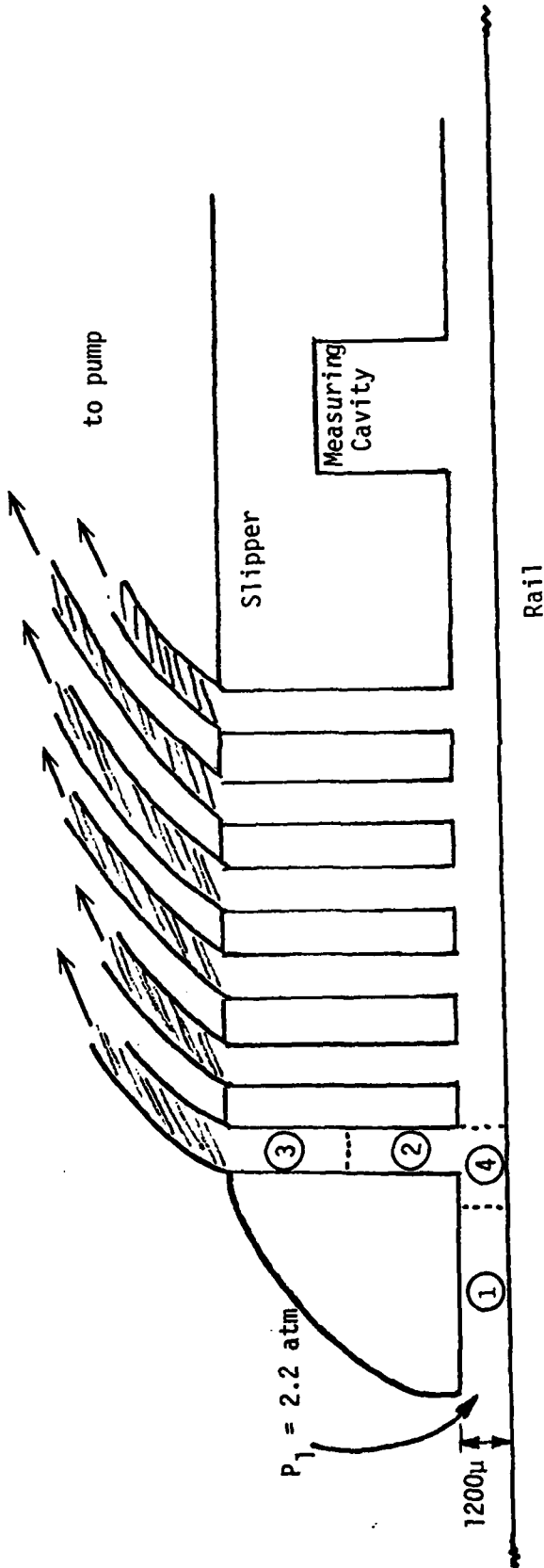
### VACUUM & AIRFLOW IN ROCKET SLED SLIPPER CAVITIES

**Problem:** To determine the vacuum levels which can be achieved in a cavity in a slipper facing the track rail.

**Discussion:** In order for accurate operation of the Transar type IVMS, a constant environment with respect to air density and composition, and refraction coefficient must be maintained. One possible solution to this is keeping a vacuum near the measurement point. The extreme environment suggests this is not simple; to gain full advantage from the decreased pressure, the pressure at the measurement region needs to be  $\sim 1$  Torr, in spite of a leak at the slipper rail interface.

A system could be designed which 1) diverts the flow of air via aerodynamical means (venturi effect, etc.), and 2) employs a mechanical vacuum pump to extract the remaining air. The vacuum system would consist of several channels (See Figure A.7.1) to break up the air flow. The analysis of the channels can be simplified to act in a power manner; i.e., effect of 6 channels is the same as  $(1 \text{ channel})^6$ . This system would be complex since each vacuum channel could draw from an adjacent channel. Also varying pressures at different points on the sled must be taken into account; the shock wave has an air pressure  $\sim 4$  atm and the aft section  $\sim 1$  atm. Other problems are the effects of turbulence and the flow due to the movement of the slipper relative to the rail.

In any such system it would be difficult to maintain a low pressure with a large leak capacity; for a standard slipper there is a  $1/8$ " gap to the rail and a 4" wide rail - a large leak. Rough calculations show it is not possible to obtain a 1 Torr vacuum with a slipper-rail gap of  $1/8$ ".



A.7.2

Approximate Dimensions

Channel ① :  $1200\mu \times (5 \times 10^4\mu) \times (2.5 \times 10^4\mu)$

② :  $(5 \times 10^3\mu) \times (5 \times 10^4\mu) \times (1 \times 10^4\mu)$

③ : (pipe cross section)  $A_0 = \pi \times (2.5 \times 10^3\mu)^2$ ,  $l = 5 \text{ cm}$

④ :  $(1.5 \times 10^4\mu) \times (5 \times 10^4\mu) \times 1200\mu$

Figure A.7.1 Schematic Sketch of Translational Interferometer Evaluation Channels.

For the purposes of answering the question of what vacuum level is achievable?, the following subjects will be discussed. And since, at high Mach numbers, the aerodynamic effects on a slipper are complicated, simplifications will be made when necessary:

- 1) Find what the limit to the size of the slipper-rail gap is in order to maintain a 1 Torr pressure in the cavity.
- 2) Does a vacuum pump exist that is capable of handling the air flow?
- 3) What are the pressures, density and flow rates in the gap?
- 4) Will a channelled system operate as intended?
- 5) Answer the overall question. Is such a vacuum feasible?

Figure A.7.2 shows idealized system of two stationary parallel plates with a hole in one acting as a pressure sink. Assume no motion between plates (rail and slipper). The actual vacuum system will be more complex due to pipe bends and gap size variations. More significantly, the rail and slipper are not stationary and their relative motion will tend to pump air into the cavity due to the boundary layer on the rail. Also restrict the problem to laminar incompressible flow; in actuality, the high Mach numbers involved make the flow compressible.

Using a common rotary vane pump to supply the vacuum with a pumping speed of 1500 liters/min., the maximum gap size allowable while maintaining a 1 Torr pressure at the hole can be calculated. Assume that a pump of the same pump speed which is suitable for the sled environment can be acquired or designed. (See Figure A.7.3). Assume the

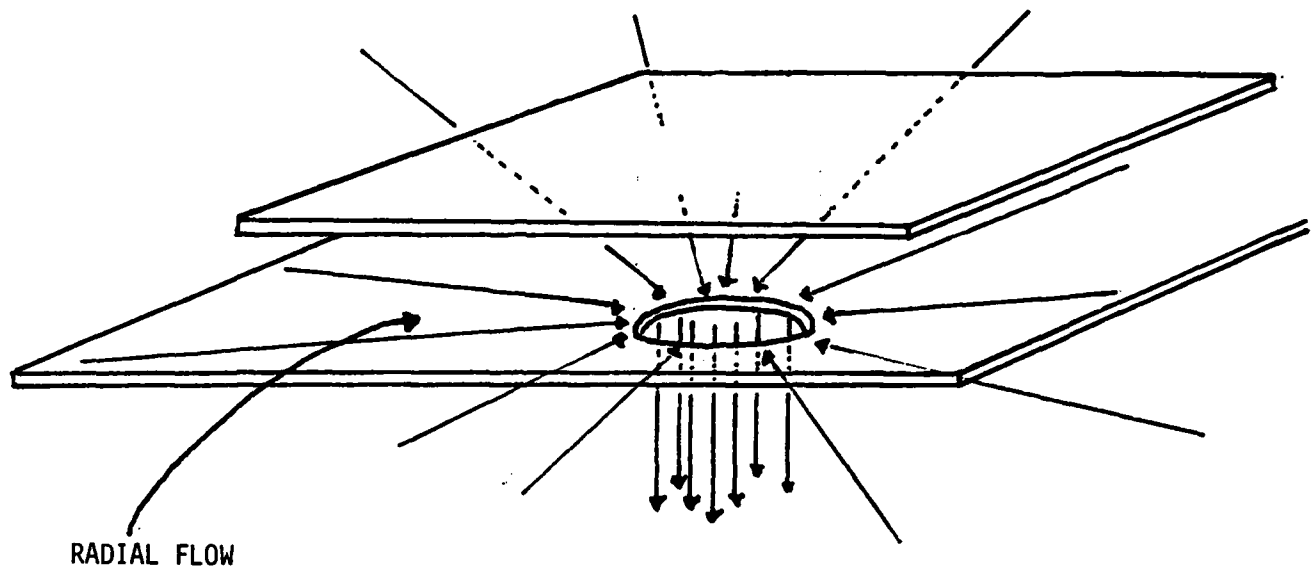


Figure A.7.2 Idealized System

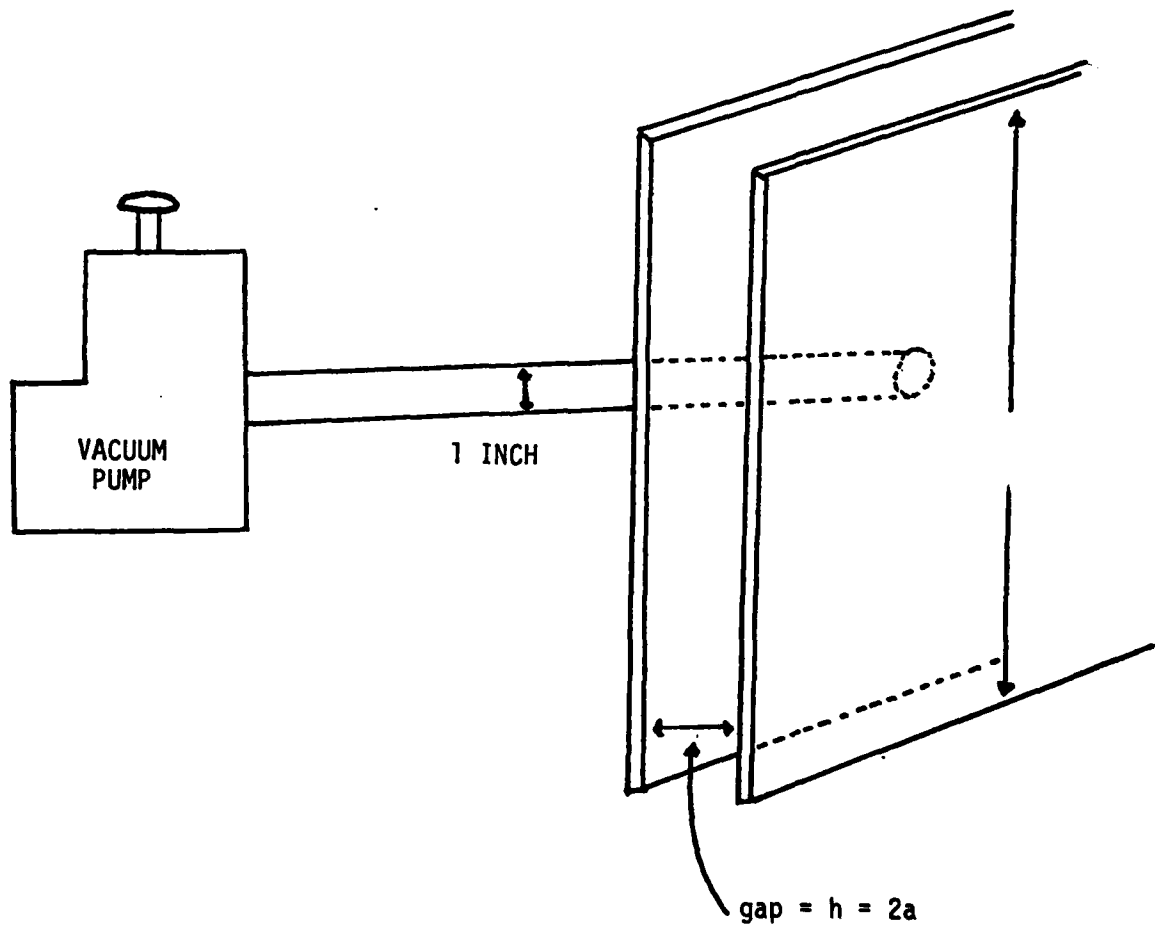


Figure A.7.3 Idealized System

hose has conductance ~600 liters/sec, then the pumping speed at the hole is about that at the pump (1500 l/min) say 24 l/sec.

$$\text{Throughput} = Q = S_n P_n \sim 24 \text{ Torr l/sec (at } P_n = 1 \text{ Torr);}$$

$$\text{also } Q = 10^{-3} \left( \frac{f\pi}{8n} \right) \frac{a^4}{l} (P_o^2 - P_n^2) \quad \text{for a single tube (from Dushman)}$$

$S_n$  = volume flow rate at hole (liters/sec)

$a$  = radius (cm)       $l$  = length (cm),  $2a$  = gap height

$n$  = viscosity =  $1.854 \times 10^{-5}$  poise

$P$  = pressure (Torr)

$$\frac{\pi f}{8} = \# \text{ microbars per Torr} = 5.236 \times 10^2 .$$

For a 1" hole in the plates, the surface area of an imaginary cylinder of height is the equivalent of  $\frac{2\pi}{2a}$  of the above tubes:

$$Q_{\text{Total}} = \frac{2\pi Q}{2a} = \frac{\pi Q}{a} \quad \text{or}$$

$$a^4 = \frac{8n}{f\pi} 10^{-3} \frac{l\pi Q}{a(P_o^2 - P_n^2)}$$

Take  $l = 15$  cm,  $P_o = 760$  torr,  $P_n = 1$  torr and  $\frac{f\pi}{8n} = 2.838 \times 10^6 \text{ torr}^{-1} \text{ sec}^{-1}$ .

Solving for  $a$ :

$$a = \left( \frac{(24 \text{ torr l/sec}) (15 \text{ cm}) \pi}{(577599 \text{ torr}^2) (2.838 \times 10^3 \text{ torr}^{-1} \text{ sec}^{-1})} \right) \\ \sim 5.86 \times 10^{-2} \text{ cm} \sim 5.86 \times 10^2 \text{ } \mu\text{m}$$

This indicates that the gap ( $h = 2a$ ), must be  $< 1170 \mu\text{m}$  in order to keep a 1 torr pressure at the sink within the specifications of the given vacuum pump capabilities (See Table 1). If the gap is 1/2 this size, the throughput is 1/32 of its previous value; i.e., then a pump with a 50 liters/min capacity is required - this size pump weighs 100 lbs. which is more sled environment oriented than the 1500  $\ell/\text{min}$  model. These gap sizes are reasonable to expect if a suitable slipper can be created; a negative lift effect coupled with the vacuum effect may be sufficient to keep the slipper on the rail.

To do this calculation it was assumed that the ambient pressure  $P_o = 1 \text{ atm}$ . Other pressures are considered in Table #1. Although the slipper air flow is in the hypersonic region, this pressure could be dissipated by the previously mentioned "pre-vacuum" cavity; even several cavities might be maintained. But more knowledge of conditions in the rail-slipper gap is needed before this can be approached.

An investigation<sup>1</sup> on wall pressures inside the slipper determined maximum pressures inside the slipper to range from 15.8 psia to 21.6 psia at corresponding Mach numbers of 1.4 and 1.74 respectively. ( $M = 1.74 \sim 2,000 \text{ ft/sec}$ ). In that investigation, designed aerodynamical down-loading of the sled kept the slipper in near constant contact with the rail. The pressure measurements were achieved using artificial slipper-gaps machined into the slipper. This suggests that with down-loading on the slipper no pressure greater than 21.6 psia is possible at  $\sim 2,000 \text{ ft/sec}$ .

In this same study, large amplitude pressure fluctuations in the measured slipper-gap pressures were observed during the first seconds of sled deceleration. No such fluctuations occurred during acceleration. This effect is likely due to the downward pitching moment of acceleration and lack of it at deceleration. So, to keep the measurement slipper in contact with the rail at initial deceleration, the down-loading due to aerodynamics must exceed that due to acceleration.

TABLE I

<u>incident gap pressure</u>	<u>gap using 1500 l/min pump</u>	<u>gap using 50 l/min pump</u>
4 atm	.67 mm	.34 mm
3 atm	.76 mm	.38 mm
2 atm	.89 mm	.44 mm
1.5 atm	1.0 mm	.50 mm
1 atm	1.2 mm	.56 mm
.5 atm	1.6 mm	.78 mm

Another report on aerodynamics of the slipper bearing<sup>2</sup>, address the region of Mach 4-10. This study is a rather indepth analysis of the types of flow, effects of aerodynamic heating and friction, etc. The parameters associated with the slipper problem are numerous and even though the Mach region is higher than that required by the contract work order, a simplified version of this investigation can be associated with a worst case of the Mach 2 region.

Viscous effects are dominant considering the small gap size and large relative velocity between rail and slipper. Boundary layers develop on the slipper and the rail. And there is an overall pressure drop from the leading edge of the slipper to the end, so any pressure variation must be a decreasing one.

The flow model of this investigation consists of:

- 1) Compression through a normal shock
- 2) Acceleration to uniform sonic conditions in the gap
- 3) The mass flow in the gap is completely determined by the gap height and free stream conditions
- 4) There is laminar stagnation in the region of the leading edge of the slipper
- 5) Turbulent boundary layer flow in the gap exists on both the slipper and rail
- 6) There exists a mergence of the two boundary layers toward a turbulent couette flow in the slipper-rail gap.

Its also assumed that the flow behaves as a perfect gas and the slipper wall remains at atmospheric temperature.

One of the most important aspects of this flow model is the mergence into couette flow. The distance through the gap at which this mergence occurs depends explicitly on the gap height and the characteristics of the two boundary layers. With a large amount of effort, both the distance

at which this occurs (actually, it does not occur at a point - it approaches it through a shear flow region) and the pressure drop created can be calculated. The report by Briggs and Korkegi gives an approximate distance for a gap height of  $\sim 1/32''$  ( $1170 \mu \leq 1/32''$ ) of  $1''$  (for  $M_\infty \sim 4$ ). So for extremely small gap heights, merge of boundary layers is rapid and the flow through the rest of the slipper gap can be approximated by couette flow. And the pressure in this region for  $M_\infty \sim 4$  is between 4 and 7 times ambient pressure.

Applying eqn (II-3)<sup>2</sup> to get the free stream height ( $l_\infty$ ) to gap height ratio gives for a gap of  $1200 \mu$ ,  $l_\infty \sim 1460\mu$ . Assuming normal shock compression, the flow enters the gap subsonically at a value near the pitot pressure and must exit at the trailing slipper edge - thus undergoing a large supersonic expansion. From one-dimensional characteristics, the flow would expand to sonic speed in the gap which acts as an elongated sonic throat. Using supersonic and Normal Shock tables<sup>3</sup>, the pitot pressure is:

$$\begin{aligned}
 P_o^1 &= P_\infty \left( \frac{1}{\frac{P_{o0}}{P_o}} \right) \left( \frac{P_{o2}}{\frac{P_{o1}}{P_o}} \right) \\
 &= (1828 \text{ lb/ft}^2) \left( \frac{1}{.1492} \right) (.7674) \\
 &= 9402 \text{ lb/ft}^2 \sim 4.4 \text{ atm} \quad (1 \text{ atm} \sim 2116 \text{ lb/ft}^2)
 \end{aligned}$$

In order to estimate the pressure drop in the merged region it is necessary to find the gap pressure when couette flow is approached. From the equation of continuity and Figure A.7.4:

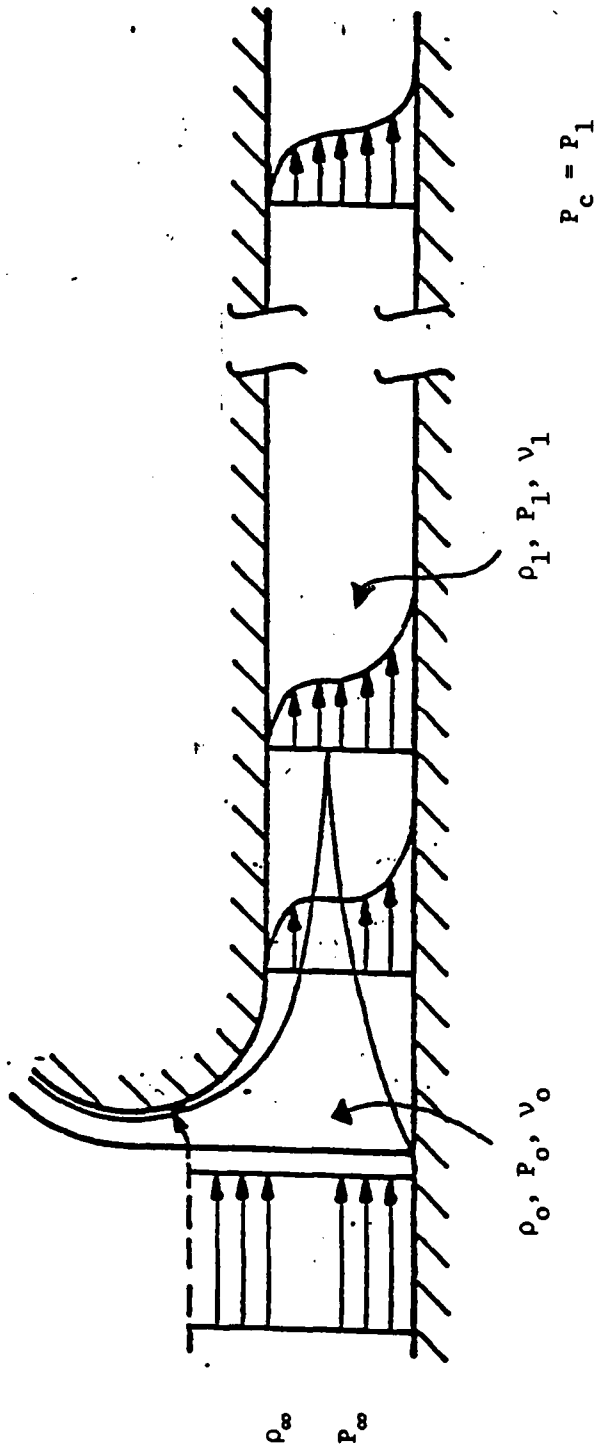


Figure A.7.4  
Pressure and Density Regions

$$\begin{aligned} \rho_{\infty} U_{\infty} l_{\infty} &= \int_0^b pu \, dy + \int_0^b \rho(U_{\infty} - u) \, dy \\ &= U_{\infty} \int_0^b p \, dy = \frac{\rho_w U_{\infty} l_{\infty}}{2} \int_0^1 \frac{\rho}{\rho_w} d \left( \frac{y}{b} \right) \end{aligned}$$

where  $b = l/2$ . Since  $T_{\infty} = T_w$ ,  $P_{\infty}/P_w = \rho_{\infty}/\rho_w$ .

Therefore,

$$\frac{P_w}{P_{\infty}} = 2 \frac{l_{\infty}}{l} \left[ \int_0^1 \frac{\rho}{\rho_w} d \left( \frac{y}{b} \right) \right]^{-1}$$

For Couette Flow<sup>4</sup>:

$$\begin{aligned} \frac{\rho}{\rho_w} &= \left[ 1 + m^2 \bar{U} (2 - \bar{U}) \right]^{-1} \quad \text{with} \\ m^2 &= \frac{\gamma - 1}{8} M_{\infty}^2, \quad \text{and } \bar{U} = \frac{2U}{U_{\infty}}. \end{aligned}$$

Noting that  $\bar{U} = (y/b)^{1/7} = \xi^{1/7}$  and substituting:

$$\frac{P_w}{P} = 2 \frac{l_{\infty}}{l} \left[ \int_0^1 \left( 1 + \frac{\gamma - 1}{4} M_{\infty}^2 \xi^{1/7} - \frac{\gamma - 1}{8} M_{\infty}^2 \xi^{2/7} \right)^{-1} d\xi \right]^{-1}$$

Substituting  $\xi = z^7$ ,  $b = 2c$ ,  $c = \left[ \frac{\gamma - 1}{8} M_{\infty}^2 \right]^{1/7}$ , this can be integrated in the manner of Reference #5 using  $N = 6$ .

Therefore, the Couette Pressure is:

$$\frac{P_c}{P_\infty} = 7 \frac{\ell_\infty}{\ell} \frac{1}{c^2 + c} \left\{ \begin{array}{l} \beta^6 \left[ \ln \left( \frac{\beta - 1}{\beta} \right) + \frac{6}{Z} \frac{1}{m} \left( \frac{1}{\beta} \right)^m \right] \\ -\lambda^6 \left[ \ln \left( \frac{\lambda - 1}{\lambda} \right) + \frac{6}{Z} \frac{1}{m} \left( \frac{1}{\lambda} \right)^m \right] \end{array} \right\}$$

which is also the lowest pressure that can exist in the gap (without external vacuum pumping, etc.).

While its been assumed for simplicity that the slipper is in "cold wall" conditions, i.e., initial conditions, the wall temperature will rise due to running friction and fluid friction, Reference #2 analyzes the case of an adiabatic wall (hot slipper) from a pressure stand point. And resulting from their considerations, for a hot slipper wall, the pressure must be constant throughout the gap and must equal the sonic value  $P_c$ . This is similar to adiabatic one-dimensional flow in a constant area channel.

Taking the values  $\ell = 1200\mu$ ,  $\ell_\infty = 1460 \mu$ ,  $c = .1805$ ,  $b = .3610$ , giving  $\beta = -1.5574$ ,  $\lambda = 3.5574$ , the resulting pressure in the Couette region is  $P_c = 4640.4 \text{ lb/ft}^2 \sim 2.2 \text{ atm}$  ( $1\mu = 10^{-6} \text{ m}$ ). Assuming this is constant throughout a large region of the slipper, and that for a gap height of  $1200\mu$ , Couette flow begins about 1" inside the leading edge of the slipper. With this in mind the simplified flow can now be applied to a region with a multi-cavity vacuum.

Quantities needed (Refer to Figure A.7.4):

- 1)  $\rho_\infty = 2.03 \times 10^{-3} \text{ 16 sec}^2/\text{ft}^4$  (or  $.065 \text{ lb/ft}^3$ , from Holloman data)
- $P_\infty = 1828 \text{ lb/ft}^2$  (from Holloman data)

2) applying shock conditions,  $\rho_o = 2.5 \times 10^{-2} \text{ lb sec}^2/\text{ft}^4$   
(.78 lb/ft<sup>3</sup>)

and  $P_o = 9402 \text{ lb/ft}^2 \sim 4.4 \text{ atm}$

$v_o = 2000 \text{ ft/sec}$

3) incident air flow (mass) per unit area

$G_o = \rho_{oo} v_o = 130 \text{ lb/ft}^2 \text{ sec}$  (agrees with Holloman data)

4) from calculations,  $P_1 = 4640 \text{ lb/ft}^2 \sim 2.2 \text{ atm}$

5) using continuity of mass flow:

$$G_1 = G_o = 130 \text{ lb/ft}^2 \text{ sec} = \rho_1 v_1$$

also the momentum eqn:

$$P_o A_o - P_1 A_1 = \rho_1 v_1^2 A_1 - \rho_o v_o^2 A_o$$

(divide out width)

$$P_o \ell_o - P_1 \ell_1 = \rho_1 v_1^2 \ell_1 - \rho_o v_o^2 \ell_o$$

After substituting the resulting values for  $v$ , and  $\rho_1$  are:

$$v_1 = 2485.6 \text{ ft/sec}$$

$$\rho_1 = .052 \text{ lb/ft}^3$$

Now consider the regions of (2)-(4). The mass flow available to these regions is  $130 \text{ lb/ft}^2 \text{ sec}$ . This flow region can be regarded as an analogous electrical circuit (Figure A.7.5). Associate  $v_o$  with  $P_1$  (of Figures A.7.1 and A.7.4) and the Resistances with the tube conductivities of each region. For the limiting cases of Figure A.7.5:

$$V_1 = \frac{R_1 + R_2}{R_o} V_o \quad \text{and} \quad V_2 = \frac{R_1}{R_o} V_o$$

(These equations are true only if  $R_o \gg (R_1 + R_2)$ .)

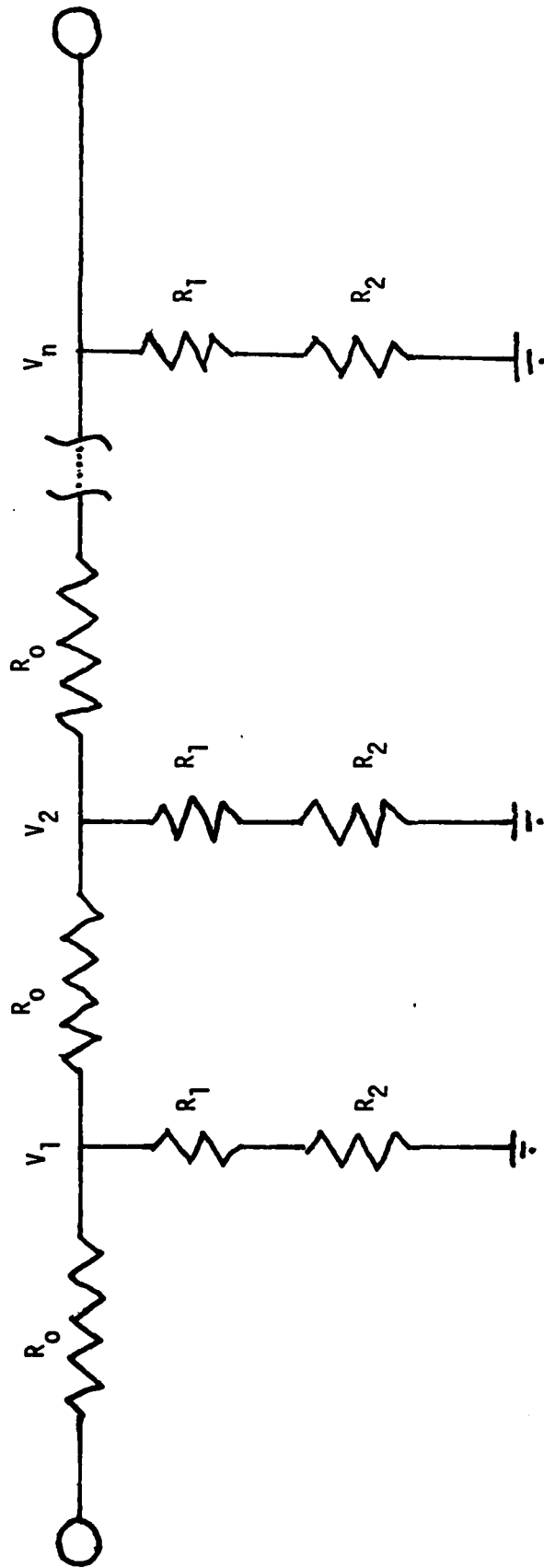
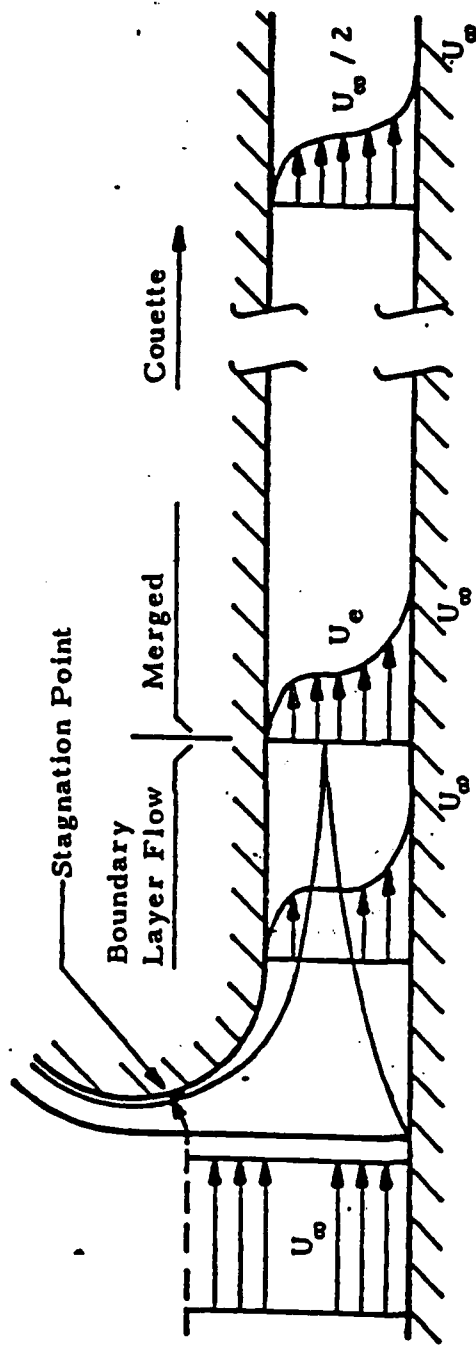


Figure A.7.5  
Electrical Analog to the Flow System



FLOW MODEL WITH CHARACTERISTIC VELOCITY PROFILES

Figure A.7.6

$$\text{and finally, } V_n = \frac{R_1 + R_2}{R_o} V_{n-1}$$

$$\text{or } V_n = \left( \frac{R_1 + R_2}{R_o} \right)^n V_o$$

$$1) \text{ if } R_1 + R_2 \ll R_o, \quad V_n \rightarrow 0$$

$$2) \text{ if } R_1 + R_2 \gg R_o, \quad V_n \rightarrow V_o$$

The purpose of the pre-vacuum cavities are to decrease the pressure, so for best results make  $R_1 + R_2 \ll R_o$  or the conductance of Region (2) + (3) should be much larger than Region (4) ( $C \propto 1/R$ )

Using the analogy, the pressure at the end of the pre-vacuum section,  $P^1$ , is:

$$P^1 = \left( \frac{\frac{I}{C_2} + \frac{I}{C_3}}{\frac{I}{C_4}} \right)^n P_1 \quad \text{for } n \text{ chambers,}$$

or

$$P^1 = \left( \frac{C_4(C_2 + C_3)}{C_2 C_3} \right)^n P_1$$

The conductance of a tube of radius  $a$ , length  $l$ , and pressures at the ends of  $P_i, P_f$ , is:

$$C = \frac{(2.838 \times 10^3)}{l} 9^4 (P_i + P_f)$$

Region 2: Assume rectangular shape can be approximated by a set of parallel tubes; 10 tubes of .25 cm radius.

$$C_2 = \frac{10 (2.838 \times 10^3) (.25)^4}{1 \text{ cm}} (P_1 + P_x)$$

$$= (1.109 \times 10^2) (P' + P_x)$$

Region 3:

$$C_3 = \frac{(2.838 \times 10^3) (.25)^4}{5 \text{ cm}} (P_p + P_x)$$

$$= 2.22 (P_p + P_x)$$

Assume  $P_p = 1$  torr,  $S_p =$  pumping speed at  $P_p \sim 15\ell/\text{sec}$ .

$$P_1 = 2.2 \text{ atm} \sim 1672 \text{ torr}$$

$$C_T = \frac{C_2 C_3}{C_2 + C_3} = \frac{(1.109 \times 10^2) (P' + P_x) (2.22) (P_p + P_x)}{(1.109 \times 10^2) (P' + P_x) + (2.22) (P_p + P_x)}$$

$$= \frac{(2.462 \times 10^2) (P' + P_x) (P_p + P_x)}{(1.109 \times 10^2) P' + 2.22 P_p + (1.131 \times 10^2) P_x}$$

Region 4: Assume this rectangular shape can also be approximated with parallel tubes; 42 tubes.

$$C_4 = \frac{42 (6 \times 10^{-2})^4 (2.838 \times 10^3) (P_1 + P')}{(1.5 \text{ cm})}$$

$$= 1.03 (P_1 + P')$$

Then substituting these expressions for  $C_T$ ,  $C_4$ :

$$P' = \left\{ \frac{(1.03) (P_1 + P') [(1.109 \times 10^{-2}) (P' + P_x) + (2.22) P_p + P_x]}{(2.462 \times 10^2) (P' + P_x) (P_p + P_x)} \right\}^n P_1$$

$$= \left( \frac{1.03}{2.462 \times 10^{-2}} \right)^2 \frac{(P_1 + P')^n P_1}{\left( \frac{(1.109 \times 10^{-2})}{(P_p + P_x)} + \frac{(2.22)}{(P' + P_x)} \right)^n}$$

let  $(P_1 + P')^n = P_1^n \left( 1 + \frac{P'}{P_1} \right)^n$  and expand using the binomial theorem:

$$P_1^n \left( 1 + \frac{P'}{P_1} \right)^n = P_1^n \left\{ 1 + \frac{nP'}{P_1} + n(n-1) \left( \frac{P'}{P_1} \right)^2 + \dots \right\}$$

For large  $n$ ,  $P'/P_1 \ll 1$  so all but  $P_1^n$  can be neglected:

$$P' = (4.184 \times 10^{-3})^n P_1^{n+1} \left\{ \frac{(1.109 \times 10^{-2})}{(P_p + P_x)} + \frac{(2.22)}{(P' + P_x)} \right\}^n$$

Let  $A = 4.184 \times 10^{-3}$ ,  $B = 1.109 \times 10^{-2}$ ,  $C = 2.22$ ; then

$$P' = A^n P_1^{n+1} \left\{ \frac{B}{(P_p + P_x)} + \frac{C}{P' + P_x} \right\}^n$$

factor out  $\frac{B}{(P_p + P_x)}$  and expand again using binomial

theorem:

$$P' = \left[ \frac{AB}{(P_p + P_x)} \right]^n P_1^{n+1} \left\{ 1 + \frac{nC}{B} \frac{(P_p + P_x)}{(P' + P_x)} + (n-1) \left[ \frac{C(P_p + P_x)}{B(P' + P_x)} \right]^2 + \dots \right\}$$

For large  $n$ ,  $P'/P_x \ll 1$  and in order to get a rough approximation for  $P'$ , neglect it:

$$P' = \left[ \frac{AB}{(P_p + P_x)} \right]^n P_1^{n+1} \left\{ 1 + \frac{nCP}{BP_x} + \frac{nC}{B} \right\}$$

Now, solve for  $P_x$  in order to complete the approximation.

$$C_3 = 2.22 (P_p + P_x) \text{ and } Q = (1 \text{ torr}) (15 \text{ l/sec})$$

$$= 15 \text{ torr l/sec}$$

$$P_x S_x + Q \text{ and } S_x = \frac{C_3 S_p}{C_3 + S_p}$$

$$\begin{aligned} \text{then } P_x &= \frac{Q (C_3 + S_p)}{C_3 S_p} \\ &= \frac{Q S_p + Q (2.22) (P_p + P_x)}{S_p (2.22) (P_p + P_x)} \end{aligned}$$

$$P_x S_p (2.22) (P_p + P_x) = Q S_p + Q (2.22) (P_p + P_x)$$

$$(2.22) S_p P_x^2 + P_x [P_p S_p (2.22) - Q (2.22)] = Q S_p - Q (2.22) P_p = 0$$

$$P_x^2 + P_x [P_p - Q/S_p] - Q/2.22 + Q P_p/S_p = 0$$

$$P_x = \left( Q/2.22 + Q P_p/S_p \right)^{1/2}$$

$$P_x = 2.79 \text{ torr}$$

with  $P_x = 2.79 \text{ torr}$ ,  $P_p = 1 \text{ torr}$ , and  $P_1 = 2.2 \text{ atm} = 1672 \text{ torr}$ :

$$P' = (1.224 \times 10^{-5})^n (1672)^{n+1} \{1 + n(2.719 \times 10^2)\}$$

and for  $n = 6$ ,  $P' = 2.005 \times 10^{-4} \text{ torr}$

Below pressures of .1 torr, the flow becomes molecular rather than viscous flow, so much of the previous analysis does not apply. Hence this figure for  $P'$  is not quite correct, but it gives the impression that the pressure is certainly  $\sim .1 \text{ torr}$  if not less than that. Also, the approximations made to achieve this answer may only

apply under special conditions; they may not be valid for a low number of channels, but there is sufficient leeway in this figure for P' to be off even by several orders of magnitude. Table 1 gives slipper-rail gaps.

Conclusions:

Many of the results arrived at in the previous analyses are quite dependent on the approximations used. These problems need a more involved analysis, but the results do give some indication that a measurement slipper can be created that will stay fixed (sliding) on the rail and a pressure level of  $\sim 1$  torr can be maintained with existing mechanical pumps and aerodynamical effects.

Another method of controlling the environment inside a measurement cavity is to pressurize it with an inert gas, say Helium. With the pressure greater inside than that of the air flowing by the cavity, the only gas in the cavity will be Helium. Helium has a low index of refraction so effects are minimized. Density in the chamber must still be known, however, and it is likely to fluctuate making measurement difficult.

Also a combination of pressurized chambers and evacuated chambers could be used to sweep debris from the track and still provide a separate vacuum chamber for the interferometer. This may solve the problems but the added complexity is a disadvantage.

Although vacuum pump might be achieved using an aerodynamically driven device, for the purposes of this analysis a conventional mechanical vacuum pump was considered which would occupy about one cubic foot in the sled.

Equations:

eqn (II-3)<sup>2</sup>

$$\frac{\rho_{\infty}}{\rho} = \left( \frac{\frac{\gamma+1}{2} M_{\infty}^2}{\gamma M_{\infty}^2 - \left(\frac{\gamma-1}{2}\right)} \right)^{\frac{\gamma+1}{2(\gamma-1)}} \left\{ \frac{\gamma M_{\infty}^2 - \frac{\gamma-1}{2}}{\frac{\gamma-1}{2} M_{\infty}^2 + 1} \right\}$$

eqn (V-6)<sup>2</sup>

$$\frac{p(x)}{p_{\infty}} = \left( \frac{\frac{\gamma+1}{2} M_{\infty}^2}{1 + \frac{\gamma-1}{2} M(x)^2} \right)^{\frac{\gamma}{\gamma-1}} \left( \frac{\frac{\gamma+1}{2}}{\gamma M_{\infty}^2 - \left(\frac{\gamma-1}{2}\right)} \right)^{\frac{1}{\gamma-1}}$$

FOOTNOTES:

1. Gallant, William, Wall Pressure Measurements on a Rocket Sled Slipper at  $M < 1.7$ . Air Force Missile Development Center, MDC-TR-67-68 (April 1967).
2. Briggs, Ronald and Korkegi, Robert, Aerodynamics of the Hypersonic Slipper Bearing, Aerospace Research Laboratories, ARL-68-0028 (February 1968).
3. Liepman, H. W., and Roshko, A., Elements of Gasdynamics, John Wiley & Sons, Inc., New York, New York, 1957.
4. Korkegi, R. H., and Briggs, R. A., Compressible Turbulent Plane Couette Flow, ARL Report 67-0223, November 1967.
5. Mirels, Harold, Boundary Layer Behind Shock or Thin Expansion Wave Moving into Stationary Fluid, NACA Technical Note 3712, Washington, May 1956.

OTHER REFERENCES:

1. Dushman, Saul, Ph.D., Vacuum Technique, John Wiley & Sons, Inc., New York, New York, 1949.
2. Shames, Irving, Mechanics of Fluids, McGraw-Hill Company, New York, New York, 1962.

## APPENDIX A.8

### POSSIBLE ERRORS IN THE FLAG INTERFEROMETER VELOCITY MEASUREMENT DUE TO SLED PITCH AND YAW

As the guidance sled pitches and yaws an error is introduced into the velocity measurement. The error can be divided into two components. First, as the sled pitches and yaws the sensing head is displaced relative to the flag and a change in the measurement beam's optical path length results. Since the specimen and optical sensing head are at different positions on the sled their displacements as the sled rotates are different, and the change in the measurement beam's path length is not necessarily indicative of a corresponding change in the position of the specimen. (A simplified configuration is shown in Figures A.8.1 and A.8.2. The second error source arises as the sled yaws, changing the angular alignment between the vertical plane through the source detector and the plane of the mirror surface. As the relative alignment of these planes changes, the sensitivity of the interferometer changes.

Motion of the specimen within shock mounts and flexing of the sled are not considered here. Refer to Appendix A.6.

#### Path Length Changes Due to Sled Pitch and Yaw

The exact magnitude of the error induced as the sled pitches and yaws, changing the measurement beam's optical path length is dependent on: 1) the relative positioning of the specimen and the sensing head, and their positions with respect to the axis of rotation of the sled, and 2) the frequency and amplitude of the vibration causing the sled to pitch and yaw. This determines the magnitude of the rotation angle over the .001 sec sampling time. Rather than calculate the magnitude of the error as a function of these parameters, a worst case analysis, assuming the most likely system design will be done here.

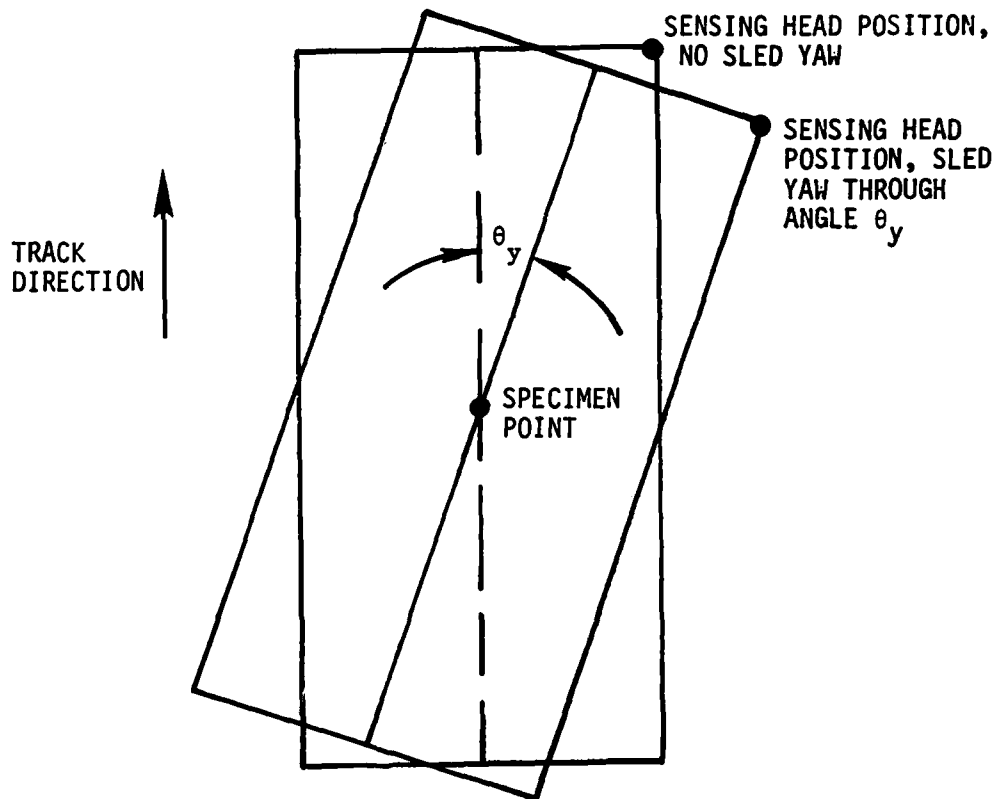


Figure A.8.1

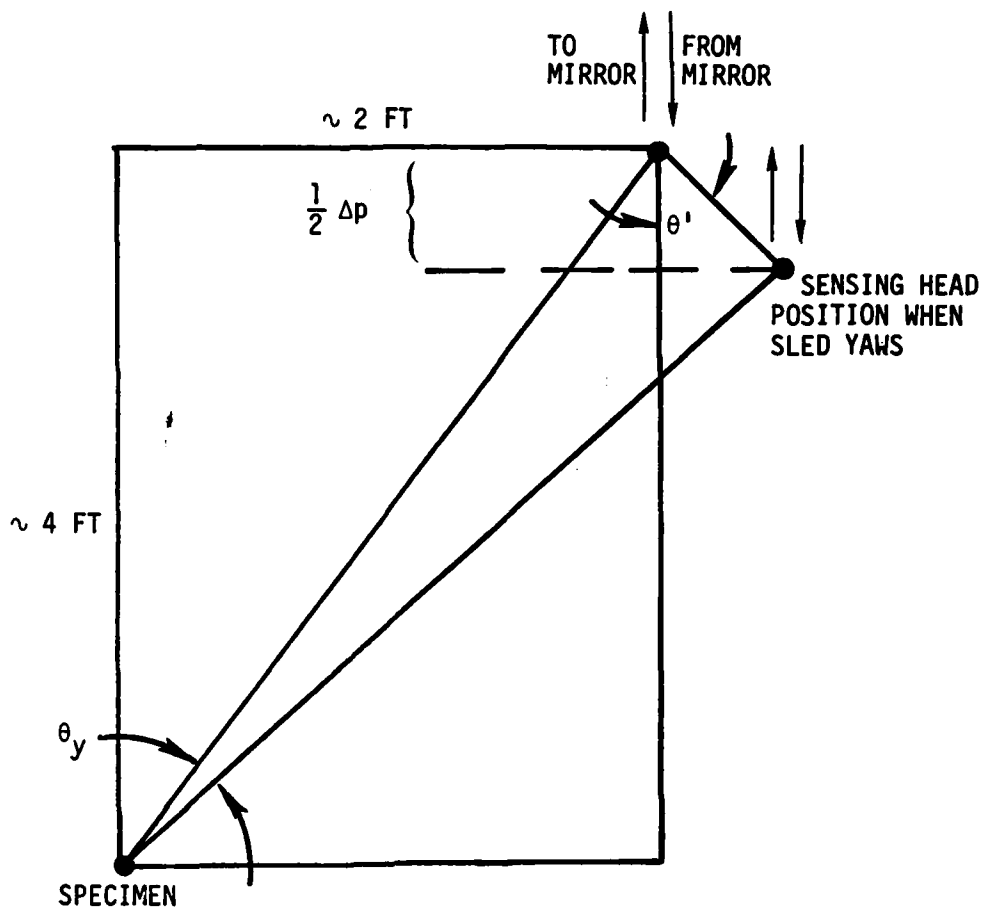


Figure A.8.2

The first simplifying assumption to be made is that the specimen is located at the axis of rotation of the sled as it pitches and yaws, and that these axes pass through the center of the sled so that the pitch and yaw angles obtain their maximum values. Therefore, any change in the measurement beam path length as the sled rotates is in error since the specimen has no corresponding motion. The sensing head position used for the analysis can be seen in Figure,1. This is the approximate design required if the existing interrupters were to be used for reflecting surfaces. (In the actual case the specimen is positioned towards the front of the sled slightly, but since the exact specimen sensing head distance is not known, the approximation of its position to the middle of the sled should still provide a good order of magnitude estimate.) For a worst case analysis it will be assumed that the vibration frequency and amplitude are high enough that the sled pitches and yaws by its maximum possible amount over the .001 sec sampling time. Then the optical path length change over the sampling time will be a maximum introducing the largest error into the velocity measurement.

The maximum pitch and yaw angles, assuming an 8 ft slipper spacing on the sled (front to back) and an all-around rail-slipper clearance of .06", are  $\pm 1.2 \times 10^{-3}$  radians.

The effect of the sled yawing can be seen with reference to Figure A.8.2.

$\Delta p$  = approximate change in optical path length as sled yaws  
 through its maximum angle  
 $L$  = specimen to sensing head position  
 $\theta_y$  = yaw angle  
 $\theta'$  = angle of line between specimen and sensing head with respect  
 to the track normal. ( $\approx \pi/3$  rads in design assumed here)

From geometrical considerations, assuming  $\Delta\theta'$  as the sled yaws  $\approx 0$ :

$$\begin{aligned}\Delta p &\approx 2L \theta_y \cos \theta' \\ &= 2\sqrt{4^2 + 2^2} \theta_y \cos (\pi/3 \text{ rads}) \text{ ft}\end{aligned}$$

Plugging in  $\theta_y = 1.2 \times 10^{-3}$  rads maximum

$$\Delta p = 5 \times 10^{-3} \text{ ft}$$

This corresponds to a velocity error of  $5 \times 10^{-3}$  ft/.001 sec = 5 ft/sec or 5000 times the allowed error. Since the sled cannot yaw through its maximum during the 1 msec measurement interval, this value is high. Even so angular accelerometers or gyroscopes will be needed to correct for this error.

#### Pitch Effects

The maximum sled-pitch angle,  $\theta_p$ , is equal to the maximum yaw angle because the slipper-rail clearance (.06") is the same in the horizontal and vertical directions. So  $\theta_p = 1.2 \times 10^{-3}$  rads. In order to calculate  $\Delta p$  due to sled pitch two assumptions are made. 1) The sensing head and specimen lie on approximately the same horizontal plane on the sled. 2) The maximum specimen sensing head spacing is approximately equal to 4 ft. Typical dual rail sleds have a first mode in pitch at about 20 hertz.

With reference to Figure A.8.3

$$1/2 (\Delta p) = \theta_p / 2 \times (4 \text{ ft} \times \theta_p)$$

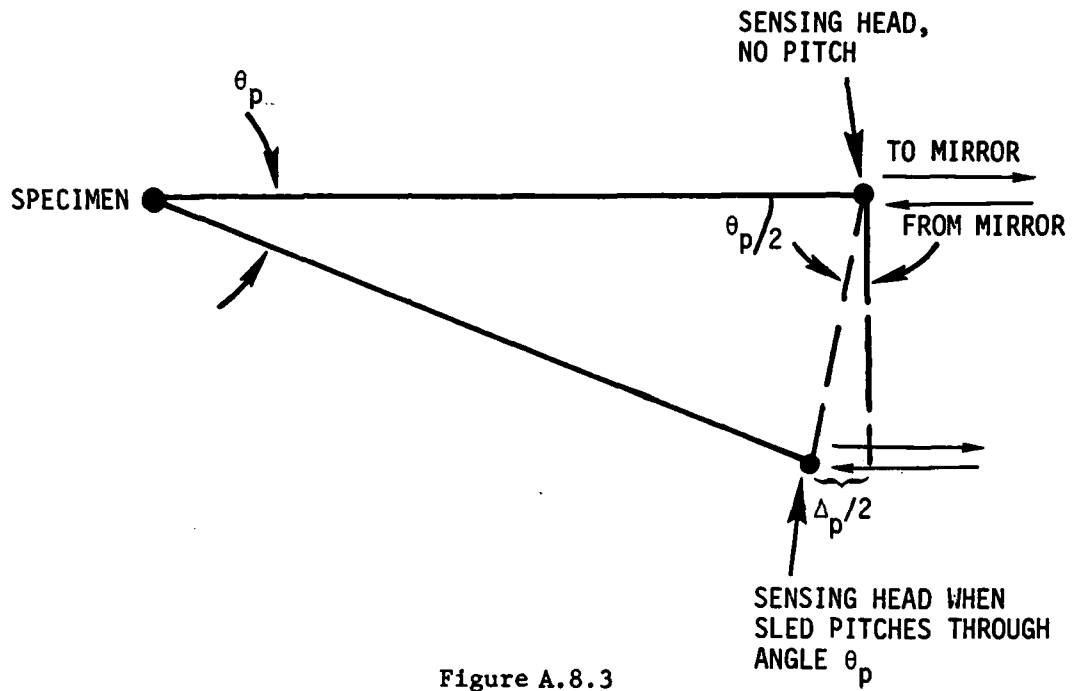


Figure A.8.3

or  $\Delta p$  (round trip) =  $4 \theta_p^2$  ft =  $6.25 \times 10^{-6}$  ft

This corresponds to  $(6.25 \times 10^{-6} \text{ ft}) / (10^{-3} \text{ sec}) = 6.2 \times 10^{-3} \text{ ft/sec}$  velocity error. This is above the allowable error of  $10^{-3}$ . If the sensing head and specimen do not lie in the same horizontal plane, though, the error will increase approximately as the sine of the angle between their separation vector and the horizontal. Therefore the error would increase further above the error budget. Gyroscopes or angular accelerometers in pitch are needed to correct for this effect, as well as for those needed for sled yaw.

Angular Errors

The change in the sensitivity of the velocity measurement due to sled yaw can be seen with reference to Figure A.8.4.

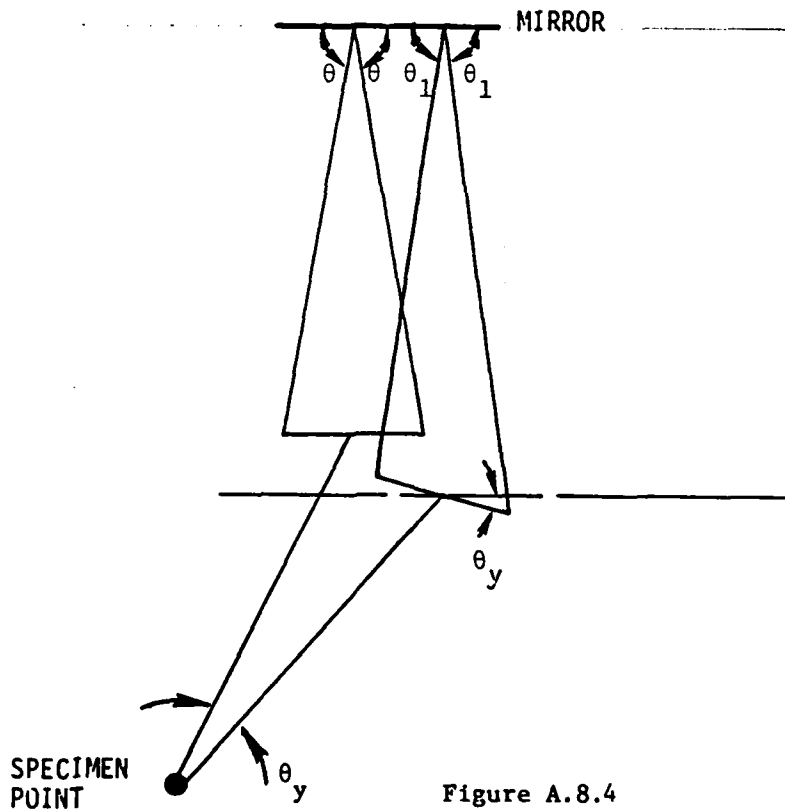


Figure A.8.4

The required quantity is  $\theta_1$ . With no sled yaw the angular sensitivity to sled motion in the direction of the track is  $\sin \theta$ . As the sled yaws the sensitivity changes to  $\sin \theta_1$ , as shown in Figure A.8.5.

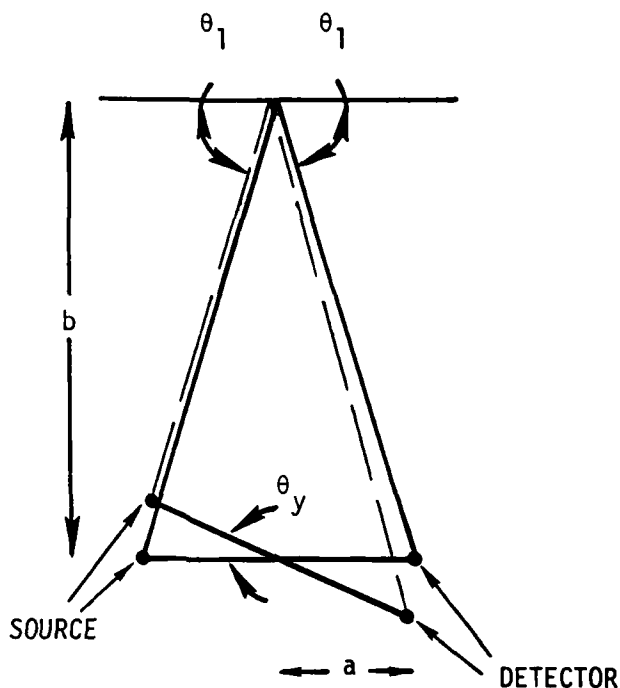


Figure A.8.5

$b$  = sensing head to mirror distance

$a$  = 1/2 source to detector distance

Since  $\theta$  (with no yaw) =  $\arctan \frac{b}{a}$ , and  $\theta' = \arctan \frac{b}{a \cos \theta_y}$   
 $\Delta \theta = 6.25 \times 10^{-9}$  rads when  $\theta_y = 1.25 \times 10^{-3}$  rads. This assumes  $b$  = distance of closest approach to mirror = 5 ft, and  $a = .04$  ft. The corresponding value of  $\Delta \sin \theta$  (sensitivity error) is  $\sim 5 \times 10^{-12}$ , therefore the angular error is negligible.

If no tracking system were used the position of the beam in the detector plane would vary. The required beam tracking could be accomplished in this case using a large area detector array that would allow mapping of the beam position vs. time. Then the angular corrections for the velocity measurement sensitivity could be made in much the same

way as on the original design proposal, except that now the laser-detector distance used for the correction would be variable.

To keep the detector array area requirements to a minimum a laser signal parallel to the average sled velocity vector would be used. Then the largest variance on the beam direction would occur as a result of sled pitch and yaw. Assuming a slipper spacing from the front to the rear of the sled of about 8 ft., and an all around slipper-rail clearance of .06" the maximum angular changes in the beam direction due to sled pitch and yaw are on the order of  $10^{-3}$  radians. If the signal were being returned from a maximum distance of 100 meters, this angle shift would necessitate use of a detector array  $2 \times 100 \text{ meters} \times 10^{-3} \text{ radians} = 20 \text{ cm}$  on a side.

REFERENCE

1. "The Holloman Track, Facilities and Capabilities", Air Force Special Weapons Center, 6585th Test Group, Test Track Division, Holloman Air Force Base, New Mexico, 1974.

## APPENDIX A.9

### TRANSLATIONAL INTERFEROMETER MODELING EXPERIMENT

Although not in the scope of this contract, a simplified experimental version of the translational interferometer shown in figure A.9.1 was assembled and tested. In these tests a rotating wheel was used to simulate relative motion of the rail. Objectives were proof of principle and identification of areas of difficulty.

Measurements were attempted of the effects on the scale factor (fringe frequency vs. velocity) of rail surface finish and angle filtering width.

System alignment difficulty was experienced until the configuration in the figure was used. Signal to noise ratio was marginally low with the simple detectors employed. Signals were observed even without a separate angle filter resulting in acceptance angles on the order of 20 degrees. This qualitatively indicated that averaging over acceptance angles occurs to a large degree which was an encouraging result.

Frequency measurements by oscilloscope agreed with theory to the accuracy (2%) of the experiment.

We attempted to make  $5 \times 10^{-7}$  resolution measurements of changes in the scale factor. Here the number of fringes per revolution were measured with a counter. Low signal to noise resulted in a large number missed counts and the equipment need to solve the problem was not available.

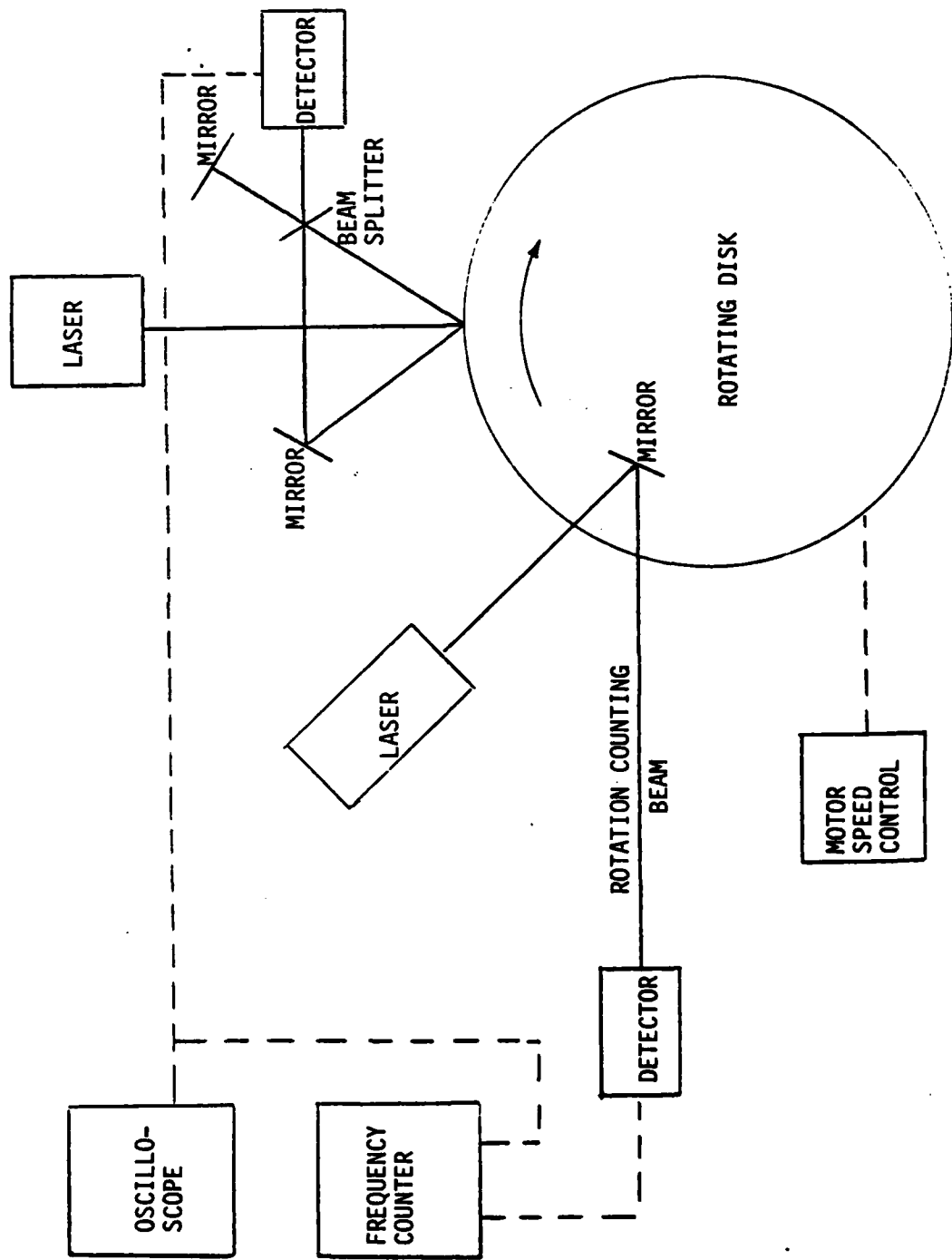


Figure A.9.1 Translational Interferometer Experiment

## APPENDIX A.10

### EFFECTS OF MECHANICAL VIBRATION ON THE ACCURACY AND SURVIVABILITY OF PROPOSED DESIGNS FOR THE IMPROVED VELOCITY MEASUREMENT SYSTEM

#### OBJECT OF ANALYSIS

The analysis contained in this report attempts to compute the first order effects of vibration on the accuracy and survivability of the various proposed velocity measurement systems. The analysis concentrates on the Translational interferometer and its components and extrapolates its findings to the other proposed designs. Typical system and component configurations are assumed in order to conduct the analysis.

#### TRANSLATIONAL INTERFEROMETER

##### Assumptions:

1. The system configuration will be that given in Figure A.10.1. The mounting plate is steel.
2. Mirrors, lenses, and components are considered integral parts of the support plate. This is a severe simplification but advisable to allow a preliminary result in an economical manner.
3. Acceleration or Force is transmitted through the center of gravity of the support plate, i.e., no coupling moment. (Tilting of the Sled and Interferometer are discussed in Appendix A.3).
4. The plate is square (ease of analysis).
5. Light source is a He-Ne laser.  $\lambda_0 = 0.6328 \mu\text{m}$ .

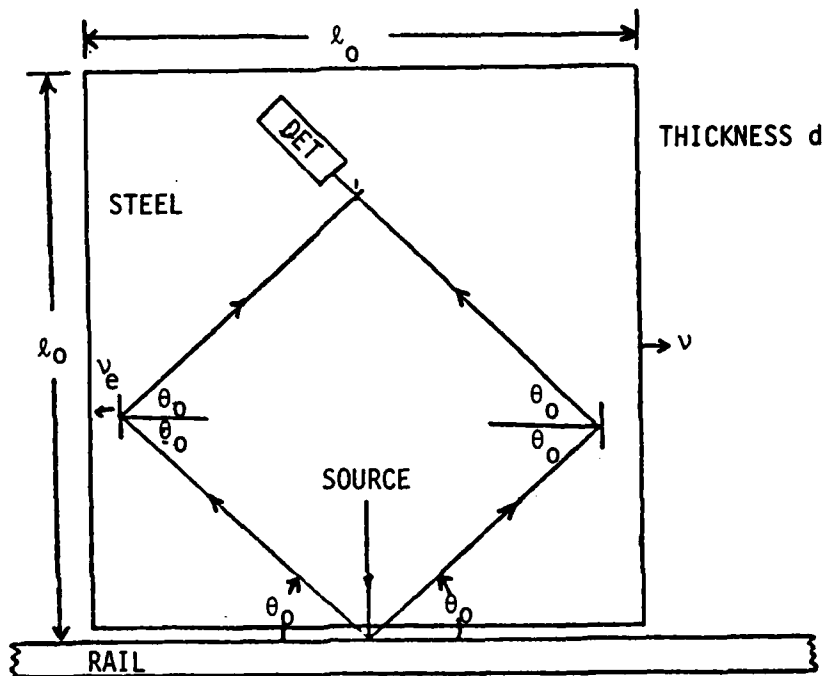


Figure A.10.1

Maximum allowed displacement of mirrors

Each leg of the interferometer will be frequency (+) shifted by  $v \cos \theta_0 / \lambda_0$  where  $v$  is the velocity of the system. The fringe rate frequency at the detector will be the difference and thus:

$$f = 2 v (\cos \theta_0) / \lambda_0 \quad (1)$$

Now we assume that the vibrations are sufficient to compress/stretch the steel mounting plate such that the left mirror moves with respect to the right mirror which we will consider fixed. This will manifest itself as an error velocity  $v_e$  of the left mirror with respect to the right mirror. Consequently, its fringe rate will be

$$f_e = 2 v_e (\cos \theta_0) / \lambda_0 \quad (2)$$

This represents an error and cannot exceed 1 part in  $2 \times 10^6$  of total fringe rate  $f$ , therefore,

$$\frac{|f_e|}{|f|} \leq 0.5 \times 10^{-6} \quad (3)$$

and from (1) and (2)

$$\frac{|v_e|}{|v|} \leq 0.5 \times 10^{-6} \quad (4)$$

at  $v = 2,000$  ft/sec  $\rightarrow |v_e| \leq 10^{-3}$  ft/sec. and in a measurement interval of  $10^{-3}$  sec, this relates to a max relative deflection  $(\Delta l_0)$  max

$$(\Delta l_0) \leq 0.3 \mu\text{m} \quad (5)$$

This must be met each measurement interval in order that the accuracy not become out of specification.

Resonant frequency of system:

The restoring force is found from the definition of Young's modulus

$$F = \frac{YA}{l_0} \Delta l = k\Delta l \quad (6)$$

or  $k = \frac{YA}{l_0} \quad (7)$

- $l_0$  - length in direction of force
- A - cross sectional area normal to force
- Y - Young's modulus

From the homogenous force equilibrium equation:

$$ma + kx = 0 \tag{8}$$

$$m \frac{d^2x}{dt^2} + kx = 0$$

the resonant frequency is found to be

$$\omega_n^2 = k/m \tag{a}$$

$$\text{thus } f_n = \frac{1}{2\pi} \sqrt{\frac{k}{m}} = \frac{1}{2\pi} \sqrt{\frac{YA}{m\ell_0}} \tag{b}$$

now from Figure 1

$$A = \ell_0 d$$

$$m = \rho v = \rho \ell_0 d$$

$$f_n = \frac{1}{2\pi \ell_0} \sqrt{\frac{Y}{\rho}} \tag{10}$$

$$f_n = \frac{32.5}{\ell_0} \text{ KHz} \quad \ell_0 \text{ in inches} \tag{11}$$

$\ell_0$ (inches)	1	2	3	4	5
$f_n$ (kHz)	32.5	16.3	10.8	8.1	6.5

Vibration frequencies close to or less than 1kHz will cause more significant errors than those much greater. The higher frequency will tend to average out, therefore, system plates as large as 5" square have a resonant frequency well above 1 kHz.

The above is for a point mass on a spring and obviously is a crude approximation. Resonant frequencies may be obtained by solving for the lowest order boundary modes from which we find:

$$\frac{2\pi f_n}{v} \ell_0 = \pi$$

$$f_n = \frac{v}{2\ell_0}$$

where  $v$  = velocity of sound in steel = 5.13 km/sec, and so we find

$$f_n = \frac{100 \text{ kHz}}{\ell_0} \quad \ell_0 \text{ in inches.} \quad (12)$$

$\ell_0$ (inches)	1	2	3	4	5
$f_n$ (KHz)	100	50	33	25	20

This shows much higher resonant frequencies for a given plate dimension. Therefore it is safe to say that (11) will give us conservative estimates.

#### General Model for a Mechanical System for Vibrational Analysis

In order to analyze more detailed components of the system, a model is needed to account for the various parts. A general model is one which has mass, spring constants and damping. Such a system can be described by the following 2nd order, linear differential equation:

$$m\ddot{x}(t) + c\dot{x}(t) + kx(t) = f(t) + \text{Boundary conditions} \quad (13)$$

where

- $m$  = mass of system
- $c$  = damping coefficient
- $k$  = spring constant
- $f(t)$  = driving force function
- $x(t)$  = displacement

Let us consider the case of forced vibration of the form

$$f(t) = f_0 \sin \omega_0 t \quad (14)$$

therefore, equation (13) becomes:

$$m\ddot{x}(t) + c\dot{x}(t) + kx(t) = f_0 \sin \omega_0 t \quad (15)$$

and we assume

$$\begin{aligned} \dot{x}(0) &= 0 && \text{(no initial velocity)} \\ x(0) &= 0 && \text{(no initial displacement)} \end{aligned}$$

The general solution to (15) is:

$$x(t) = \mu_1 e^{-\alpha t} \cos \beta t + \mu_2 e^{-\alpha t} \sin \beta t + \mu_3 \cos \omega_0 t + \mu_4 \sin \omega_0 t \quad (16)$$

$$\text{where } \alpha = \frac{c}{2m} ; \quad \beta = \left[ \frac{k}{m} - \frac{c^2}{4m^2} \right]^{1/2} \quad (17)$$

Let us define some useful quantities:

recall  $\omega_n$  is resonant frequency of system

$$r \equiv \omega_0 / \omega_n \quad (18)$$

$$d \equiv C / C_c$$

where  $C_c$  is critical damping coefficient, i.e., when  $\beta = 0$

$$\text{from (17) we get } C_c = 2m\omega_n \quad (20)$$

$$\alpha = d\omega_n \quad (21)$$

$$\beta = (1-d^2)^{1/2} \omega_n \quad (22)$$

note that:

$d = 0$	no damping
$0 < d < 1$	underdamped
$d = 1$	critically damped
$d > 1$	overdamped

(23)

Let us look at steady state solution to (16) using reference (1) to get  $\mu_3$  and  $\mu_4$ .

$$x_{ss}(t) = \frac{(f_0/k) \sin(\omega_0 t - \phi)}{\{(1-r^2)^2 + (2rd)^2\}^{1/2}} \quad (a)$$

(24)

$$\phi = \tan^{-1} \left( \frac{2rd}{1-r^2} \right) \quad (b)$$

but from (6)  $f_0/k = \Delta l_0$ . This is static deflection under load  $f_0$ .

Now let  $x = \max x(t)$  (this is obviously when  $\sin(\omega_0 t - \phi) = 1$ ) and we can define a magnification factor  $\frac{x}{\Delta l_0}$  and get

(25)

$$\frac{x}{\Delta l_0} = \frac{1}{\{(1-r^2)^2 + (2rd)^2\}^{1/2}} \quad (26)$$

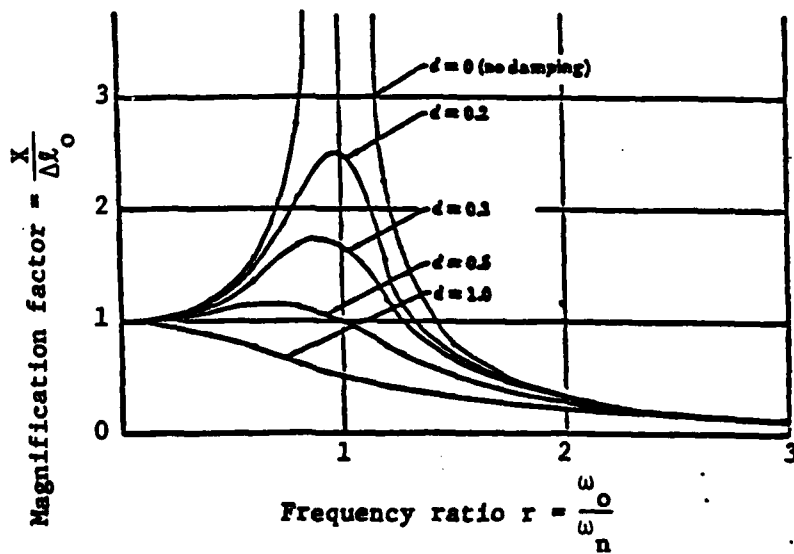


Figure A.10.2

From the above analysis, we can draw some preliminary conclusions:

1. For minimum deflection/magnification,  $r \gg 1$

$$\omega_n \gg \omega_o$$

2. Some damping should always be present to insure that if  $f(t)$  has a harmonic at  $\omega_n$ , its effect will not be devastating.
3. Damping insures  $\alpha$  will be as large as possible thereby the transients will die out more rapidly.

Lens/Mirror Mount Analysis:

In this section, we attempt to analyze a typical lens/mirror mount assembly. A typical mount is proposed and analyzed.

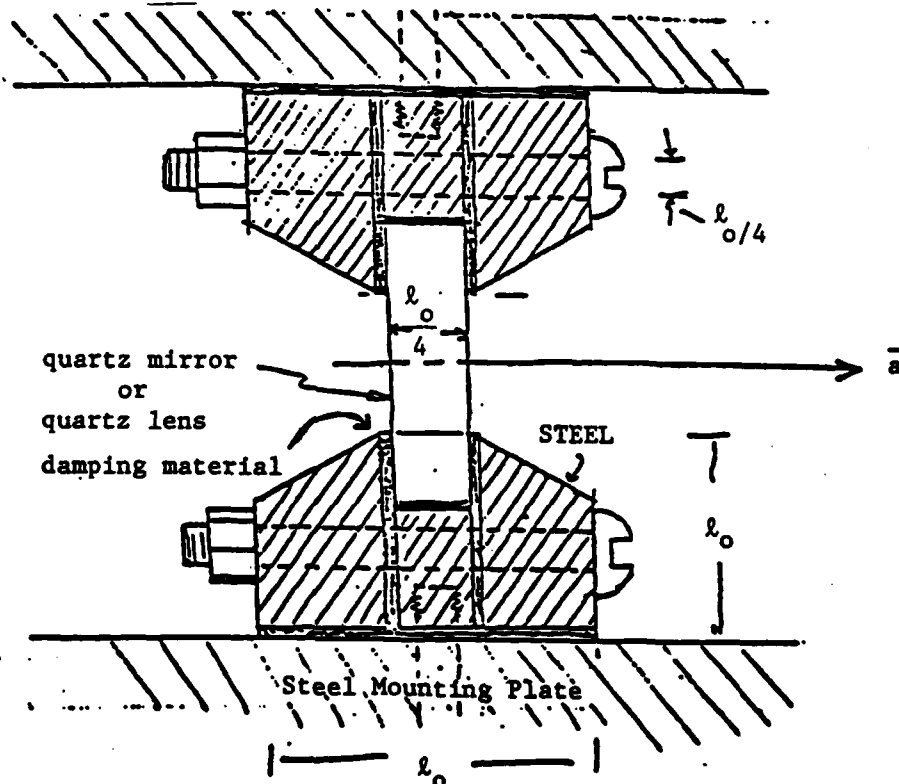


Figure A.10.3

DATA:  $\rho_s = 7.7 \times 10^3 \text{ kg/m}^3$  ;  $\rho_q = 2.7 \times 10^3 \text{ kg/m}^3$   
 $Y_s = 21 \times 10^{10} \text{ nt/m}^2$  ;  $Y_q = 71.7 \times 10^{15} \text{ nt/m}^2$

Neglect mass of damping materials.

Volume of mount  $V_m \sim 2\ell_o^3$   
 Diameter of lens  $\sim \ell_o$   
 Height of lens  $\sim \ell_o/4$

What is the spring constant of the steel portions? This would normally be  $k_s$ , however, the steel portion is made up of screws and various pieces. Let us assume some degradation occurs because of this -10%.

$$k_{\text{steel}} = 0.9 k_s \quad (27)$$

Actually, this is a best case analysis since the degradation is probably far greater. However, if it does not stay in spec with these values, it will not for lower values.  $k$  for mount system has to be a weighted average.

$$k_m = \frac{M_{\text{steel}} k_{\text{steel}} + M_q k_q}{M_{\text{steel}} + M_q} \quad (28)$$

from (27) we get

$$k_m = 15.9 \times 10^{10} \ell_o \text{ nt/m} \quad (29)$$

( $\ell_o$  in m)

Resonant Frequency of Mount

$$M_m = M_{\text{steel}} + M_q \quad \text{so from (27) we get}$$

$$M_m = 15.9 \times 10^3 \ell_o^3 \text{ kg} \quad (30)$$

from (9)  $\omega_n = \sqrt{\frac{k}{M_m}}$  so from (29) & (30)

$$\omega_n = \frac{3162}{l_o} \text{ sec}^{-1} \quad (31)$$

$$f_n = \frac{0.503}{l_o} \text{ kHz} \quad (l_o \text{ in m}) \quad (32)$$

Accuracy/Survivability Requirements for a 1 in. Mount

Let us assume  $l_o = 1 \text{ in} = .0254 \text{ m}$ . This value is selected to be representative but not necessarily optimum as the optimum diameter will change as the design changes.

The maximum allowed deflection to remain accurate was found by (5) to be  $0.3\mu\text{m}$ . Let us assume a harmonic of  $f(t)$  is  $\omega_n$  ( $r = 1$ ), what damping is necessary to keep deflection below  $0.3\mu\text{m}$ ? Assume  $a_o = 200 \text{ g's}$ .

Max deflection at 200 gs is from(6):

$$\Delta l_o = F/k = \frac{a_o}{k/m} = \frac{a_o}{\omega_n^2} \quad (33)$$

$$(\Delta l_o)_{200} = \frac{200g}{\omega_n^2} \quad \text{and for } l_o = 1 \text{ in.}$$

$$(\Delta l_o)_{200} = 0.13\mu\text{m}$$

$$\frac{x}{(\Delta l_o)_{200}} = \frac{0.3}{0.13} = 2.31$$

What value of  $d$  to keep  $x/\Delta l < 2.31$ . From (26),

$$d \geq 0.22$$

From (19) & (20)  $C = dC_c = d(2m\omega_n)$  and  $l_o = 1 \text{ in}$ .

$$C = 1.41 \times 10^4 \text{ kg/sec.} \quad (34)$$

This is minimum damping necessary.

Survivability - What magnification factor will cause it to break at 200 g's? Take  $l_0 = 1$  in.

Failure is determined by Tensile strength

$$(\Delta l_0)_F = \frac{TS \cdot l_0}{Y} \quad (35)$$

TS = tensile strength = 80,000 psi

Y = Young's modulus -  $30 \times 10^6$  psi

For  $l_0 = 1$  inch:

$$(\Delta l_0)_F = 68 \mu\text{m}$$

Therefore,

$$\frac{X}{(\Delta l_0)_{200}} = \frac{68}{0.13} = 523 \quad \text{and from (26) with } r = 1$$

$$d \geq 9.56 \times 10^{-4} \quad (36)$$

Equation (36) implies that only a slight amount of damping in all that is necessary to protect the mounting system from failing at 200 g's assuming worst case conditions.

#### Conclusion:

1. This best case analysis does not rule out the translational interferometer from effects of the vibration environment. More detailed analyses and tests are indicated.

#### Flag Interferometer

Appendix A.6 "Specimen to Measuring Point Velocity" discusses

similar first order analysis on the various components of the flag interferometer. One calculation not performed was to find static compression of the 2 meter I-Beam along the length of the beam. If we use equation (33) in this report, we find that a 1 g acceleration will result in 1.4  $\mu\text{m}$  deflection. If we use a distributed force derivation for the static compression we get the same formula as (33) except for a factor of 1/2. Therefore, at 1 g, it is safe to say we would see approximately 0.7 - 1.4  $\mu\text{m}$  compression. To keep it below 0.3  $\mu\text{m}$ , we need to isolate the beam from lateral acceleration to at least 1/2 g.

Since little lateral acceleration is required during the run (the track is straight) this requirement is theoretically possible. Practical problems in designing shock mounts and perhaps null servos to achieve the 0.5 g limit are anticipated.

REFERENCE

1. W. G. McLean and E. W. Nelson, Engineering Mechanics, 2nd Ed., Schawn Publishing Co., New York, N.Y., 1962.

## APPENDIX A.11

### REQUIREMENTS ON PINHOLE SIZE & DIAMETER OF LASER BEAM

The necessary angular divergence of the laser beam used on the flag interferometer is determined by two requirements. The first is that as the sled approaches successive flags the received signal must come from either the first or second flag from the sled. It was suggested in the proposal that a signal be received from the flag closet to the sled until it is approximately 5 feet in front of the sled, at which point the signal will "jump" from this interrupter to the one 13 feet behind it (18 feet from the sled). The divergence should not be larger than this value or it would allow a signal to be returned from both flags simultaneously.

The second requirement is that as the sled pitches and yaws, changing the angle of the rays striking the mirror on the flag, a signal must still be returned. (But, again, from either one flag or the other, and not both.)

Another consideration is that a geometry should be used that will allow the smallest beam divergence, because the divergence will affect the power requirements of the source laser. As the beam divergence increases the intensity of the signal received at a fixed aperture decreases.

#### I. Determination of Beam Divergence Required to Just Intercept Two Successive Flags.

Figure A11.1 shows two mirror positions.

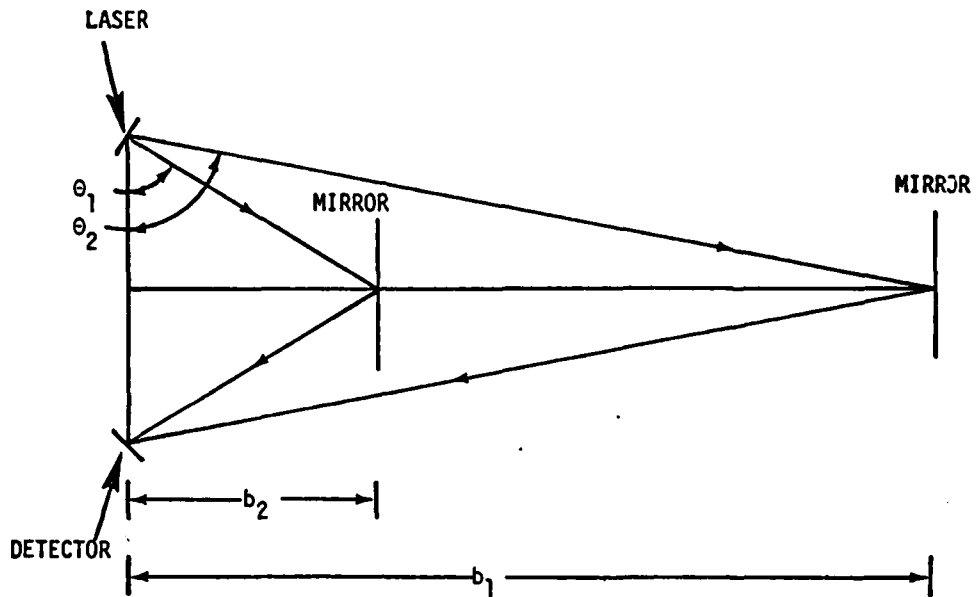


Figure All.1

Angular spread on the beam necessary =  $\theta_2 - \theta_1 = \Delta\theta$

$b_1$  = distance to interrupter at 18 ft.

$b_2$  = distance to interrupter at 5 ft.

$a$  = 1/2 source to detector distance = .04 ft. (from proposal).

Then from geometry

$$\theta_1 = \arctan 5 \text{ ft}/.04 \text{ ft}$$

$$\theta_2 = \arctan 18 \text{ ft}/.04 \text{ ft}$$

$$\Delta\theta = \theta_2 - \theta_1$$

and  $\Delta\theta < 5.8 \times 10^{-3}$  radians divergence in laser beam required to just prevent return of a signal from both flags.

$\Delta\theta$  is the maximum angular divergence allowable in the laser beam, because at a larger value than this a signal could be returned from the mirrors on the flag at 5 ft. and at 18 ft. simultaneously.

II. DETERMINATION OF BEAM DIVERGENCE REQUIRED TO ALLOW FOR PITCH AND YAW EFFECTS

Assuming the sled rides on 2 slippers per rail, the maximum angular shift of the beam is set by the distance between the two slippers, and the clearance between the slipper and the rail.

From "The Holloman Track: It's Facilities and Capabilities," the all around clearance between the slipper and the track = .06". The approximate distance between the forward and rear slipper is about 8 ft.

To see what the yaw effects on beam direction are, one needs the geometry in a horizontal plane. (See Figure All.2)

From Geometry:  $\theta_y \approx \frac{.12''}{8 \text{ ft.}} = 1.25 \times 10^{-3}$  radians

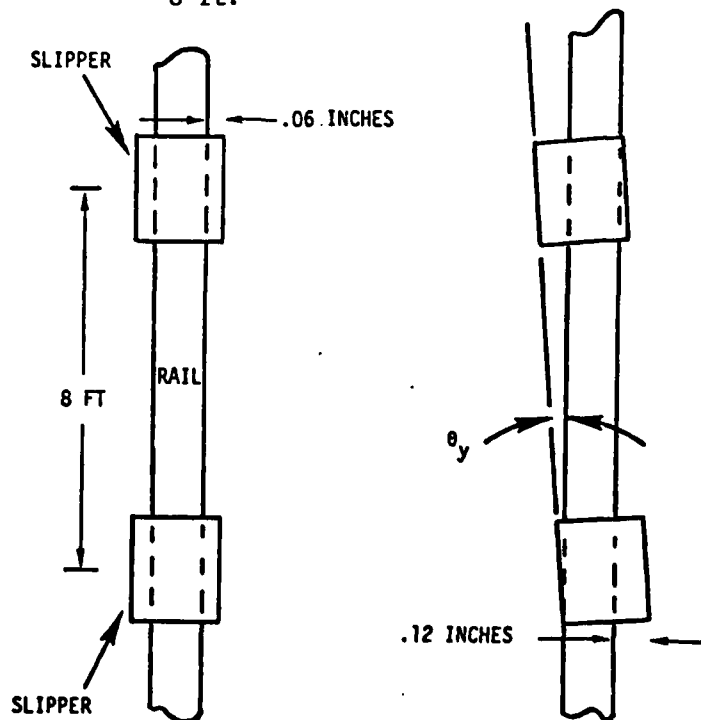


Figure All.2

Since the sled could pivot through this same angle in the opposite direction the total angular change is twice this value in the horizontal plane.  $\theta_y = \pm 1.25 \times 10^{-3}$  radians.

Since the relative dimensions to calculate the effect due to sled pitch are the same (.06" clearance, and 8 ft. length),  $\theta_p$  = angular change due to pitch (in the vertical plane) must also =  $\pm 1.25 \times 10^{-3}$  radians.

The largest angular change due to pitch and yaw is smaller than the beam divergence required to return an (approximately) continuous signal from successive flags. So as the sled pitches and yaws it may cause the return signal to "jump" from one flag to another, but the beam will still return from one of the flags (See Figure All.3).

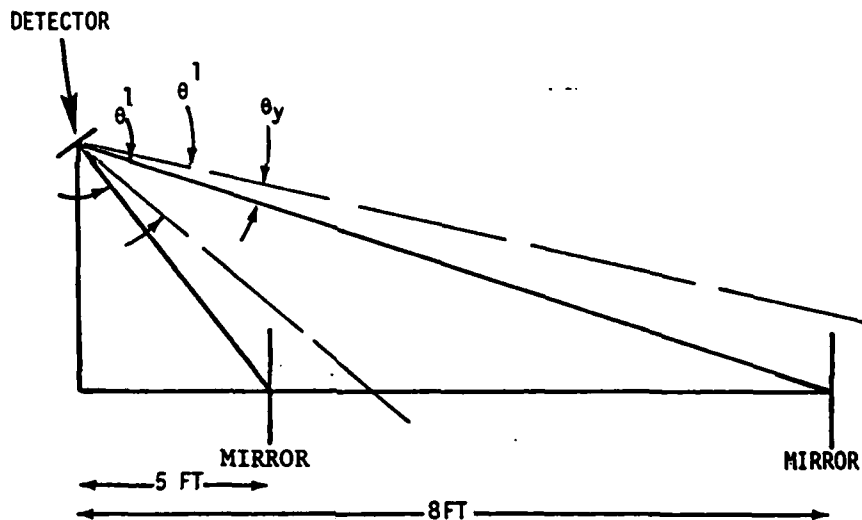


Figure All.3

Therefore the requirement on the beam divergence is just that set by the condition that as the signal leaves a flag at ~5 ft. from the sled it will just begin to return from the flag at 18 ft. For continuous velocity measurements, two overlapping systems would be used.

Assuming a symmetrically divergent beam, the requirement is that the beam diverge by  $5.8 \times 10^{-3}$  radians in both the horizontal and ver-

tical planes. This defines a square in the interrupter plane of length  $5.8 \times 10^{-3}$  radians  $\times d$ , where  $d$  = the distance from the laser source to the flag.

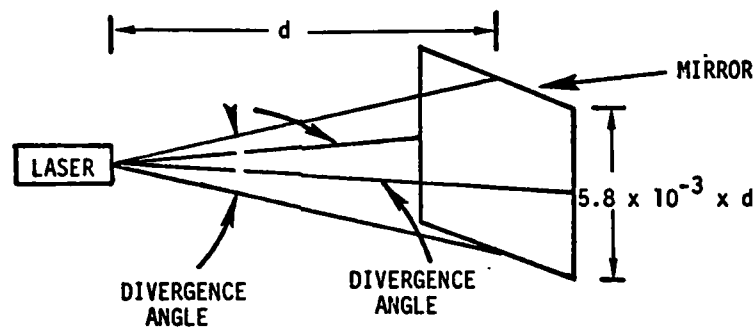


Figure A11.4

A symmetrically divergent beam would define a circle in the interrupter plane. For the circle to contain the above square within it, its radius would have to equal 1/2 of the square's diagonal, or

$$r_{\text{circle}} = \sqrt{2 \times (5.8/2 \times 10^{-3} \times d)^2}$$

So the required angular divergence would be

$$4.1 \times 10^{-3} \times d/d = 4.1 \times 10^{-3} \text{ radians.}$$

An elliptical or rectangular beam would result in less attenuation but for simplicity consider the circular beam.

To see what type of attenuation this divergence induces in the received signal, it is necessary to know the total divergence of the beam as it travels to the flag and back to the detector, and also the size of the intercepting aperture at the detector.

The requirement on the aperture diameter comes from the following consideration (See Figure A11.5).

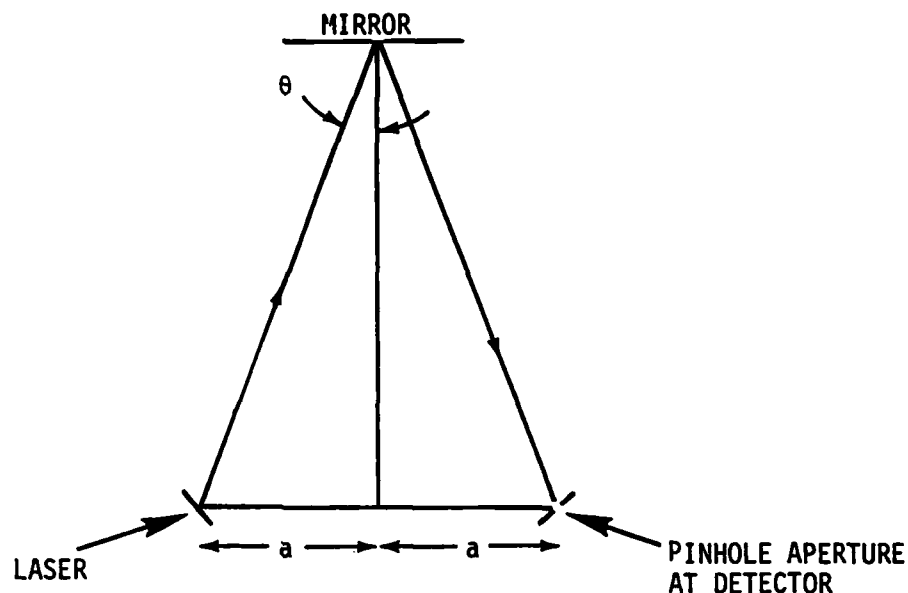


Figure All.5 :

For the error in  $\cos\theta$  to be <1 part per 2 million a must be known to  $\pm .005''$ , and b must be known to  $\pm .5''$ . (From original proposal.) (1) Therefore, since a is measured as 1/2 the distance between the source and the detector, the source laser diameter, and the pinhole diameter must be less than  $2 \times .005''$  for a to be known to  $\pm .005''$ .

So therefore the maximum value of the pinhole aperture =  $.01''$ .

Now, let d = the source to flag distance. As the diverging beam travels to the flag and back to the detector, the total area intercepted by the beam in the detector plane is the same as if the beam had just traversed a distance  $2d$  from its source.

The angular spread of the beam in each direction is  $4.1 \times 10^{-3}$  radians, so at a flag-source distance of 18 ft., the diameter of the

circular image in the receiver plane =  $2 \times 18' \times 4.1 \times 10^{-3}$  radians =  
.15 ft. with a corresponding radius of 1/2 this value or  $r \approx .07$  ft.

The ratio of the intercepted beam intensity to the emitted intensity (power) is equal to the ratio of the detector aperture area to the area of the laser image on the detector plane, or, equivalently, to the ratio of their radii squared.

$$\begin{aligned} \text{intercepted intensity} &= \frac{(r_{\text{aperture}})^2}{(r_{\text{image}})^2} \times \text{original beam intensity} \\ &= \frac{(.005'')^2}{(.07 \text{ ft})^2} \times \text{original beam intensity} \\ &= 3.5 \times 10^{-5} \times \text{original beam intensity} \end{aligned}$$

Conclusion: The power intensity intercepted by the detector used in the flag interferometer is down by a factor of  $3.5 \times 10^{-5}$  from the original laser (source) power, if no tracking system is used. An elliptical beam would result in an attenuation of only  $1.4 \times 10^{-4}$ . Since the number is so small, the signal to noise requirements at the detector may have to be met using some form of tracking system.

Addendum to the above calculation:

If the angular divergence of the laser beam were smaller than that specified to just intercept the flag at 5 ft. ahead and that at 18 ft. ahead of the sled, there would be a finite signal "drop-out time". But a problem arises in using the 5 ft. and 18 ft. distance flags to calculate the necessary beam divergence.

If the sled yaws by an angle  $\theta_y$ , so as to increase the value of  $\theta$  (See Figure 6) the beam could simultaneously intercept two flags out ahead of the sled and return a signal from both of them.

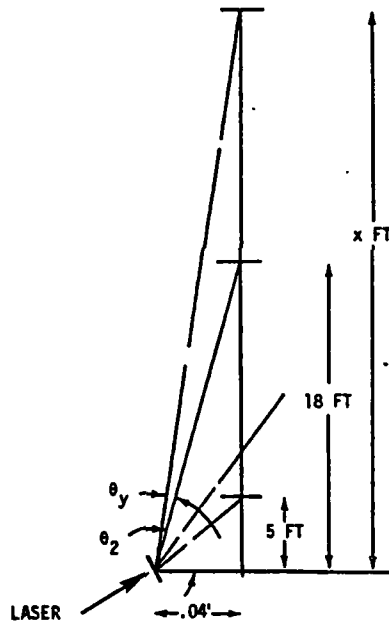


Figure All.6

$\theta_y$  = yaw angle

$\theta_2$  = angle of ray  
striking mirror  
on flag 18 ft.  
ahead of the 18 ft.  
sled.

If  $\theta_y$  = its maximum value of  $+ 1.25 \times 10^{-3}$  radians, then  $x$  (ft.) in the figure can be found from:

$$\arctan (x \text{ ft.}/.04 \text{ ft.}) = \theta_2 + \theta_y$$

$$\text{and } \theta_2 = \arctan 18 \text{ ft.}/.04 \text{ ft.}$$

Therefore,

$$\frac{x \text{ ft.}}{.04 \text{ ft.}} = \tan (\arctan \frac{18 \text{ ft.}}{.04 \text{ ft.}} + 1.25 \times 10^{-3} \text{ radians})$$

$$\text{or } x \text{ ft.} = 41 \text{ ft.}$$

So the laser could return a signal from two flags simultaneously, the maximum distance of the furthest one being 41 ft., and the other flag being the one 13 ft. closer to the sled. This is because the beam divergence required to intercept two flags decreases with distance along the track relative to the sled.

One way to avoid this problem would be to make the beam divergence smaller, but this would increase the signal drop-out time, as stated above.

Another way to ensure that a signal would return from only one flag at a time would be to make the width of the mirrors attached to the flags such that a signal could not be returned from further than 18 ft. ahead of the sled. (See Figure All.7).

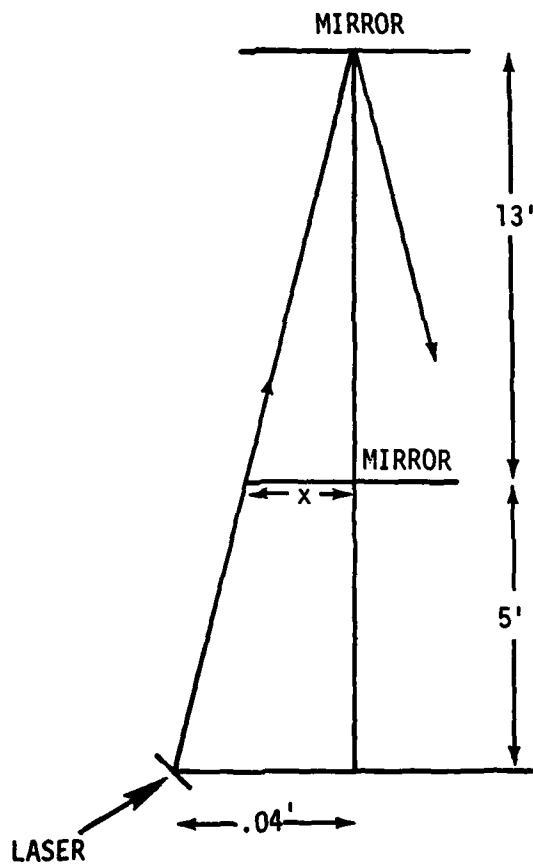


Figure A11.7

Flag width = 2 x.

As can be seen from the diagram, any flag further than 18 ft. could not return a signal to the detector. The signal would be cut off by the flag in front of it.

To determine this flag width x use

$$\theta = \text{arc tan } 18 \text{ ft.}/.04 \text{ ft.}$$

and  $\theta = \text{arc tan } 13 \text{ ft.}/x \text{ ft (from geometry)}$

Therefore,  $x \text{ ft.} = 13 \text{ ft.}/18 \text{ ft.} \times .04 \text{ ft.} \approx .03 \text{ ft.}$  and flag (mirror) width required is  $2 \times .03 \text{ ft.} = .06 \text{ ft.}$

Another consideration is that the signal returned to the detector falls off as the square of the distance from the sled to the flag. Therefore, as a signal is being received at the detector any "noise" from the flag 13 ft. further ahead could have a negligible effect on the reception of the required signal.

APPENDIX A.12

APPLICABILITY OF A TWO-COLOR LASER TO THE PROBLEM OF  
CORRECTING FOR INDEX OF REFRACTION FLUCTUATIONS  
ON THE FLAG INTERFEROMETER SYSTEM

The flag interferometer system measures the displacement of the sled over an interval of time. To measure this displacement accurately it is necessary to know the index of refraction along the portion of the optical path that is changing due to the displacement. If a part per 2 million accuracy is required, the index of refraction, which is directly related to the wavelength of the light along the displacement path, must be known to this accuracy. Therefore  $\Delta n/n = 1$  part per 2 million =  $5 \times 10^{-7}$ .

A possible way to measure the index of refraction is by the use of a two-color laser for the measuring beam in the interferometer.<sup>(1)</sup> Theoretically, the value of the index of refraction along the part of the optical path that is changing due to the sled displacement can be calculated by observing the difference in the number of fringes received with the different wavelengths of light.

The calculation is as follows:

Let  $\lambda_1$  = wavelength of laser #1

$\lambda_2$  = wavelength of laser #2

$N_1$  = number fringes induced with  $\lambda_1$

$N_2$  = number fringes induced with  $\lambda_2$

$C_1$  = speed of light of 1st laser

$C_2$  = speed of light of 2nd laser

$n_1$  = the index of refraction of laser #1

$n_2$  = the index of refraction of laser #2

$$\left(\frac{n_2}{n_1}\right)_{\text{air}} \times \left(\frac{\lambda_1}{\lambda_2}\right)_{\text{vacuum}} = \left(\frac{\lambda_1}{\lambda_2}\right)_{\text{air}}$$

and from  $N_1 = 2d/\lambda_1$  and  $N_2 = 2d/\lambda_2$  you get

$$\left(\frac{N_1 - N_2}{N_1}\right)_{\text{air}} = \left(1 - \frac{\lambda_1}{\lambda_2}\right)_{\text{air}}$$

Where the quantities subscripted (air) refer to the actual wavelength along the optical paths used in the measurement.

So if  $N_1$  and  $N_2$  are measured, the ratio  $(\lambda_1/\lambda_2)_{\text{air}}$  is found from Equation 2, and Equation 1 relates  $(\lambda_1/\lambda_2)_{\text{air}}$  to  $(n_2/n_1)_{\text{air}}$ .

The value of either  $n_2$  or  $n_1$  is then calculated because of the relation

$$\frac{n_2}{n_1} = \frac{1 + \beta_2 \rho/\rho_s}{1 + \beta_1 \rho/\rho_s}$$

where  $\rho$  = the density of air in the medium you are calculating the index of refraction for,  $\beta_2$  and  $\beta_1$  are the values of  $\beta$  for the two wavelengths of light. Since  $\beta_2$  and  $\beta_1$  are known values,  $\rho/\rho_s$  can be solved for, and with it both  $n_2$  and  $n_1$ .

To see what type of accuracy is available using this system, it is required to see what degree of change in the index of refraction along the optical path used for the measurement will induce a measurable change in the quantity  $N_2 - N_1$  (from above).

$N_2$  and  $N_1$  are measurable to  $\pm 1$  fringe accuracy so the difference between them is measurable to  $\pm 2$  fringes. Therefore the smallest  $\Delta n$  "visible" with the 2 color system, is one just large enough to induce a change in  $N_2 - N_1$  of 2 fringes. Or  $\Delta(N_1 - N_2)_{\text{minimum}} = 2$  fringes.

The corresponding  $\Delta n$  is found as follows:

$$\left( \frac{N_1 - N_2}{N_1} \right)_{\text{air}} = \left( 1 - \frac{\lambda_1}{\lambda_2} \right)_{\text{air}}$$

Therefore

$$\Delta(N_1 - N_2)_{\text{air}} = \Delta \left[ N_1 \left( 1 - \lambda_1 / \lambda_2 \right)_{\text{air}} \right]$$

Since  $N_1$  is  $\gg \Delta N_1$

$$\begin{aligned} \Delta(N_1 - N_2)_{\text{air}} &\approx N_1 \times \Delta \left( 1 - \lambda_1 / \lambda_2 \right)_{\text{air}} \\ &= N_1 \times \Delta \left( \lambda_1 / \lambda_2 \right)_{\text{air}} \end{aligned}$$

$$\text{(using equation 1)} = N_1 \times \left( \lambda_1 / \lambda_2 \right)_{\text{vacuum}} \times \Delta(n_2 / n_1)_{\text{air}}$$

The sensitivity of measurements of  $\Delta(N_1 - N_2)_{\text{air}}$  is  $\pm 2$  fringes, so the minimum detectable value of  $\Delta(n_2 / n_1)$  is found from the relation,  $N_1 \times \left( \lambda_1 / \lambda_2 \right)_{\text{vacuum}} \times \Delta(n_2 / n_1)_{\text{air}} = \pm 2$  fringes.

Using a laser with a blue and a red component

$$\lambda_1 = 6328 \text{ \AA} \quad \beta_2 = .000297$$

$$\lambda_2 = 4546 \text{ \AA}$$

$$\beta_1 = .000291$$

At 2000 fps  $N_1 \approx 2 \times 10^6$  fringes/ $10^{-3}$  sec.

$$\begin{aligned}\text{Therefore } \Delta(n_2/n_1)_{\text{air}} &= 2 \text{ fringes} / 2 \times 10^6 \text{ fringes} \times 4546 \text{ \AA} / 6328 \text{ \AA} \\ &= 7.2 \times 10^{-7}\end{aligned}$$

This is the minimum detectable change in  $n_2/n_1$  using the two-color laser, at 2000 fps.

The sensitivity obtainable in measuring  $\Delta\left(\frac{n_2}{n_1}\right)$  varies inversely with velocity, therefore at 1000 fps  $\Delta\left(\frac{n_2}{n_1}\right)_{\text{air}} \approx 1.4 \times 10^{-6}$ , and at 500 fps =  $2.8 \times 10^{-6}$ .

How does this relate to  $\Delta N$  for one of the wavelengths. Look at variations in  $n_2/n_1$  from its value at STP.

$$\Delta\left(\frac{n_2}{n_1}\right) = \frac{(1+\beta_2)}{(1+\beta_1)} - \left(\frac{1+\beta_2}{1+\beta_1} \frac{\rho/\rho_s}{\rho/\rho_s}\right)$$

Where  $\rho$  = the density of the air along the optical path.

$\rho_s$  = the density of air at STP.

$$\text{Now } (1 + \beta_2)/(1 + \beta_1) = 1.000297/1.000291$$

and  $\Delta(n_2/n_1)_{\text{air}}$  (minimum measurable) is  $7.2 \times 10^{-7}$ .

$$\text{Therefore } \frac{1.000297}{1.000291} - 7.2 \times 10^{-7} = \frac{1 + \beta_2}{1 + \beta_1} \frac{\rho/\rho_s}{\rho/\rho_s}$$

$$\text{And } \rho/\rho_s = .91$$

This defines the minimum density change from STP that generates a measurable change in  $n$ . So since the change in the index of refraction  $n_1$  from its value at STP =  $(1 + \beta) - (1 + \beta\rho/\rho_s)$ , and  $\rho/\rho_s$  is known,  $\Delta n$  can be solved for,

If you are using the 6328 Å line for the measurement =  $\lambda_1$

$$\begin{aligned}\Delta n_1 &= (1 + \beta_1) - (1 + \beta_1 \rho/\rho_s) \\ &= (1.000291) - (1 + .000291 \times .91) \\ &= 2.6 \times 10^{-5} .\end{aligned}$$

So the minimum detectable change in  $n$  at 2000 fps, from its known value at STP using a 2 color laser =  $2.6 \times 10^{-5}$ . This decreases by an order of magnitude as the sled velocity decreases to 250 fps. This is not as good a resolution as required by the .001 fps accuracy at any velocity but may provide the best resolution achievable on measuring the index of refraction along the displacement path.

As the sled velocity decreases below 2000 fps the ratio  $\rho/\rho_s$  which will induce a measurable change in  $n$  decreases .

$$\text{At 1000 fps } \rho/\rho_s \approx .79 \text{ and } \Delta n_1 = 6.1 \times 10^{-5}$$

#### Error Due to Change in Shock Parameters Over the Sampling Time

There is an error introduced into the index of refraction measurement which arises as a result of changing shock parameters, and temperature fluctuations. These effects cause an apparent sled displacement to be measured which is not distinguishable from the actual displacement.

Suppose  $N$  = the number of fringes induced over the 1/1000 sec measurement interval. Part of the measured fringe pattern is due to

the sled displacement, and part of it is due to the apparent displacement caused by the variation in the optical path length due to atmospheric variations and changing shock parameters.

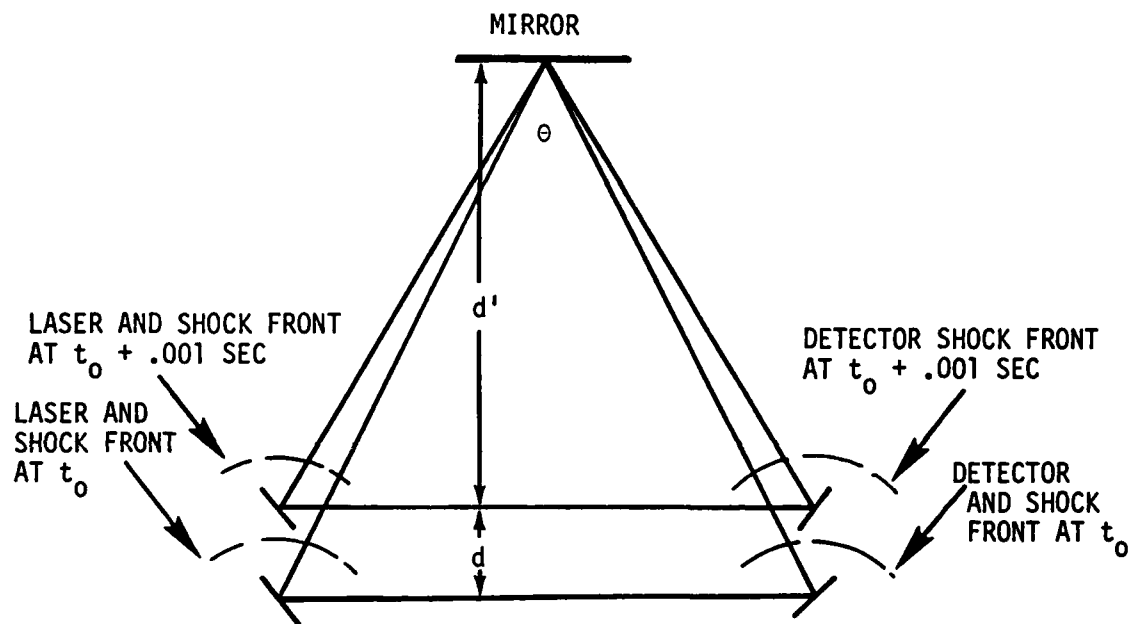


Figure A.12.1

$\theta \sim 0^\circ$  so

$$N = \frac{2d}{\lambda} + \left( \frac{2d'}{\lambda_a} - \frac{2d'}{\lambda_b} \right)$$

where  $\lambda_a$  = the average wavelength over  $d'$  at  $t_0$

$\lambda_b$  = the average wavelength over  $d'$  at  $t_0 + 1/1000$  sec

$N$  = number of fringes induced over 1/1000 sec

(if  $\lambda_a = \lambda_b$  then

$N = 2d/\lambda$  and there is no error)

Using a 2 color laser you can't tell what part of the difference in fringes  $N_1 - N_2$  occurred as a result of displacement through the medium, and what part of  $N_1 - N_2$  occurred as a result of changing atmospheric parameters along  $d'$ .

From Appendix A.4 and A.3 the apparent displacement  $d'$  over 1/1000 sec arising as a result of shock changes and atmospheric fluctuations has a maximum value about an order of magnitude less than the specifications of around  $10^{-7}$  ft. If  $d' = 10^{-7}$  ft, and  $d$  is 1 ft, (assuming the sled is traveling 1000 fps), then

$$N_1 - N_2 = \left( \frac{2d}{\lambda_1} - \frac{2d}{\lambda_2} \right) + 2d' \left[ \left( \frac{1}{\lambda_{1a}} - \frac{1}{\lambda_{1b}} \right) \left( \frac{1}{\lambda_{2a}} - \frac{1}{\lambda_{2b}} \right) \right]$$

$$\text{or } N_1 - N_2 = 2d \left( \frac{1}{\lambda_1} - \frac{1}{\lambda_2} \right) + 2d' \left[ \left( \frac{1}{\lambda_{1a}} - \frac{1}{\lambda_{1b}} \right) - \left( \frac{1}{\lambda_{2a}} - \frac{1}{\lambda_{2b}} \right) \right]$$

where  $\lambda_1$  = the wavelength of laser 1 over the interval  $d$

$\lambda_2$  = the wavelength of laser 2 over the interval  $d$

$\lambda_{1a}$  = the  $\lambda$  of laser #1 over  $d'$  at  $t_0$

$\lambda_{1b}$  = the  $\lambda$  of laser #1 over  $d'$  at  $t_0 + 1/1000$  sec

$\lambda_{2a}$  = the  $\lambda$  of laser #2 over  $d'$  at  $t_0$

$\lambda_{2b}$  = the  $\lambda$  of laser #2 over  $d'$  at  $t_0 + 1/1000$  sec

$2d' \left[ \left( \frac{1}{\lambda_{1a}} - \frac{1}{\lambda_{1b}} \right) - \left( \frac{1}{\lambda_{2a}} - \frac{1}{\lambda_{2b}} \right) \right]$  is the fraction of  $N_1 - N_2$  that is caused by changes in the shock parameters over the sampling time.

$$N_1 - N_2 = 2 \text{ ft} \times \left( \frac{1}{\lambda_1} - \frac{1}{\lambda_2} \right) + 2 \times 10^{-7} \text{ ft} \times \left[ \left( \frac{1}{\lambda_{1a}} - \frac{1}{\lambda_{1b}} \right) - \left( \frac{1}{\lambda_{2a}} - \frac{1}{\lambda_{2b}} \right) \right]$$

Since  $\left( \frac{1}{\lambda_1} - \frac{1}{\lambda_2} \right)$  and  $\left( \frac{1}{\lambda_{1a}} - \frac{1}{\lambda_{1b}} \right)$  and  $\left( \frac{1}{\lambda_{2a}} - \frac{1}{\lambda_{2b}} \right)$  are all

of the same order of magnitude then

$$\left[ \left( \frac{1}{\lambda_{1a}} - \frac{1}{\lambda_{1b}} \right) - \left( \frac{1}{\lambda_{2a}} - \frac{1}{\lambda_{2b}} \right) \right] \ll \left( \frac{1}{\lambda_1} - \frac{1}{\lambda_2} \right)$$

and therefore the part of  $N_1 - N_2$  induced by the changing shock parameters,  $2 \times 10^{-7} \text{ ft} \times \left[ \left( \frac{1}{\lambda_{1a}} - \frac{1}{\lambda_{1b}} \right) - \left( \frac{1}{\lambda_{2a}} - \frac{1}{\lambda_{2b}} \right) \right]$  is less than a  $10^{-7}$  part of the value of  $N_1 - N_2$ . So the effect of shock changes or temperature fluctuations on the measurement of  $N_1 - N_2$  or equivalently, on  $n_1$  is negligible.

#### CONCLUSION:

The optical path length changes over one measurement interval, using the flag interferometer, are too short to generate enough fringes to measure  $n$  (refractive index) to 1 part per 2 million ( $5 \times 10^{-7}$ ).

The best accuracy obtainable using a two-color laser (He-Ne, He-Cd) to measure  $n$  is about 2 orders of magnitude down, or  $\Delta n/n \approx 3 \times 10^{-5}$ .

APPENDIX A.13

FEASIBILITY OF TEMPERATURE MEASUREMENT

In Appendix A.4, variations in optical path length due to temperature fluctuations were discussed. These temperature fluctuations change the index of refraction. In order to correct for these changes in index of refraction the temperature changes need to be measured.

For any system involving a laser beam, the ambient environment has a profound effect on path length, direction, and power requirements. It is apparent that in order to keep the accuracy required by the system specifications the effects of temperature, density, pressure and wind velocity on the index of refraction need to be analyzed. The following analysis assumes only that the data acquired is correct and at least closely applicable to the situation.

Assume that the changes in the index of refraction are due to fluctuations in temperature, air density, humidity, pressures, etc. Starting with the equation for index of refraction of air<sup>1</sup>:

$$(1) \quad n = \left\{ k_1 \frac{P_d}{T} + \frac{k_2 e}{T} + \frac{k_3 e}{T^2} + \frac{k_4 P_c}{T} \right\} \times 10^{-6} + 1$$

$P_d$  = partial pressure

$k_1, k_2, k_3, k_4$  = atmospheric constants

$$= (1-3 \times 10^{-4}) P_t \quad (P_t = \text{total atmospheric pressure})$$

and

$$P_d + P_c = P_t$$

$$P_c = (3 \times 10^{-4}) P_t = \text{Partial CO}_2 \text{ pressure (.03\% content)}$$

e = partial H<sub>2</sub>O pressure - seasonal variance

Summer 9 torr average }  
 Fall-Spring 2-5 torr } from Dr. Kunkel<sup>3</sup>

For practical purposes, neglect the humidity and CO<sub>2</sub> pressures and use the equation given by Tatarski<sup>2</sup>:

$$n = (77.6 \times 10^{-6}) \frac{P}{T} + 1 \quad (k_1 = 77.6 \times 10^{-6} \text{ }^\circ\text{k/mbar})$$

Then for  $\Delta n = n_2 - n_1$ :  $n_1$  and  $n_2$  = index of refraction at two different positions

$$\Delta n = (7.76 \times 10^{-5}) \left\{ \frac{P_2}{T_2} - \frac{P_1}{T_1} \right\}$$

Contract specifications are for accuracy up to 1 part in 2 million, so take a maximum allowable change  $\Delta n = .5 \times 10^{-7}$

$$\frac{P_2}{T_2} - \frac{P_1}{T_1} = \frac{.5 \times 10^{-6}}{7.76 \times 10^{-5}}$$

and assume for the distances involved,  $P_1 = P_2 = 875 \text{ mbars}$

$$\frac{1}{T_2} - \frac{1}{T_1} = 7.364 \times 10^{-6} \text{ }^\circ\text{k}^{-1}$$

or

$$T_2 = T_1 \left\{ (7.364 \times 10^{-6} \text{ }^\circ\text{k}^{-1}) T_1 + 1 \right\}^{-1}$$

These results suggest that a 1 part in 2 million correction may be needed for temperature changes on the order of .7 °k in the range

280-310 °k, (refer to Table 1).

Phase II of a report on velocity measuring systems<sup>4</sup> has a large quantity of plotted data of temperature vs. time, temperature vs. spatial track coordinates, and temperature profiles from varying seasons.

Summary of Data:

- 1) Over the time of a sled run, ~ 25 sec, the temperature will not vary appreciably (it may vary spatially but not temporally at each point)
- 2) Temperature profiles show spatial variance according to season.<sup>4</sup>

Winter - the maximum difference in temperature over length of track ranges from .5 to 5°C at different times. The 5°C maximum above is 4.5°C between bench marks ( ~ 3000 ft).  
In the data taken temperature varies between -3° and 12°C.

Spring - .5-5°C over length of track. A maximum of 4°C between bench marks. Temperature varies between 16-28°C
- 3) Daytime has predominantly strong turbulence; rain and wind reduce temperature fluctuations but wind stirs up dust, and rain increases moisture content of air.
- 4) There is an isothermal period when the temperature profile remains relatively constant - several hours before sunset and after sunrise.

This data suggests that very high accuracy sled runs should be done during the isothermal periods of the day. Also, if the temperature does not vary more than .5°C peak to peak very few temperature measurements need to be made in order to make corrections. But more data is

TABLE 1

$T_1$ °k	$T_2$ °k	$\Delta T$ °k	$T_1$ °k	$T_2$ °k	$\Delta T$ °k
280	279.42	.58	296	295.36	.64
282	281.42	.58	298	297.35	.65
284	283.41	.59	300	299.34	.66
286	285.40	.60	302	301.33	.67
288	287.39	.61	304	303.32	.68
290	289.38	.62	306	305.31	.69
292	291.37	.63	308	307.30	.70
294	2943.36	.64	310	309.29	.71

Any of the above temperature differences would produce a difference in  $\Delta_n$  of  $5 \times 10^{-7}$  which in turn corresponds to the velocity accuracy goal of .001 ft/sec at 2000 ft/sec.

needed to support this view; specifically, more knowledge of temperature fluctuations along the track at heights < 1 ft.

Another problem needing consideration is that of the water brake troughs. These may need to be covered with thin plastic in order to keep evaporation effect on the environment minimal.

We can also relate  $\Delta n$  to the structure constant  $C_n^2$  and correlate the same temperature changes; it is also possible to check the linearity or nonlinearity of the constant  $C_n^2$ . Then for the change in the index of refraction<sup>3</sup>:

$$C_n^2 = (n_2 - n_1)^2 r^{-2/3} = \Delta n^2 r^{-2/3}$$

$$C_n^2 = (7.76 \times 10^{-5}) \left( \frac{P_2}{T_2} - \frac{P_1}{T_1} \right)^2 r^{-2/3}$$

or solving for  $\frac{P_2}{T_2}$  ....:

$$\frac{P_2}{T_2} - \frac{P_1}{T_1} = \frac{C_n r^{1/3}}{(7.76 \times 10^{-5})} \quad P_2 = P_1 = 875 \text{ mbars}$$

We are interested in correcting the optical path length for temperature fluctuations causing a  $\sim 1$  part per 2 million change in the index of refraction. So we can tabulate the temperatures needed to cause a maximum  $C_n^2 \sim 10^{-12} \text{ m}^{-2/3}$  for various distances  $r$ ; vary  $r$  from 20 cm - 550 cm (See Table 2).

The procedure used by Kunkel<sup>3</sup>, is derived from vertical measurements and adapted to horizontal fluctuations. This is only valid for a region the same size as which the vertical fluctuations were determined over. Also, those measurements were taken at a height of 8m above ground and

TABLE 2

$T_1$ °k	$T_2$ °k					
	r = .20 m	r = .50 m	r = 1.00 m	r = 2.00 m	r = 3.50 m	r = 5.50 m
280	279.3	279.1	278.9	278.6	278.3	278.0
282	281.3	281.1	280.8	280.5	280.2	279.9
284	283.4	283.1	282.8	282.5	282.2	281.9
286	285.3	285.0	284.8	284.5	284.2	283.9
288	287.3	287.0	286.8	286.5	286.2	285.9
290	289.3	289.0	288.8	288.4	288.1	287.8
292	291.3	291.0	290.7	290.4	290.1	289.8
294	293.3	293.0	292.7	292.4	292.1	291.8
296	295.2	295.0	294.7	294.3	294.1	293.7
298	297.2	297.0	296.7	296.4	296.0	295.7
300	299.2	299.0	298.7	298.3	298.0	297.7
302	301.2	300.9	300.7	300.3	300.0	299.6
304	303.2	302.9	302.6	302.3	301.9	301.6
306	305.2	304.9	304.6	304.3	303.9	303.6
308	307.2	306.9	306.6	306.2	305.9	305.6
310	309.2	308.8	308.6	308.2	307.9	307.5

Tabulated Figures of Temperatures needed to cause a  $C_n^2 \sim 10^{-12}$  for distances separating temperature measurement points.



changes in path length for the interferometer are due to temperature fluctuations at a height of < 1 ft. So the validity of these tabulations can only be for a worst case; in actuality, a larger horizontal temperature gradient is needed to cause a  $C_n^2 \sim 10^{-12}$  than a vertical gradient.

Wind also has some effect on the index of refraction in air; air at a velocity is at a different density than that of still air. Related by Bernoulli's principle:

$$\frac{P_0}{\rho_0} + \frac{v_0^2}{2} = \frac{P_1}{\rho_1} + \frac{v_1^2}{2}$$

$v_0$  = initial wind velocity

$P_0$  = initial air pressure

$\rho_0$  = initial air density

$v_1$  = new velocity

$P_1$  = new pressure

$\rho_1$  = new density

with  $v_0 = 0$ , and let  $P_0 = P_1 = P$  then

$$\frac{P}{\rho_0} = \frac{P}{\rho_1} + \frac{v_1^2}{2}$$

or

$$P \left( \frac{1}{\rho_0} - \frac{1}{\rho_1} \right) = \frac{v_1^2}{2}$$

$$\frac{1}{\rho_0} - \frac{1}{\rho_1} = \frac{v_1^2}{2P}$$

then

$$\rho_1 = \frac{2P\rho_0}{2P - \rho_0 v_1^2}$$

If  $P$ ,  $\rho_0$  and  $v_1$  are known (measurable) then  $\rho_1$  can be calculated and the change in the index of refraction can be found:

$$\rho_1 - \rho_0 = \frac{2P\rho_0}{(2P - \rho_0 v_1^2)} - \rho_0$$

and from the ideal gas law,  $P = \rho RT$ , i.e.,  $\frac{P}{T} = \rho R$ , then:

$$\Delta n = \frac{(7.76 \times 10^{-5}) R \rho_0^2 v_1^2}{[2P - \rho_0 v_1^2]}$$

Take conditions:  $P = 1828 \text{ lb/ft}^2$ ,  $v_1 = 15 \text{ ft/sec}$ ,  $\rho_0 = 2.5 \times 10^{-3} \text{ lb sec}^2/\text{ft}^4$   
also  $7.76 \times 10^{-5} \text{ }^\circ\text{k/mbar} = 3.715 \times 10^{-5} \text{ }^\circ\text{k/lb/ft}^2$

$$R = 8.314 \text{ Joules/}^\circ\text{k mole} = 53.3 \frac{\text{ft lbs}}{16 \text{ mole } ^\circ\text{R}} = 32.933 \frac{\text{ft}^2}{^\circ\text{k sec}^2}$$

(for air)

$$\Delta n = \frac{\left(3.715 \times 10^{-5} \frac{^\circ\text{k}}{\text{lb/ft}^2}\right) \left(32.933 \frac{\text{ft}^2}{^\circ\text{k sec}^2}\right) \left(2.5 \times 10^{-3} \frac{\text{lb sec}^2}{\text{ft}^4}\right) \left(15 \frac{\text{ft}}{\text{sec}}\right)^2}{\left[2(1828 \text{ lb/ft}^2) - \left(2.5 \times 10^{-3} \frac{\text{lb sec}^2}{\text{ft}^4}\right) (15 \text{ ft/sec})^2\right]}$$
$$= 4.707 \times 10^{-10}$$

for  $n_0 = 1.000292$ ,  $n_1 = 1.00029200047$

This result suggests that a correction is not needed for wind velocity (density changes) since the change in the index is negligible. Using the same procedure, but solving for velocity, a maximum  $\Delta n \sim 5 \times 10^{-7}$  gives  $v \sim 450$  ft/sec. So whenever the wind velocity is  $> 450$  ft/sec, a correction is in order; wind will obviously have no effect!

In order to correct for a change in the index of refraction due to temperature fluctuations, the temperature must be known between points where the minimum change to cause an error occurs. The temperature does not change appreciably with time (assuming stable weather, no clouds, etc.) and also does not change more than a net  $5^\circ\text{C}$  over the length of the track. However, changes  $\sim 1^\circ\text{C}$  may occur frequently enough over short distances ( $< 500$  ft) to correct for.

Several ways to measure the temperature have been suggested: 1) 50,000 ft (track length) thermocouple wire with magnetic (or electric) reed relays actuated by the passing of the sled. 2) liquid crystal temperature indicators mounted trackside and read by sensing head on the passing sled, and 3) thermistors mounted similarly to the thermocouple set-up. All three of these ideas have prohibitive costs ( $> \$100,000$ ). Another possible method which will involve a detailed analysis is the use of density determination by laser doppler back-scattering from air molecules.

If only on the order of 10 temperature indicators are required the problem is reduced. This might be the case if sled runs can be restricted to times when  $\Delta T \sim .5^\circ\text{C}$  when maximum accuracy is required.

All of these methods require knowledge of how frequently (spatially) these changes in density or temperature occur in order to take measurements at distances less than that which a maximum change can occur; another reason for an experiment.

### CONCLUSION

In order to give a complete answer on frequency of temperature or density measurements needed to correct the index of refraction, more information (data) is needed on the temperature structures at height's < 1 ft. above the ground. But a rough guess would be  $\sim 20$  ft/measurement. Some other effects that may need consideration in regard to the index of refraction are 1) refraction of the beam due to a wind velocity gradient normal to beam, not just density changes due to wind and 2) convection effect at close proximity to the ground. Overall, the temperature-index of refraction problem appears to be correctable.

#### REFERENCES

1. Beam, B.R., and Dutton, E.J., Radio Meteorology, National Bureau of Standards Monograph 92, 1966.
2. Ishimaru, Akira. Wave Propagation and Scattering in Random Media, Volume 2. Academic Press, 1978.
3. Kunkel, Ken, Personal letter to Walt Naumann, 2 July 1979.
4. Watkins, M.C., "Phase II Technical Summary Report on Study of Laser Applications to Velocity Measuring System", Aircraft Armaments, Inc., Report No. ER-3570, June 1964.

APPENDIX A.14

TRANSONIC BOW WAVE EFFECTS ON THE FLAG  
INTERFEROMETER VELOCITY MEASUREMENT

Appendix A.3 calculated effects on the flag interferometer velocity measurement that would arise due to the laser beam traversing the supersonic bow shock region in front of the sensing head. This calculation was made with the assumption that the sensing head could be positioned in such a way that it rode out ahead of the bow shock of the sled itself. This is feasible in the supersonic (above about Mach 1.3) speed regime, where the sled bow shock has a stand-off distance of only a couple of feet in front of the sled.

At the lower velocities, however, a problem arises since the stand-off distance of the shock front increases with decreasing velocity. For instance, in the transonic speed regime, at around Mach .98, the sled shock region can extend out close to 40 ft in front of the sled. At transonic velocities it would not be possible to keep the optical paths out of the influence of the sled shock.

It is difficult to calculate exact values for shock effects in the transonic regime because experimental data is limited and difficult to locate. Therefore, the results in this report are only approximations, but should be an indication of the magnitude of the problem. Most of the results applied to this analysis were taken from two articles. AN EXPERIMENTAL INVESTIGATION OF TRANSONIC FLOW PAST TWO-DIMENSIONAL WEDGE AND CIRCULAR-ARC SECTIONS USING A MACH-ZEHNDER INTERFEROMETER, by A. E. Bryson,<sup>(1)</sup> and THE AERODYNAMIC PERFORMANCE OF SMALL SPHERES FROM SUBSONIC TO HIGH SUPERSONIC VELOCITIES by A. C. Charters and R. N. Thomas.<sup>(2)</sup>

For purposes of analysis a typical sled and rail geometry is used. The pertinent dimension is the diameter of the sled creating the shock, which is estimated at four feet. (See Figure A.14.1).

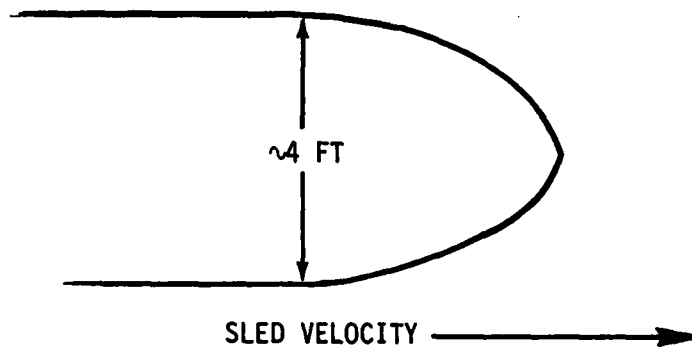


Figure A.14.1

Typical Sled Shape

#### Analysis of Error

There are 3 major components to the error that arises in the measured velocity due to the effects of the bow shock. The analysis of the first two effects closely follows that of Appendix A.3 for the supersonic shock, except that now the shock region of interest is that arising from the sled itself rather than from the sensing head.

As the laser beam traverses the shock region it is refracted. Above Mach 1 where a finite discontinuity in air density occurs across the shock front, the optical beam will also be refracted by an angle dependent on the magnitude of the discontinuity. The total angle the ray is refracted through on its way to the mirror surface and back induces an error because the sensitivity of the interferometer to sled displacement is directly dependent on the angle the optical paths make with the direction of the sled velocity.

The second effect is that, as the shock parameters change due to changing sled velocity over the .001 sec sampling time, the optical path length is changing due to increasing or decreasing transit time through the shock region. This introduces an apparent displacement of the sled which is indistinguishable from a signal generated by the

actual sled displacement, and as such introduces an error into the velocity measurement.

The third source of error arises if the shock stand-off distance is large enough relative to the laser-mirror spacing that the shock extends out past the mirror and the entire optical path falls within a shock region. Then the index of refraction value required to interpret the measured fringe count would be that behind the displaced part of the shock region. If the velocity is to be known to .001 fps at 2000 fps the index of refraction must be measured to a part per 2 million accuracy.

### Error due to Refraction of Beam Propagating Through the Sled Shock

As the laser beam used for the flag interferometer velocity measurement propagates through the shock region in front of the sled it is refracted. The net refraction angle is dependent on the shock parameters, and the angle between the ray and the lines of constant density within the shock. (See Figure A14.2).

An estimate of the error due to refractive effects can be calculated using geometrical considerations and the theoretical values for the shock density vs. Mach number. The exact form of the equation for the error and the relative parameters are dependent in a complex way on the sled geometry, the interferometer positioning with respect to the sled, and on the Mach number. For purposes of analysis certain simplifying assumptions will be made here.

To first order the net angle the ray is refracted through depends only on the net density gradient at right angles to the path of the beam. Therefore, the density profile across the shock will not be necessary, but the density gradient normal to the shock will be considered to depend only on the value of the difference between the stagnation density from that at the mirror.

A good approximation to the refraction effects can be made assuming the sled shock front in the region of interest is parallel to the mirror surface. This greatly simplifies the refraction equations, since the value of angles with respect to the normal to the shock front are the same as those with respect to the sled velocity vector. This is also not an unreasonable assumption in the transonic region (See Figure A.3.3 for shock front form at Mach 1.17). This assumption will be made in the first part of the analysis that follows.

The third assumption is that the density of air at the laser

source equals the stagnation density for the sled shock. Whether this is the case or not depends on the positioning of the sensing heads relative to the sled, but it should be a good approximate value, and is also the worst case value.

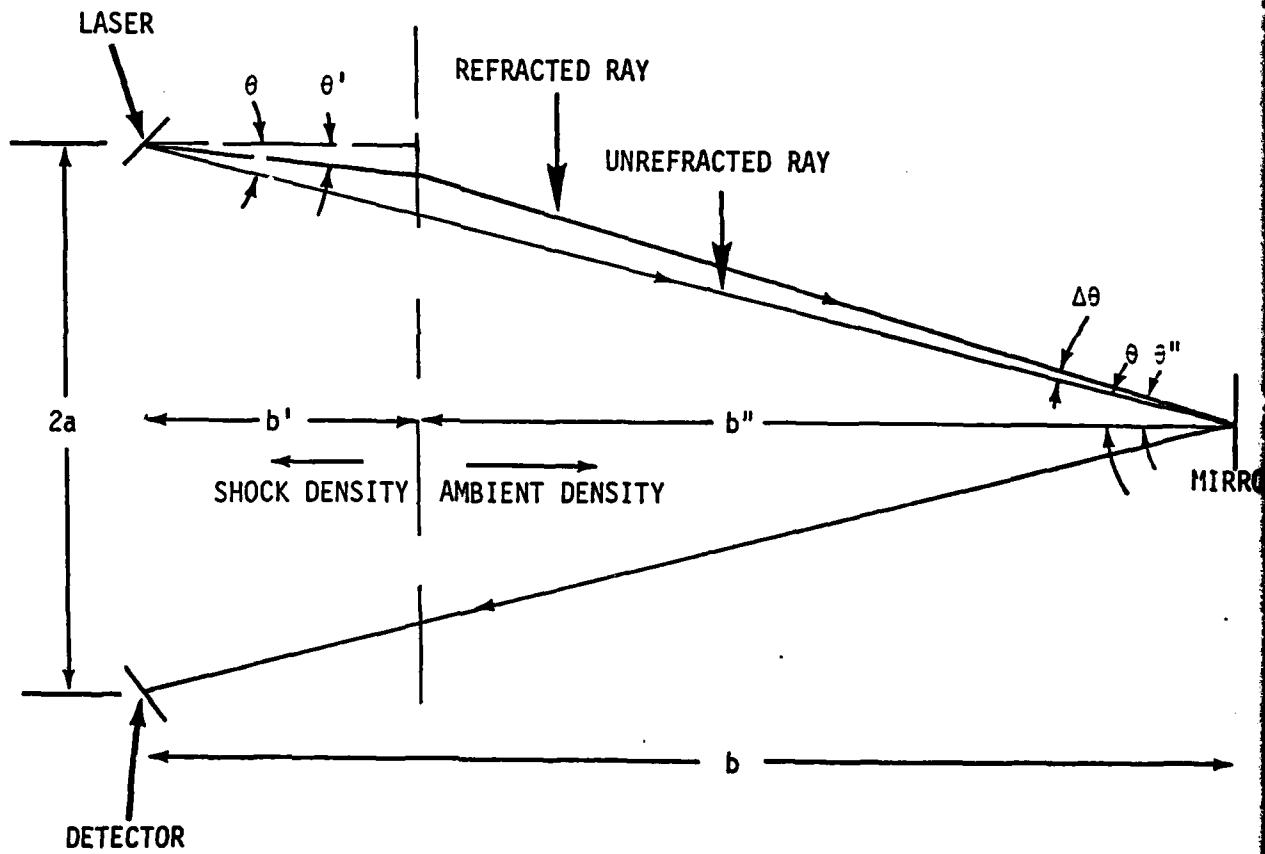


Figure A.14.2

List of Symbols used for the Analysis:

- $\theta$  =  $\arctan a/b$  = angle of undeflected ray with respect to sled velocity vector and shock normal
- $a$  = 1/2 (Laser-detector distance)
- $b$  = sled-mirror distance
- $b'$  = shock stand off distance
- $b''$  = distance from shock front to mirror
- $\theta'$  = angle of ray behind shock with respect to sled velocity vector and shock normal
- $\theta''$  = angle of ray in front of shock with respect to sled velocity vector and shock normal
- $n'$  = index of refraction behind shock (stagnation point)
- $n''$  = index of refraction in air (in front of shock)
- $\Delta b$  = the sled displacement over the measuring interval
- $\Delta d$  = the measured change in optical paths (fringe count)
- $\Delta\theta$  =  $\theta'' - \theta$  = the difference between the deflected and undeflected rays' angles with respect to the sled velocity vector.

The required quantity is  $\Delta b$ , the sled displacement over the sampling time. If an undeflected ray is assumed, this quantity will be calculated as the change in the optical path multiplied by the cosine of the angle  $\theta = \arctan a/b$ . This is in error, because the actual angle of the ray with respect to the sled velocity is  $\theta''$ . The magnitude of the error introduced into the velocity measurement will then depend on the difference between the values of  $\cos\theta$  and  $\cos\theta''$ . Using the previously mentioned assumptions, this difference can be calculated as follows:

From geometrical considerations,

$$b' \tan \theta' + b'' \tan \theta'' = a$$

Since  $\theta'$  and  $\theta'' \ll \pi/2$ ,  $\sin \sim \tan$ , and  $b' \sin \theta' + b'' \sin \theta'' \sim a$ ; and applying the laws of refraction

$$\sin \theta' = (n''/n') \sin \theta''$$

Combining the two results

$$\begin{aligned} \theta'' &= \arcsin \left[ \frac{a}{\frac{n''}{n'} b' + b''} \right] \\ &= \arcsin \left[ \frac{a}{b' \left( \frac{n''}{n'} - 1 \right) + b} \right] \end{aligned}$$

The fractional error introduced into the velocity measurement is  $(\cos\theta'' - \cos\theta)/\cos\theta \sim \cos\theta'' - \cos\theta$ , because  $\cos\theta$  is very close to 1.

$$\begin{aligned} &\cos\theta'' - \cos\theta \\ &= \cos \left[ \arcsin \left( \frac{a}{b' \left( \frac{n''}{n'} - 1 \right) + b} \right) \right] - \cos (\arctan a/b) \end{aligned}$$

Remembering that the exact form of this equation, and the relevant parameters depend on the exact positioning of the laser and detector, and on the sled shape and Mach number, a rough approximation to the magnitude of the error can be obtained with reference to the shock parameter tables, and an assumed geometry for the interferometer.

Using the original design dimensions proposed for the system,  $a = .04$  ft and  $b =$  the sled-mirror distance, the cosine error discussed above can be calculated for different values of sled velocity in the transonic regime.

As an example, let  $b = 5$  ft (distance of closest approach), and see what happens at Mach 1.3. Here  $b' \sim 1$  sled diameter = 4 ft, and  $n''/n \sim .9997$  (using the tabulated value of the density change across the shock, and the fact that  $n \sim 1 + \beta \rho/\rho_0$ ). Then  $\Delta \cos \theta \sim 2 \times 10^{-8}$ , well within the tolerance for the measurement.

At constant sled velocity ( $b'$  constant) an inspection of the equation for the error in  $\cos \theta$  shows that as  $b$  increases the error decreases, therefore the largest error occurs at the distance of closest approach between the sled and reflecting surface. The error in the angle, increases as the shock stand-off distance  $b'$  increases, but this increase is only as the sin of the inverse power of  $b'$  multiplied by  $\frac{n''}{n'} - 1$  which, in the range of Mach numbers of the rocket sled is a negligible quantity compared to the values of  $b$ . This means that the refractive effects due to the transonic and subsonic shocks on the velocity measurement should be negligible, and about two orders of magnitude below the specification tolerance.

### Error Due to Changes in the Shock Parameters Over the Sampling Time

The fringe count generated over the .001 sec sampling time arises from changes in the length of the optical path of the laser beam as it travels to the mirror and back to the detector. If the changes in this optical path length occur as a result of any other cause than sled displacement, an error is introduced into the velocity measurement.

If the sled is accelerating, the change in the free stream Mach number over the .001 sec sampling time will induce a corresponding change in the density of air behind the shock, and in the length of the shock region in front of the sled. Near the maximum acceleration this change in the shock parameters will have a significant effect on the velocity measurement.

In Appendix A.3 it was shown that the apparent displacement,  $\Delta p$ , due to changing shock parameters could be calculated approximately as:

$$\Delta p = \beta \times [\Delta(\Delta o) \left( \frac{\rho'_{\text{shock}} - \rho_s}{\rho_s} \right) + \Delta o \left( \frac{\rho'_{\text{shock}} - \rho_{\text{shock}}}{\rho_s} \right) ]$$

where  $\beta$  = dependent on  $\lambda$ , = .000291 at He-Ne line

$\Delta(\Delta o)$  = change in stand-off distance over .001 sec

$\rho'_{\text{shock}}$  = value of density of air behind shock at the end of the measuring interval

$\rho_{\text{shock}}$  = the density of air behind the shock at the start of the time interval

$\rho_s$  = the density of air at standard conditions

$\Delta o$  = the shock stand-off distance

Results from the article by Charters and Thomas, show that at around Mach .99 the flow is still supersonic in form but the stand-off distance of the sphere shock front is about 7 diameters.

Applying this result to the sled problem, the value of  $\Delta o$  in the above equation is approximately 30 ft at Mach .99. If a maximum sled acceleration of 200 g's is assumed,  $\Delta M$  over the measuring interval is  $\sim .006$  (.990 to .996), and, interpolating from the attached tables (NACA Rpt. #1135) the corresponding change in the value of  $\rho_{shock}/\rho_s$  is  $1.02 \times 10^{-2}$ . This is the value of the  $\frac{\rho'_{shock} - \rho_{shock}}{\rho_s}$  term in the above equation.

The change in the shock stand-off distance for  $M = .006$  is quite small compared to the magnitude of the stand-off distance. Therefore, the term multiplied by  $\Delta(\Delta o)$  in the equation for  $\Delta p$  will be negligible compared to the second term in the equation, and  $\Delta p$  can be approximated as

$$\Delta p = \Delta o \frac{\rho'_{shock} - \rho_{shock}}{\rho_s} \times \beta$$

Using a value of  $\beta = .000291$  for the .6328 micron He-Ne laser line,  $\Delta p \approx 10^{-4}$  ft or two orders of magnitude above the part per million tolerance, around Mach 1.

Conclusion: The effect of sled acceleration on the shock parameters in the transonic speed region will induce errors on the order of a part per 10,000 (worst case) on the sled velocity measurement. This is two orders of magnitude worse than the 1 part per million specifications at Mach 1.

### Measurement of the Index of Refraction Within Shock Region

The experimental results reported in the above mentioned paper by Charters and Thomas show a shock stand-off distance at Mach 0.99 of about seven diameters, for a small spherical projectile. Also, around Mach 1 and below, the shock stand-off distance for circular arc shapes with thickness ratios around 1 are close to that for blunt-nosed bodies, so the spherical projectile stand-off results are approximately applicable to the guidance sled in the transonic regime. This means that just below Mach 1 it is reasonable to expect a shock stand-off distance of  $7 \times 4 \text{ ft} \approx 30 \text{ ft}$  in front of the sled. The shock density in the region of interest approaches the free stream density as the Mach number decreases, but the stringent requirement on the index of refraction measurement makes some sort of correction necessary. The relationship between the index of refraction in a region and the air density is defined by  $\eta = 1 + \beta \rho / \rho_s$ , where  $\beta \approx .000291$  for  $.6 \mu$  wavelength,  $\rho$  = the air density in the medium, and  $\rho_s$  = the air density at standard conditions. Estimating the free-stream density to be close to  $\rho_s$ , if the average air density behind the displaced region of shock is greater than  $1.003 \times \rho_s$  the change in the value of the index of refraction from that of the free stream conditions in the area is greater than 1 part per million. Depending on where in the shock region the mirror is at the time of the measurement,  $\rho$  will be greater or less than  $1.003\rho_s$ .

Assuming a distance of closest approach between the laser and mirror of 5 ft, as proposed in the original system design, and the approximated stand-off distance of 30 ft at Mach .99 it can be seen that the entire optical path lies within the first one-sixth of the shock region. With reference to the attached tables (copied from NACA Report #1135, Equations, Tables and Charts for Compressible Flow) the value of  $\rho/\rho_0$  (where  $\rho$  = the free stream density and  $\rho_0$  = the stagnation density) is .6392 at Mach .99. The gradient in the region of interest is difficult to gauge, but approximating a linear density decrease the

air density 5 ft ahead of the stagnation point at Mach .99 would be roughly 1.5 times the free stream air density so a correction for the index of refraction difference from its free stream value would be required.

If the index of refraction within the shock region is required, the most accurate measurement obtainable would probably be that using a two-color laser. Stationary temperature measuring devices would be impractical because the air flow behind the shock varies so rapidly temporarily and spatially around Mach 1. A two-color laser has the advantage that it measures the index of refraction continuously over the part of the optical path that is changing due to the sled displacement. This is precisely the measurement required in order to analyze the fringe count.

In a previous report (Appendix A.12) it was calculated that the best accuracy achievable in measuring  $n$  with a two-color laser is about a part per 10,000 or two orders of magnitude down from the required accuracy.

This may be the best measurement achievable, though, in the shock region.

Effect of Air Turbulence in a Shock Region of Laser Beam Propagation

Normal air turbulence has a degenerative effect on the internal structure of a laser beam propagating through the atmosphere. Phase coherence across the beam face is degraded and variations in the angle of arrival of the rays composing the beam can result. It is reasonable to expect the same type of effect to arise as a beam propagates through a shock region. In the transonic speed regime large segments of the optical path of the beam lie within shock regions. The effect of turbulent regions within the shock on the signal propagation may be quite sizable, but no pertinent data on the problem has been located as yet. The non-equilibrium conditions existing in a shock region make a theoretical approach to the problem difficult. Experimental results would be necessary to accurately predict the magnitude of the effect.

Conclusions:

The worst bow shock induced errors on the flag interferometer velocity measurement arise when the sensing head lies behind the sled shock region.

If the optical paths lie entirely within a shock region the index of refraction within the shock must be measured to interpret the fringe count. If this were done using a two-color laser the best accuracy achievable with the system would be about two orders of magnitude below the specifications.

The second major source of error is that changes in the density behind the shock region over the .001 sec measuring time could induce velocity errors as large as  $10^{-4}$  ft per .001 sec. This is about two orders of magnitude outside of tolerance.

Refraction effects in the transonic shock region will not be of major concern if the optical paths are kept close to the direction of the shock normals. Turbulent refraction effects may degrade the beam structure, but the magnitude of this effect is not known. An estimate of the effect would require some experimental results.

If these error sources were not eliminated the best accuracy achievable with the flag interferometer would be about 2-3 magnitudes worse than .001 fps at 1000-2000 fps required.

#### REFERENCES

1. A. E. Bryson, "An Experimental Investigation of Transonic Flow Past Two-Dimensional Wedge and Circular Arc Sections Using a Mach-Zehnder Interferometer" (1952), NACA Rpt. 1094.
2. A. C. Charters, R. N. Thomas, "The Aerodynamic Performance of Small Spheres from Subsonic to High Supersonic Velocities" (1945), Journal of the Aeronautical Sciences.
3. Heberle, Wood, Gooderum, "Data on Shape and Location of Detached Shock Waves on Cones and Spheres", (1950), NACA TN 2000.
4. "Equations, Tables and Charts for Compressible Flow", Ames Research Staff, NACA Rept. 1135.

APPENDIX A.15

CONSIDERATIONS ON USING EXTENDED (100 METER) MIRROR SPACINGS

ON THE FLAG INTERFEROMETER SYSTEM

In the original design of the flag interferometer system the interrupter surfaces, spaced 4 meters (13 feet) apart, were used to return a signal. The longest optical path length used was 11 meters (36 feet) (to the interrupter and back). This design calls for the installation and upkeep of approximately 4000 mirror surfaces. If the maximum sled to mirror spacing could be increased to about 100 meters then the number of mirrored surfaces required would be cut down to approximately 150. This would mean a considerable reduction in the installation and maintenance requirements of the system.

In looking at the feasibility of extending the mirror spacings, the possibility of changing the system geometry to eliminate some of the problems that arise has been considered.

For example, it has been suggested that the laser source and detector mirror be positioned coaxially, the optical signal impinging on the mirror surface perpendicularly. (See Figure A.15.1)

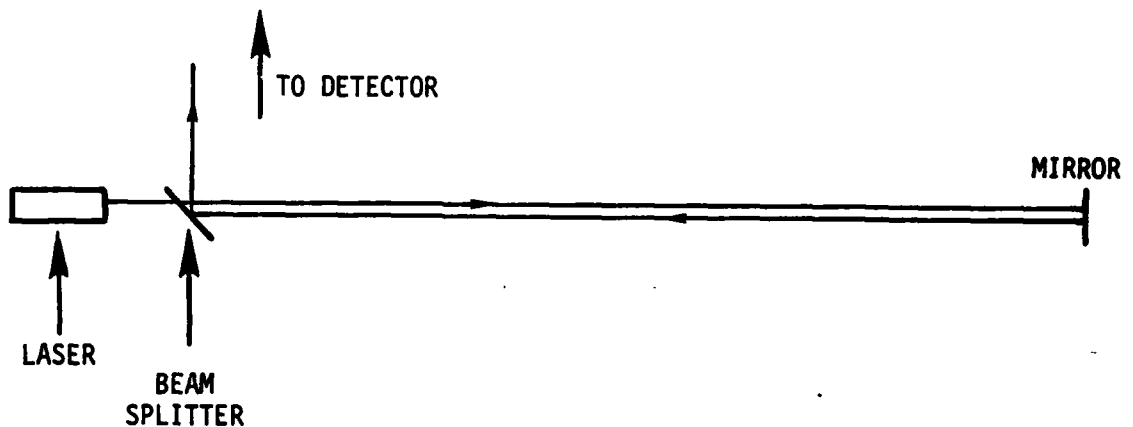


Figure A.15.1

This geometry would require a movable mirror surface to avoid sled impact, but would reduce the systems sensitivity to beam deflection and mirror misalignment, since the velocity movement sensitivity depends on the cosine of this angle and  $d\cos\theta/d\theta$  decreases with  $\theta$ . This would mean that the tolerance of angular shifts due to temperature gradients and atmospheric turbulence would be increased. If a tracking system could be used it would increase the signal power at the detector by many orders of magnitude, since a well collimated signal could be used, rather than a divergent one.

This would significantly increase the signal to noise ratio and would make any kind of averaging process required to correct for spatial incoherence more feasible. The greater the degradation of the internal beam structure is, the more important aperture averaging may be to signal interpretation.

#### I. ATMOSPHERIC CONSIDERATIONS

Increasing the optical path lengths used in the interferometer from 11 meters (36 feet) to 100 meters (328 feet) will increase the effects of atmospheric signal degradation. There are four major effects on the optical signal that will affect the velocity measurement.

The first effect is overall signal attenuation due to molecular and aerosol scattering and absorption. Molecular attenuation arises from the presence of the atmospheric gases themselves, while the aerosol effect refers to that from suspended particles in the air (dust, sand, etc.).

The second is the effect of atmospheric turbulence on the structure of the beam, and on its direction of propagation. The beam will cross regions of varying index of refraction as it propagates and will be bent in random directions as a result. Whether the beam as a whole is deflected or the internal structure of the beam is degraded depends

on the relative sizes of the turbulent eddys.

Third, the vertical temperature gradient that exists above the ground will cause deflection of the beam as a whole. If the optical paths lie close to the rail, the temperature gradients in the vicinity of the rail will also increase this angular deflection.

The last effect is highly dependent on the size and distribution of aerosol particles along the beam's path. As the beam diffracts around these obstacles its internal structure can be effected and splotches will appear on the signal in the receiver plane.

#### Effects of Atmospheric Turbulence on the Signal

The original design for the flag interferometer used divergent beams to track the flags (see Fig. A15.2, Design 1). This system incurred excess signal attenuation. It was calculated in Appendix number A.11 that the signal at the detector would be decreased to as much as  $10^{-5}$  of the original output power using this method. Since the output of most He-Ne lasers is on the order of a few milliwatts the signal to noise requirements of the interferometer system would not be met if this type of attenuation were to occur.

If a divergent beam is used for the signal, angle filtering is accomplished by using small aperture detectors. Since the angle filtering requirements on the system are so stringent, very small apertures are required, and only a small fraction of the beam is returned to the detector. If, on the other hand, a collimated beam is used for the signal, the sampling angle across the face of the beam will be constant, and the whole of the incoming beam at the detector could be used for a signal. Of course, angle of arrival fluctuations across the face of the beam will occur due to oscillation effects, as well as angular change of the entire beam due to turbulence induced beam wander and beam bend-

ing due to temperature gradients in the atmosphere. Random angle of arrival fluctuations can be averaged out across an aperture, and the errors due to the other effects are no larger than if a divergent beam was used for the signal.

If a collimated beam is to be used, though, either some form of tracking system is required to keep the beam on the detector, or a large area detector is needed to intercept the returned signal. If a tracking system were to be used it must have a very fast response, and must be able to retrack the beam very rapidly after signal dropouts occur. If no tracking system were used the beam spot on the detector plane would vary. If some form of detector system that allowed mapping of beam position vs. time were used the angular corrections required for determining the sensitivity of the velocity measurement could be made. (See Figure A15.2).

This would be the same case as in the original system design, except that now the laser-detector distance would be variable. The same angular correction can be made, though, if the beam position on the detector vs. time is known. The only practical way to accomplish this would be to use a beam direction for the signal that was parallel to the sled velocity vector on the average. Then the major angular changes of the beam would be those due to sled pitch and yaw, which are on the order of  $10^{-3}$  radians. A useable detector area of about  $10^{-3}$  rads x 200 meters = 20 cm on a side would be required. A problem which arises in this system is that some mechanism for removing the mirrors ahead of the sled must be found. Some investigation of this problem is being conducted.

Whether a tracking system of some sort, or a large area detector array, or some combination of the two were to be used, the beam profile in the detector plane will be an important factor in determining the system errors.

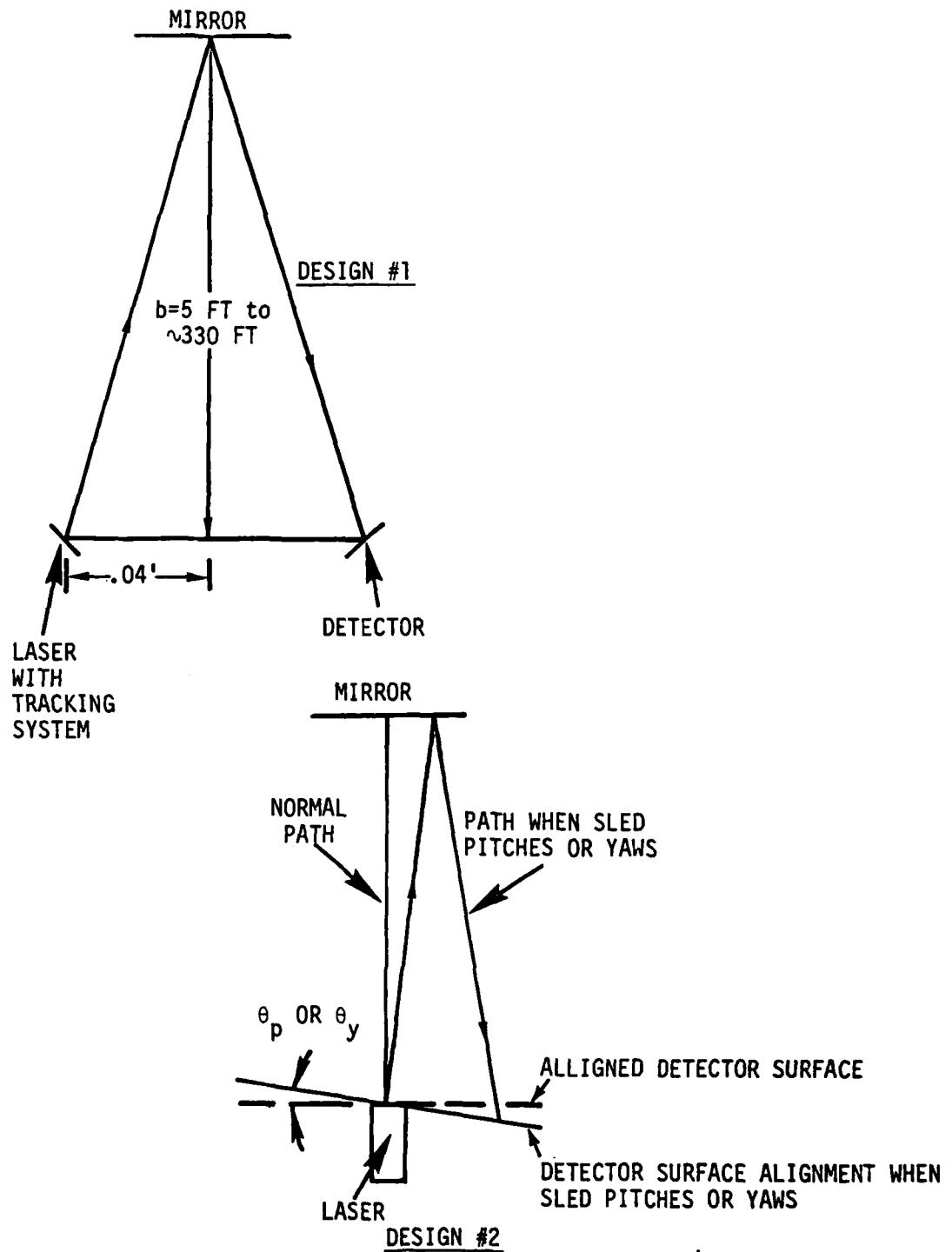


Figure A15.2 Flag Interferometer Designs

Since the optical requirements of the interferometer can't be met using divergent beams for tracking, the following discussions will assume that a collimated laser beam is used, with a gaussian irradiance profile. Also the maximum propagation path of the beam to and from the detector will be assumed to be 200 meters.

The refractive index of air depends on the air temperature. The approximate relationship between the two quantities is

$$n = 1 + \frac{80 \times 10^{-6} p}{T}$$

with  $p$  in millibars and  $T$  in degrees kelvin. At standard atmospheric conditions  $p \approx 1$  bar and  $T$  is around  $300^\circ$  K. Therefore  $\frac{dn}{dT}$  is equal to about  $10^{-6}/^\circ\text{K}$ . So as the air temperature varies,  $n$  varies as  $10^{-6} \Delta T$ .

The air temperature in the boundary layer of atmosphere above the ground doesn't vary continuously, but rather turbulent eddies exist. These are regions where the temperature is approximately constant over a distance dictated by the size of the eddy. This size varies with height above the ground, but basically energy is introduced into the atmosphere from the sun's heating, with a characteristic length  $l_0$ , the outer scale of turbulence. This defines the largest eddy size. These break up into smaller turbulent regions due to atmospheric mixing until an eddy size  $l_0$  (the inner scale of turbulence) is reached where the energy is dissipated viscously into the atmosphere. At sea level, the size of these smallest eddies is a couple of millimeters, depending on the time of day and the exact height above the ground. The larger eddies are on the order of meters, and vary approximately as the 4/3 power of height above ground.

The basic theory of turbulence effects on beam propagation shows that if the beam diameter is very small compared to the size of the smallest eddy,  $l_0$ , then the beam will be bent as a whole as it enters regions

of differing index of refraction. If the beam size is approximately equal to or larger than this size,  $l_0$ , then the internal structure of the beam will be degraded, since different parts of the beam can experience different changes in refractive index and interference between parts of the beam which experience small angular deflections occurs (see Figure A15.3).

Actually, even when the beam is smaller than  $l_0$ , the internal structure of the beam can be degraded if the beam's path through the distorting medium is long enough. The lateral coherence length for the beam is the distance across the face of the beam where the rms phase shift just equals  $\pi$ . This lateral distance is dependent on the wavelength of the laser, the properties of the medium, and the length of the beam's path through the medium.

Tatarski (Wave Propagation in a Turbulent Medium, V.I. Tatarski, 1961) defines a phase structure function  $D_\phi$  for a beam, where  $D_\phi$  is the rms phase shift across the beam at two points separated by a cross distance  $\rho$ . (See Figure A15.4).

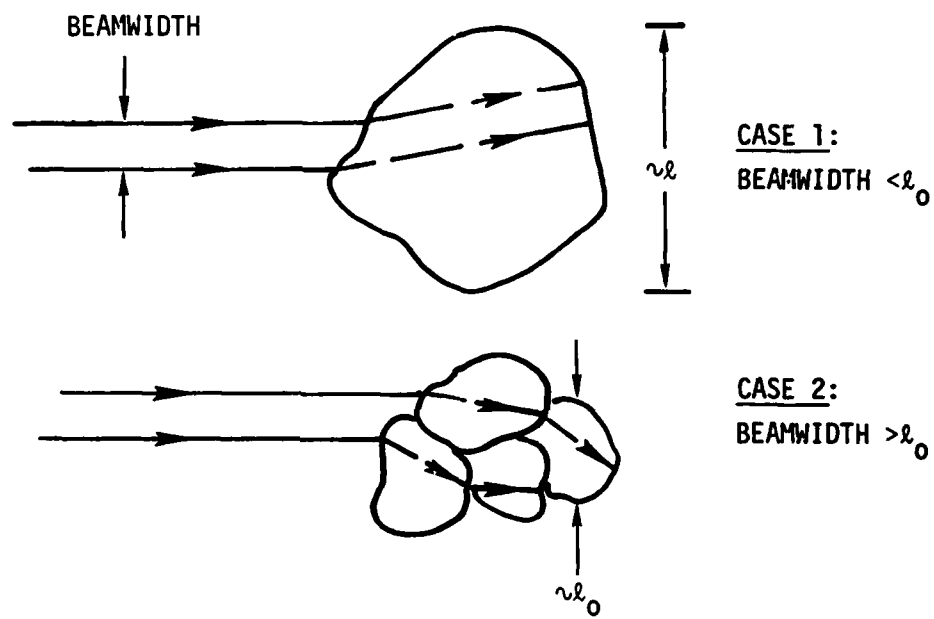


Figure A15.3 Beam Structure

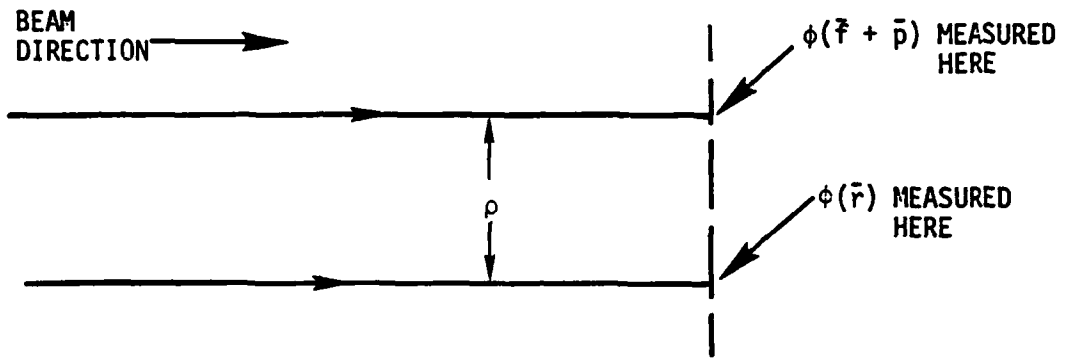


Figure A15.4 Phase Structure Definition

For plane waves, using the approach of geometrical optics, Tatarski calculates this phase structure function  $D_{\phi}$ , as

$$D_{\phi} = 2.91 k^2 L C_n^2 \rho^{5/3}$$

where  $k$  = the wave number,  $\frac{2\pi}{\lambda}$

$L$  = the length of the path through the medium

$C_n^2$  = the index of refraction structure parameters

$\rho$  = the distance between the two points the phase is observed at

$\lambda$  = wavelength of light used

The approximation of geometrical optics is valid when  $\lambda \ll \ell_0$ , ( $\ell_0$  is the inner scale of turbulence), and  $\sqrt{\lambda L} \leq \rho < L_0$ . The first condition is met, since  $\ell_0$  is on the order of millimeters. The upper bound on the second condition is definitely met, since  $L_0$  is on the order of meters. But the lower bound is met only approximately since  $\sqrt{\lambda L} \approx 1$  cm for a 200 meter path, and  $\rho \approx 1$  mm, an order of magnitude difference. Experimental results show Tatarski's equation to be valid down to 3mm in the atmosphere over a 70 meter path (Ref. 5), so it is reasonable to assume its approximate validity for a beam diameter on the order of a millimeter propagating approximately twice this distance.

To find the value of the lateral coherence length for a 1mm, 6398 $\text{\AA}$  laser beam, propagating 200 meters through the atmosphere, the strength of the atmospheric turbulence must be known. The strength of the turbulence affecting the laser beam propagation is defined by the quantity  $C_n^2$ , the index of refraction structure function. This quantity is derived from a measure of the average temperature difference between two points, separated by a distance intermediate between the outer and inner scales of turbulence. This difference, averaged over time, is related to the index of refraction difference between the same 2 points using the

relation between temperature and index of refraction and assuming isobaric air heating. The quantity  $C_n^2$  is the square of the average index of refraction difference between 2 points divided by the distance between the points raised to the two thirds power.

$$C_n^2 = \langle [n_1 - n_2]^2 \rangle / (r_1 - r_2)^{2/3}$$

As such, it has units of meters<sup>-2/3</sup>. This quantity is independent of the distance between the two points as long as it is smaller than the outer, and larger than the inner scales of turbulence.

The strength of the turbulence decreases with distance from the ground  $C_n^2$  varying roughly as  $h^{-4/3}$ . This is to be expected since the turbulence arises as a result of heat interchange between the ground and the atmosphere. Convective heating in the immediate vicinity of the ground can cause the strength of the turbulence to increase above that predicted by the  $h^{4/3}$  variance.

The highest value of  $C_n^2$  tabulated 8 meters above the ground at Holloman AFB was  $10^{-13}$  meters. Putting in the height correction, the value of  $C_n^2$  around 1/2 meter off the ground would be around  $10^{-12}$ . A value of  $C_n^2$  equal to  $10^{-12} \text{ m}^{-2/3}$  corresponds to very strong turbulence, and as such is probably reasonably well achieved by keeping the optical paths a good distance from the rail. Strong temperature fluctuations will occur in the vicinity of the rail due to its heating of the surrounding atmosphere. The size of the inner scale of turbulence will decrease and the value of  $C_n^2$  will increase closer to the rail. The exact magnitude of these effects is difficult to gauge and could only be predicted accurately experimentally. But it is reasonable to assume that the beam of a laser placed a meter away from the rail should be far enough away from its thermal effects to make the  $10^{-12} \text{ m}^{-2/3}$  value of  $C_n^2$  corresponding to very strong atmospheric turbulence, reasonable.

Using the value of  $C_n^2$  of  $10^{-12} \text{ m}^{-2/3}$ ,  $L = 200$  meters, and  $\lambda = 6328\text{\AA}$ , the coherence length for the beam will be  $\sim 5.5$  mm, about 5 times larger than the proposed beam diameter of 1mm. Therefore, over the entire width of the beam the phase change due to turbulence effects should be smaller than  $\pi$ . The rms phase change predicted by the phase structure constant  $D_\phi$  would be

$$2.92 \times \left( \frac{2\pi}{.6328\mu} \right)^2 \times 200 \text{ meters} \times (1\text{mm})^{5/3} \times 10^{-12} \text{ m}^{-2/3}$$

$$\approx .6 \text{ rads}$$

Related to the turbulence induced phase variance across the beam is the phenomena of beam spread. The irradiance pattern in the receiver plane is dependent on the strength of the turbulence, which determines the size of the turbulent eddies relative to the beam. The instantaneous irradiance pattern in the receiver plane defines the short term beam radius, and the long term irradiance pattern defines the value of  $\rho_L$ , the long term radius. The short term radius refers to the symmetrical spread of the beam around its centroid, while  $\rho_L$  defines the beam wander, as the direction of the beam centroid varies with time. (Figure A15.5)

The equations for determining the magnitude of these effects, as derived by R.L. Fante, (reference 2) are dependent again on the strength of the turbulence of the propagation medium, the beam diameter, propagation distance, and wavelength.

The long term irradiance spread for a gaussian beam is derived as:

$$\langle \rho_L^2 \rangle \approx \frac{4L^2}{k^2 D^2} + \frac{D}{4} \left( 1 - \frac{L}{F} \right)^2 + \frac{4L^2}{k^2 \rho_0^2}$$

where  $F$  = the radius of curvature of the beam

$F = 0$  for a collimated beam

$L$  = the length of the path through the medium

$k$  = the wavenumber of the light used

$D$  = the original beam diameter

$C_n^2$  = the index of refraction structure function

and  $\rho_0$ , the long term average lateral coherence length is defined as

$$\rho_0 = \left[ .626 k^2 L C_n^2 \right]^{-3/5}$$

If a well collimated beam is used  $F = 0$ , and the above equation reduce to:

$$\left\langle \rho_L^2 \right\rangle = \frac{4L^2}{k^2 D^2} + \frac{4L^2}{k^2 \rho_0^2}$$

The first term in this equation is the beam spread due to diffraction at the aperture and the second is that due to turbulence induced diffraction effects.

The appropriate equation for the short term beam spread, as derived by Fante, depends on the relative sizes of  $L$ ,  $\rho_0$ , and  $D$ . For a 1 mm diameter collimated gaussian beam, with a 6328Å wavelength, propagating 200 meters through the atmosphere, the value of  $\rho_0$  is

$$2.2 \times 10^{-10} \times (C_n^2)^{-3/5}$$

Using a value of  $C_n^2$  of  $10^{-12}$ , this = 3.5 mm.

Therefore the correlation length is approximately equal to the beam diameter,  $D$ .

The second quantity of interest in determining short term beam spread effects is  $kD^2$ . Again assuming a 1 mm, He-Ne beam this has a value of 10 meters.

Four cases are discussed by Fante. They are:

- i)  $\rho_0 \ll D < L_0, L \leq kD^2$
- ii)  $\rho_0 \sim D$  and  $L \leq kD^2$
- iii)  $L \gg kD^2$
- iv)  $\rho_0 \gg D$  and  $L \approx kD^2$

An inspection of these conditions shows none of them to be directly applicable to the situation considered here. The relevant quantities in case iii) are,  $L = 200$  meters,  $kD^2 = 10$  meters, therefore  $L$  is an order of magnitude larger than  $kD^2$ . If this difference constitutes a "very great compared to" condition, the effect of the turbulence, predicted by Fante is to cause the beam to break up into patches. This would be a serious problem if it was to occur.

H.T. Yura in a paper in the Journal of the Optical Society of America entitled "Short-Term Average Optical Beam Spread in a Turbulent Medium," sets the condition as  $L \geq kD^2$ , and  $L \leq kD^2$ . For the case  $L \geq kD^2$  he says the beam can be expected to break up into multiple patches or blobs. The individual splotch will have a characteristic diameter equal to the diffraction limited spot size obtained for the system. For this same case the motion of the beam centroid will be comparable to the angular size of the short term radius,  $\rho_s$ , (Figure A15.5) beam centroid wander being negligible.

For the case  $L \sim kD^2$ , Yura's results show that  $\rho_L \approx \rho_s$ , so beam wander is on the same order of magnitude as the total beam spread. Splotching should not occur in this range.

Since  $L$  is approximately an order of magnitude larger than  $kD^2$ , the actual case is probably intermediate between the two discussed above. If beam splotching does occur to a certain extent, but remains small and close together, the error introduced into the signal could be negligible.

Since the pertinent dimensions for the Flag Interferometer beam

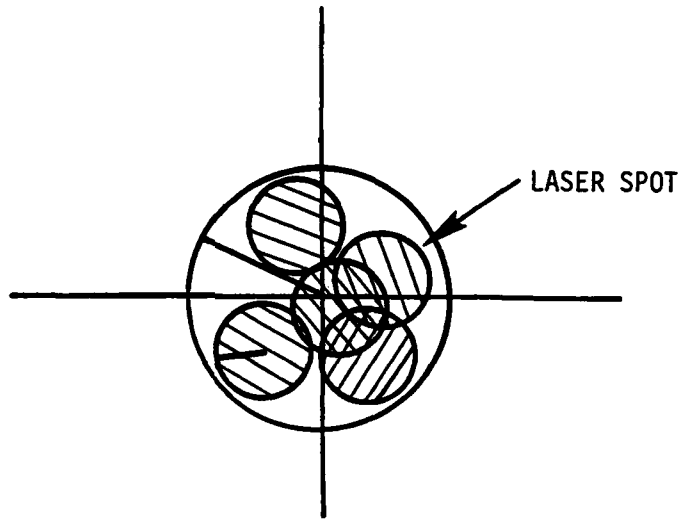


Figure A15.5

system are not well into the region of one approximation or another the best way to predict the atmospheric effects on the beam is through experimentation. This is true also since the relevant quantities are directly dependent on the exact value of  $C_n^2$  which is not known in the immediate rail environment. Also, its variance with distance from the rail and ground is not known.

As discussed above, if  $L > \text{or} \sim kD^2$  the long and short term beam spread will be approximately equal. Then, using the equation for  $\rho_L$  above, and  $L = 200$  meters,  $D = 1$  mm,  $\lambda = 6328 \text{ \AA}$ ,  $\rho_0 = 3.5$  mm, the value of  $\rho_L$  is about 1.8 mm, therefore the radius of the beam increases by a factor of 1.8 over the 200 meter path. The effects of beam spread then, cause no significant problem, as relates to power attenuation in the receiver plane. The beam wander, reflected in the motion of the beam centroid will thus also be of the same order of magnitude as the instantaneous beam spread, and will also be negligible.

#### Conclusion:

Signal degradation and attenuation due to atmospheric turbulence effects on the Flag Interferometer signal beam are small enough to allow increase of the mirror spacing above the 13 ft value originally proposed. The results of a preliminary investigation into the degradation effects on the signal show that it might be possible to increase the mirror spacing to 100 meters. Experimentation in the track vicinity is recommended to more accurately predict the beam profile vs. distance, and determine the maximum useable mirror spacing.

#### Atmospheric Attenuation of the Laser Signal

The laser beam intensity will decrease with distance as it propagates through the atmosphere. The causes of this attenuation are

molecular scattering and absorption of the atmospheric gases, and scattering of the beam as it is incident on suspended aerosol particles (e.g., dust and sand).

The atmosphere has a good window at  $6328\text{\AA}$  and so the effect of molecular absorption on the light beam will be negligible.

Furthermore, in standard atmospheric propagation the molecular scattering coefficient is on the order of  $10^{-13} \text{ km}^{-1}$ . (Reference 7). This means that over a path of 1 kilometer in length the beam intensity will be 99.9% of the original intensity.

The attenuating effect of aerosol particles on the laser signal is highly dependent on the size of the particles and on their density. Three atmospheric models were developed by the Air Force Geophysical Lab. The models are for an urban, a rural, and a maritime environment (Ref. 9). The maritime model has the largest value of  $\sigma_a$  and hence the greatest attenuation effect on the signal. It takes into account the effect of salt particles from the evaporation of sea spray in the atmosphere. It is probably reasonable to assume that over the path lengths involved here (200 meters) the maritime model attenuation is roughly the same as that due to sand and dust in the desert environment (ignoring effects of debris scattered by the shockwave). The attenuation due to aerosol scatter is then calculated as

$$E_e = E_{e0} \exp(-\sigma_a x)$$

where  $\sigma_a$  = the combined aerosol attenuation coefficient

$E_{e0}$  = the initial irradiance

$E_e$  = the irradiance at the detector a distance  $x$  from the source

$x$  = the source-detector distance

The value of  $\sigma_a$  at  $6328\text{\AA}$  for the maritime model is approximately  $.15 \text{ km}^{-1}$  (Ref. 9). Therefore, over a 200 meter path length (.2 km),  $E_e = .97 E_{e0}$ .

If this model predicts the approximate attenuation for the track environment, signal attenuation due to aerosol scattering could be ignored.

Conclusion:

Signal attenuation over a 200 meter path length at  $6328\text{\AA}$  due atmospheric absorption and scattering should be negligible.

IV. EFFECT OF THE VERTICAL TEMPERATURE GRADIENT ABOVE THE GROUND ON THE LASER SIGNAL PROPAGATION

As a light ray propagates through a medium with a refractive index gradient (temperature gradient) at the right angles to its path of propagation, the ray is deflected towards the region with the greater index of refraction. The net deflection of the beam is proportional to the magnitude of the gradient and the length of the ray's path through the medium. Specifically, the net deflection, call it  $\epsilon$ , is calculable approximately as (Ref. 10)

$$\epsilon \approx L/n_1 (dn/dy)_1$$

where  $\epsilon$  = the net deflection angle  
L = the path length through the medium  
dn/dy = the refractive index gradient of right angles to the ray (Figure A.15.6).

(the subscript "1" refers to the index of refraction and it's gradient along a non-deflected path. If the deflection is small these values are approximately correct over the whole path).

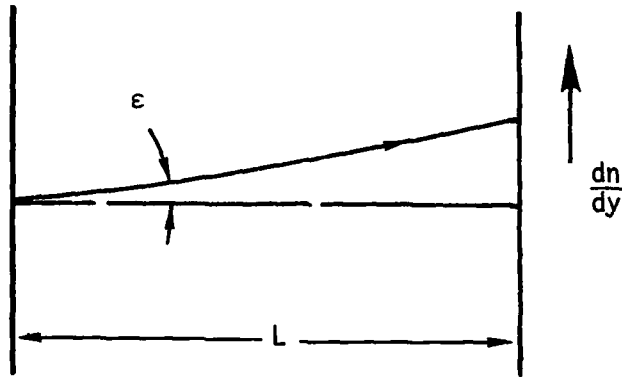


Figure A.15.6

The flag interferometer velocity measurement is dependent on the angle of the optical path displaced over the sampling time with respect to the sled velocity vector. The velocity measured with the interferometer is directly proportional to the cosine of this angle. Therefore, the 1 part per 2 million accuracy requirement on the velocity measurement sets a corresponding limit on the angular deflection of the light beam used for the measurement.

The relationship between the net deflection angle of the ray and the error introduced into the velocity measurement depends on the system design used.

Assuming a collimated beam is used for the signal, either a tracking system or a large area detector is required. If a tracking system is used the error generated by vertical temperature gradients can be seen with reference to the diagram below.

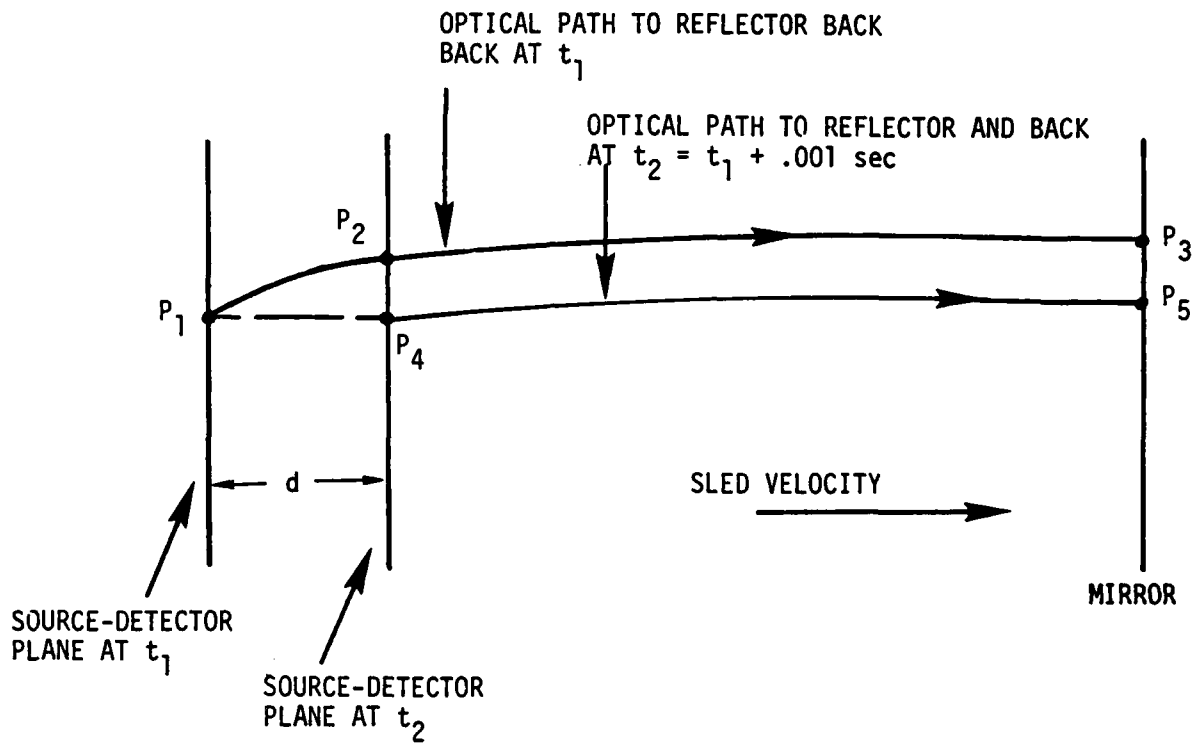


Figure A15.7 View of Deflected Signal Beam in Vertical Plane Parallel to Sled Direction.

In the diagram,  $d$  = the sled displacement over the sampling time. The deflection of the beams in a horizontal plane will not be affected by vertical temperature gradients. Therefore, the error introduced will be to cause the displaced portion of the optical path,  $\overline{P_1P_2}$  on the diagram, to require two angular correction factors, one due to its deflection in the horizontal plane, and one due to its deflection in the vertical.

The error introduced into the velocity measurement due to the vertical temperature gradient will be proportional to the cosine of the net deflection angle over the propagation path at  $t_1$ , if a tracking system is used, and the detector lies in the same horizontal plane as the laser source. The reason for this is that in order to keep the beam centered on the detector the tracking system must aim the beam up (or down) by an amount equal to the net deflection angle of the ray over the path from the laser to the reflector. In this way, the angle in the vertical plane that the beam impinges on the reflector surface is  $0^\circ$  with respect to the normal to the mirror, therefore the beam will propagate back to the detector along its same path in this vertical plane. As can be seen from the diagram, the deflection angle that is required for the velocity correction is that between the sled velocity vector and  $\overline{P_1P_2}$ . (Actually the ray curves over this distance, but to first order the assumption of a straight line can be made.)

The allowable vertical temperature gradient can be found with reference to the allowable error in the velocity measurement. Since the error introduced is equal to  $1 - \cos \epsilon$ , the maximum allowable value of  $(1 - \cos \epsilon)$  is 1 part per 2 million =  $5 \times 10^{-7}$ , or  $\cos \epsilon$  (min) = .9999995.

$$\text{But, } \cos \epsilon = \cos (L \frac{dn}{dy}),$$

Therefore, the maximum allowable value of  $L \frac{dn}{dy}$  is  $\text{arc cos}$

(.9999995,) or  $10^{-3}$  rads. Using a path length of 200 meters,  $dn/dy$  maximum =  $5.0 \times 10^{-6}$ /meter.

The relationship between  $n$  and  $T$  is

$$n = 1 + \frac{80 \times 10^{-6} P}{T}$$

with pressure,  $p$ , in millibars, and temperature,  $T$ , in degrees Kelvin.  $P \approx 1$  bar at normal conditions, and  $T$  is approximately  $300^\circ\text{K}$ . Then the relationship between temperature and pressure gradients is given by,

$$\frac{dn}{dy} \approx 10^{-6} \frac{dT}{dy}$$

Therefore, the temperature gradient corresponding to  $5 \times 10^{-6}$ /meter refractive index gradient is 5 degrees/meter.

Under normal atmospheric conditions this gradient would not be exceeded however, within the first foot or so above the ground in midday or within the immediate vicinity of the heated rail surface the temperature gradients can be quite high. Therefore, the laser should be positioned in such a way that the optical paths are not within the immediate vicinity of the rail or ground.

Conclusion:

The vertical temperature gradients existing above the ground and above the rail will not introduce a significant error if the optical paths used in the interferometer are not subject to a cross path temperature gradient greater than  $5^\circ$ /meter.

### Aerosol Effects

Particulate matter suspended in the atmosphere in the path of the laser beam will cause either momentary signal dropouts or degradation of the internal beam structure by the effect of its shadow on the detector. The beam profile at the detector is therefore dependent on the sizes and concentrations of these aerosols, and any other airborne objects. The effect of beam diffraction around particulate matter will depend on the dimensions of the particulates intercepted by the beam, and their distance from the source.

The subsonic bow shock may kick up debris out in front of the sled. The concentrations of particulates from this effect could be expected to decrease with increasing height above the ground. So one way to reduce the problem would be to run the signal beam higher above the track.

Another serious consideration in designing a sled borne interferometer is the effect of airborne particulates impacting on the optical components used in the system. These particulates would cause erosion of the optical surfaces. Insects impacting on the laser emitting surface or on the detector could cause complete signal loss for the duration of the sled run. Water droplets in the air, either from air moisture, or the water brake system may impinge on the interferometer surfaces with enough force to cause some damage. Again, the magnitude of the problem is difficult to gauge without more detailed knowledge of the size of the particulates and their concentration in the atmosphere.

## BIBLIOGRAPHY

1. Yura, H.T. (1972) Short-Term Average Optical-Beam Spread in a Turbulent Medium, JOSA 63:567-572.
2. Fante, R.L. (1975) Optical Beam Propagation in Turbulent Media, Air Force Cambridge Research Laboratories, Hanscom AFB, MA.
3. Chiba, T. (1971) Spot Dancing of the Laser-Beam Propagated Through the Turbulent Atmosphere, Applied Optics, Vol. 10: 2456-2461.
4. Lawrence, R.S. & Strohbehn, J.W. (1970) A Survey of Clear-Air Propagation Effects Relevant to Optical Communications, Proceedings IEEE, Vol. 51: 1523-1545.
5. Clifford, Bouricius, Ochs, Ackley (1971) Phase Variations in Atmospheric Optical Propagation, JOSA 61: 1279-1284.
6. Tatarski, V.I. (1961), Wave Propagation in the Turbulent Medium, McGraw-Hill.
7. MacInnis, W.H. (1977) Laser Test Range Propagation Model, M.S. Theses, Air Force Inst. of Teh., Wright-Patterson, AFB, Ohio.
8. Peckham, L.N. & Davis, R.W. (1973), A Simplified Propagation Model for Laser System Studies, Air Force Weapons Lab, #TR-72-95 (Rev.).
9. Shettee and Fenn, Models of Atmospheric Aerosols and Their Optical Properties from Optical Propagation in the Atmosphere, AGARD Conference Proceeding #183, 2.1-2.20, Springfield, VA: National Technical Information Service, 1976.
10. Liepmann, H.W. and Roshko, A. (1957) Elements of Gas Dynamics, John Wiley & Sons.

## APPENDIX A.16

### OPTICAL DISTORTION IN AMBIENT AIR

As a beam of coherent light propagates through the atmosphere, the beam is distorted as it passes through regions of differing index of refraction. Index of refraction variances occur as the air is heated due to the sun. The relationship between the index of refraction of the air and the temperature is given by:

$$n \approx 1 + \frac{80 \times 10^{-6} P}{T}$$

with P in millibars, and T in  $^{\circ}\text{K}$ . Under normal conditions at sea level  $T = 300^{\circ}\text{K}$ , and P is on the order of 1000 millibars. Therefore  $dn/dT$  is equal to approximately  $10^{-6}/^{\circ}\text{K}$ . Pressure is assumed constant. This is likely a good assumption since aircraft are required to set altimeters using a measuring station within 100 nautical miles. This means under worst conditions an error of less than 200 ft (70 m) in altitude or 7 millibars in pressure or about a  $2 \times 10^{-6}$  in n would occur. For the 10 miles track and the stable meteorological conditions required a change of much less than  $5 \times 10^{-7}$  is likely which corresponds to the required accuracy. The above applies to constant elevation. A small

correction for elevation change in the track would be advisable since the 15n change in elevation of the track would produce a pressure induced n change of  $5 \times 10^{-7}$ .

The air temperature in the boundary layer of the atmosphere above the ground doesn't vary continuously, but rather turbulent eddies exist (reference number 1). These are regions where the air temperature is approximately constant over a distance defining the size of the eddy. In the atmosphere energy is introduced due to solar influx on a size scale  $L_0$ , the outer scale of turbulence. This defines the size of the largest eddy. Due to atmospheric mixing these eddies are broken up into smaller ones until an eddy size  $l_0$  is reached, called the inner scale of turbulence. At this point the heat is dissipated viscously into the atmosphere. At sea level  $l_0$  is on the order of millimeters.

The inner scale of turbulence is an important quantity in trying to determine beam profiles at varying distances from a laser source. The relative size of the beam compared to this inner scale of turbulence determines what happens to the beam profile as it propagates through the atmosphere. If the smallest eddies it propagates through are of a size

smaller than the diameter of the beam, the internal structure of the beam will be degraded, because separate lateral areas of the beam will pass through different eddies and be refracted differently. If, on the other hand, the beam is small compared to the smallest eddy the beam as a whole will be bent on passing through the regions of varying index of refraction. If the beam diameter is larger than  $l_0$  beam spreading will occur and the internal beam structure will be affected.

The amount of turbulence existing in the atmosphere is dependant on the sizes of the eddies and the variance in the index of refraction from one point to another. The index of refraction structure function  $C_n^2$  is defined in such a way as to be a measure of the strength of atmospheric turbulence (reference 1). Its value is obtained by taking the time average square variance of the index of refraction between two points separated by a distance intermediate between the inner and outer scales of turbulence. Dividing this quantity by the separation distance raised to the  $2/3$  power yields a quantity which is relatively independent of distance. In practice this quantity is derived by measuring the difference in the temperature between the two points, and using the relationship between the index of refraction and the temperature in the atmosphere to derive the structure function for the index of refraction.

In the first couple of meters of the atmosphere, the outer scale of turbulence has a value on the order of magnitude of a meter, while that of the inner scale of turbulence is a couple of millimeters, these dimensions decreasing with increasing turbulence. As the eddy sizes decrease the beam diameter becomes larger relative to their dimensions, and the degradive effects of the turbulence on the internal beam structure will increase.

Atmospheric turbulence increases nearer to the ground,  $C_n^2$  varying approximately as  $h^{-4/3}$ . Within the first few centimeters from the ground the turbulence increases more rapidly than this. This same effect will occur in an area close to any heated object. For this reason it is

important to keep the Flag Interferometer signal beams a distance from the rail or rail support structure.

When the laser beam undergoes refractive effects caused by turbulent regions larger than its diameter, beam wander occurs. The beam as a whole is deflected from its original direction of propagation and the irradiance pattern in the receiver plane varies. As this occurs the angle of arrival of the total beam at the receiver changes.

When the refractive effects are caused by regions of turbulence on a scale smaller than the beam diameter the phase and angle of arrival of two rays at a lateral distance across the beam will vary. The magnitude of this variance depends on the strength of the turbulence in the propagation medium, on the length of the beam's path, and on the lateral distance between the two points.

Another effect of the smaller turbulent eddies on the beam is to induce beam spread. This is distinct from beam wander in that it refers to the increase in the beam diameter at an instant of time in the receiver plane, rather than to the change in arrival at the beam centroid.

The theory of wave propagation through turbulent media can be used to predict the magnitude of the phase shift across the beam due to these atmospheric effects. A phase structure function is defined by Tatarski (reference 1) which relates to mean square variance in phase across a laser beam, at two points separated by a lateral distance,  $\rho$ . This function is defined as

$$D_{\phi}(\rho) = \langle [\phi(\rho_1) - \phi(\rho_2)]^2 \rangle .$$

where  $\phi(\rho_1)$  is the phase of the wave at  $\rho_1$ , and  $\phi(\rho_2)$  is the phase of the wave at a cross-beam distance  $\rho_2 - \rho_1$  away.

The value of the above function was determined by Tatarski (Reference 1) using the approximation of geometrical optics. For a plane wave propagating through a medium with index of refraction structure  $C_n^2$ ,

$$D_\phi(\rho) = 2.92 C_n^2 \rho^{5/3} L k^2$$

$L$  is the length of the propagation path and  $k$  - the wave number for the beam. The approximation of geometrical optics is good if the wavelength of light being used is small enough that  $\lambda \ll \ell_0$ , where  $\ell_0$  is again the inner scale of turbulence, and if the relation between  $\lambda$  and  $L$  is such that  $\sqrt{\lambda L} \lesssim \rho < L_0$ . This condition arises out of diffraction effects which will change the phase structure function value over sufficiently long path lengths.

Using the phase structure function a lateral coherence length for the beam can be defined. This is the cross-beam distance over which the rms phase change is no greater than  $\pi$ . This then describes the spatial coherence remaining in the beam profile at a distance  $L$ , from the source.

The basic requirement on the beam propagation path length is that it not be of such a length as to cause the beam diameter to be wider than its lateral coherence length. As mentioned in the introduction, the accuracy requirements for the system require measurement of the sled displacement to within one wavelength of light. If a lateral area of the beam in the receiver plane with dimensions exceeding the coherence length is "read out" over one sampling time the error in the signal will be above this limit, unless some type of aperture averaging was used.

The coherence length for a beam propagating 200 meters through a worst case atmosphere (a  $C_n^2$  value of  $10^{-12}$ ) is, using Tatarski's phase structure function for plane waves, and from the above  $D\phi(\rho) = \pi^2$ ,

$$\rho = \left( \frac{2.92 k^2 C_n^2 L}{\pi^2} \right)^{-3/5} = 5.5 \text{ mm}$$

The diameter of the beam being considered for use on the Flag Interferometer system is on the order of 1 mm, so the coherence across the beam face should be effected somewhat less than the maximum and system performance is undetermined.

Another application of the coherence length formula given above is to predict the error that arises as the beam is displaced over the sampling time. This arises from the cross-track component of the sled vibration. As the sled moves from side to side the beam propagates through a varying region of space. The maximum value for this displacement, since the all around rail to slipper clearance is 1.5mm, is 3mm. The coherence length for the beam calculated above is 5mm. Therefore the maximum displacement of the beam due to cross-track sled motion is also marginal for introducing significant errors onto the signal.

The temporal fluctuations of the turbulence structure function of the atmosphere are on the order of 100 hertz. Therefore, there is not a significant change of the turbulence structure over the .001 sec. sampling time, and changes in the optical path length of the beam due to the variation with time of the atmospheric turbulence will be minimal.

Using another mathematical treatment of atmospheric turbulence effects on light beams, given by Fante (reference 2), the beam spread and beam wander effects can be estimated. Fante's derivation is done without recourse to the approximation of geometrical optics, and as such should be applicable to arbitrary path lengths.

As a laser beam propagates through the atmosphere the beam diameter is increased by diffraction effects as the beam is incident on the various turbulent eddies in its path. In addition, the larger eddies will cause motion of the entire beam leading to "wander" of the beam centroid in the receiver plane. The irradiance pattern in the receiver plane can be specified by two quantities. One is the short term beam

diameter  $\rho_s$ , arising from the diffraction effects, which defines the instantaneous beam diameter in the receiver plane. The second quantity is  $\rho_L$ , the long term beam diameter which defines the spread of the time average irradiance pattern.

Fante's derivation for  $\rho_L$ , for a collimated beam, with a Gaussian irradiance distribution with zero beam curvature yields,

$$\langle \rho_L^2 \rangle = 4L^2/k^2D^2 + 4L^2/k^2\rho_o^2$$

where  $\rho_o$ , the long term average lateral coherence length is  $\rho_o = [.626 k^2 L C_n^2]^{-3/5}$ , and

- L = the path length through the medium
- k = the wave number of the light used
- D = the original beam diameter
- $C_n^2$  = the index of refraction structure function

The first term in this equation for  $\rho_L$  is the beam spread due to diffraction at the aperture, and the second is that arising from turbulence induced diffraction effects.

Assuming a 200 meter path length and a  $C_n^2$  value of  $10^{-12}$ , the value of  $\rho_L$  for the Flag Interferometer beam is 1.75 mm or twice the original beam diameter. This wander is less than that caused by the lateral sled vibrations and as such should be well within the beam following capabilities of the system.

The short term beam spread defining the value of  $\rho_s$  is not predicted as easily because the amount of beam spreading that will occur is dependent on the exact size of the eddies encountered by the beam on its path to the detector. Fante discusses the beam effects arising in 4 different cases according to the relative values of the parameters.

The relevant values for the Flag Interferometer do not fit exactly any of the four categories, but are intermediate between them. For  $L \gg kD^2$  the beam is expected to break up into small patches on the receiver plane. The value of  $kD^2$  for a  $\lambda = .6\mu\text{m}$ , 1mm diameter beam is 10 meters, an order of magnitude below the path length value of 200 meters. This is not really "a very small compared to" condition, but does indicate that some degradation of the internal beam structure may occur.

Yura (reference 3) defines the two cases  $L \leq kD^2$  and  $L > kD^2$ . In the latter case he says the beam can be expected to break up into multiple patches. The individual patch diameter will have a diameter approximately equal to the diffraction limited spot size obtained for the system. Further, the extent of the beam centroid wander will be comparable to the short term radius  $\rho_s$ . Therefore  $\rho_s$  is around the same order of magnitude as  $\rho_L$ , the value of which was calculated above to be just about twice the original beam diameter. Therefore signal attenuation in the receiver plane due to beam spread will be small since the beam will be spread into an area at the detector on the order of only twice its original size. Therefore a good portion of the beam can be used for a signal and should be well localized.

These results, although promising, are qualitative in nature and do not specify if the required accuracy can be met. Needed are data on  $C_n^2$  at the test track and at positions around the rails followed by a quantitative error analysis. Alternatively, a test using an interferometer can be conducted.

REFERENCES

1. Tatarski, V.I., Wave Propagation in a Turbulent Medium, McGraw Hill 1961.
2. Fante, R.L., Optical Beam Propagation in Turbulent Media, Air Force Cambridge Research Laboratories, Hanscom AFB, MA, August 1975.
3. Yura, H.T., Journal of the Optical Society of America 63, p. 567-572 (1972).

FIL

2